Université de Liège
Faculté des Sciences
Département des Sciences et Gestion de l'Environnement

Using remote sensing (optical and radar) and modeling to support the irrigation management of cereals in a semi-arid region: a case study of the Tadla irrigated perimeter in Morocco

Benabdelouahab Tarik

Thèse présentée en vue de l'obtention
du grade de Docteur en Sciences

Décembre 2015

Composition du jury :

Président : Dr. Christian Barbier (CSL)
Promoteur : Pr. Bernard Tychon (ULg)
Co-promoteur : Dr. Riad Balaghi (INRA-Maroc)
Lecteurs : Pr. Pierre Defourny (UCL)
Dr. Dominique Derauw (CSL)
Pr. Dirk Raes (KU Leuven)
Dr. Joost Wellens (ULg)

Années académique 2015-2016

Avec l'appui de:

For my parents and my wife who keep me walking

Thanks for your great support and continuous care

Acknowledgment

The completion of this thesis would have not been possible without their precious contributions and support throughout or during my doctoral study in the University of Liège. I am very grateful to all of them.

First of all, I would like to express my sincerest thanks and appreciation to my supervisor Professor Dr. Bernard Tychon for his supervision and valuable guidance during the research period. His sincere technical advice and moral support allowed me to complete this work. I am thankful to Dr. Riad Balaghi, from INRA, who motivated me to undertake this Ph.D. study, and for his advice and suggestions and for spending his valuable time on the evaluation of this study. Also, special thanks to Dr. Christian Barbier for spontaneously accepting to promote my study. I learned a lot from his style of supervision and I really benefited from his knowledge and long experience in SAR analysis. I am very grateful to Dr. Dominique Derauw for his support and encouragement and for his professional suggestions and, rich knowledge and experience in the SAR analysis have had a great contribution to this thesis. Dominique, I have really appreciated your friendship. My gratitude also goes to Professor Dr. Mohamed Badraoui for his support and encouragement.

I would like to express my sincere gratitude to all members of jury to accept to evaluate this work.

I am thankful to the University of Liège and the National Institute of Agronomic Research (INRA) for their logistic support during this work.

Sincere gratitude goes to Noury Hassan, Hamid Riani, Jaafar, Hassan Gradess and Lahssen Aarab, Adil Assous and Abdelatif Assous, without their assistance it would not have been possible for me to carry out the field work.

Very keenest thanks extended to my PhD colleagues, staff members and my friends, with whom I shared very important moments during these

years, Pr, Hassan Mrabet, Dr. Moussa Eljaroudi, Dr. Joost Wellens, Dr. Djaby Bakary, Dr. Badr Benjelloun, Dr. Rachid Hadria, Abdoul Aziz Diouf, Marie Lang, Catherine Hyemen, Abdoul Hamid Sallah, Dr. Farid Traore, Dr. Julien Minet, Antoine Denis, Claire Simonis, Dr. Louis Amani, Pr. Adil Salhi, Hamza Iaaich, Pr. Ibrahim Elboukari and Françoise Dasnoy, for their support when it was most need. Many thanks for the good company, moral support and friendship.

I am thankful to the Belgian Technical cooperation (CTB) and National Institute of Agronomic Research (INRA) for their financial support for the study. Thanks extended to the ISIS program and ESA for their valuable financial and technical support for images acquisition.

I would like to express my honest and sincere thankfulness to my parents, my sister and my father in law for their spiritual support and blessing. Last but not least, my wife Dr. Hayat Lionboui, and kids Alae and Ahmed, I reserve offer all my thanks to them for their unlimited support and endless patience that encouraged and gained me strength to complete the study.

Summary

Irrigated agriculture is an important strategic sector in Morocco, it accounts for about 45%, on average, of the agricultural Gross Domestic Product, contributing thus to food security and employment. It occupies 15% (about 1.5 million ha) of the total cultivated area in the country. Irrigation scheme managers need to ensure that water is optimally used in the irrigated perimeters and that water shortages are avoided. For large areas under irrigation, this can be achieved through water monitoring at plot level using modeling and satellite-based methodologies. The main objective of this research was to assess the use of optical and radar remote sensing and of crop modeling in the irrigation monitoring and management of wheat in the irrigated perimeter of Tadla. The potential of spectral indices derived from SPOT-5 images was explored for comparing, quantifying and mapping surface water content changes at regional and local levels. Indices were computed using the reflectance in red, near infrared and shortwave infrared bands. Our findings show that the normalized difference water index ($NDWI_{Rog}$) could be used to estimate and map the surface water content of wheat plots, from bare soil to fully covered soil. Backscatter threshold values derived from SAR images were used to detect irrigation water supplies in wheat plots and the optimal acquisition frequency of SAR images was determined in order to ensure continuous monitoring. A field crop model (AquaCrop) was adjusted to simulate durum wheat yields and the temporal evolution of soil moisture status in order to manage and schedule irrigation water supplies and assess their impact on yield. Currently, the approaches described in this paper are being applied independently. This research was intended, therefore, to provide tools to help policy-makers and

stakeholders improve irrigation monitoring and mitigate wheat water stress at the field and irrigation perimeter levels in semi-arid areas.

Keywords: irrigation management, spectral index, wheat, backscattering, SAR, semi-arid, Morocco.

Résumé

L'agriculture irriguée est un secteur stratégique au niveau des régions semi-arides et l'un des principaux contributeurs à la sécurité alimentaire et à l'emploi. Elle occupe 15% de la superficie totale cultivée au Maroc (environ 1,5 millions d'hectares), et contribue à hauteur de 45% en moyenne de la valeur ajoutée en agriculture. Actuellement, les gestionnaires de périmètres veillent à ce que l'utilisation de l'eau d'irrigation soit optimale et ainsi éviter une pénurie d'eau au niveau des périmètres irrigués. Ceci peut être accompli, sur de grands périmètres, à travers un suivi de l'eau d'irrigation à l'échelle de chaque parcelle en utilisant des méthodologies basées sur le satellite et la modélisation. La présente recherche a été positionnée par rapport à cette problématique, avec un objectif principal de soutenir le suivi et la gestion de l'irrigation du blé à travers les outils de la télédétection optique et radar et de la modélisation. Le potentiel des indices spectraux a été examiné pour comparer, quantifier et cartographier le changement de teneur en eau de surface à l'échelle d'un périmètre et au sein des parcelles. Les indices spectraux, dérivés des images SPOT-5, ont été déterminés à partir de la réflectance des bandes moyenne infrarouge, proche infrarouge et rouge. D'après nos travaux de recherche, le $NDWI_{Rog}$ est approprié pour estimer et cartographier la teneur en eau de surface des parcelles de blé. A partir des valeurs du coefficient de rétrodiffusion dérivées des images SAR, la valeur de seuil de rétrodiffusion a été établie pour détecter les apports en eau d'irrigation au niveau des parcelles de blé. En outre, la fréquence d'acquisition optimale des images SAR a été déterminée afin d'assurer une surveillance continue. Le modèle de cultures (AquaCrop) a été ajusté et testé pour simuler les rendements de blé dur aussi bien que l'évolution temporelle de l'état de l'humidité du sol. AquaCrop a été utilisé aussi pour établir une planification des apports en eau d'irrigation et estimer leur

impact sur les rendements. Actuellement, les approches présentées laissent entrevoir une valorisation opérationnelle et elles sont appliquées indépendamment. Cette recherche fournit des méthodes pour la gestion et la planification afin d'aider les décideurs et les parties prenantes à améliorer la surveillance d'irrigation et atténuer le stress hydrique de la culture du blé à l'échelle de grands périmètres irrigués dans les régions semi-arides.

Keywords: irrigation, indice spectral, blé, rétrodiffusion, SAR, semi-aride, Maroc.

List of symbols

$\alpha_{i,j}$	Local incidence angle	-
$\theta_{i,j}$	Look angle corresponding to pixel 'i,j'	-
$\sigma^0_{i,j}$	Backscattering coefficient	dB
°C	Celsius	-
CC	Canopy cover	%
CCo	Initial canopy cover	%
CCx	Maximum canopy cover	%
CDC	Canopy decline coefficient	%
CGC	Canopy growth coefficient	%
D_a	Bulk density	$g.cm^{-3}$
ET	Cumulative crop evapotranspiration	mm
ET_0	Reference evapotranspiration	mm
FC	Field capacity	mm
$G(\theta i,j)^2$	The gain	-
HIo	Reference harvest index	%
K	The constant parameters (the calibration factor)	-
Ks	Hydraulic conductivity	$cm.h^{-1}$
n	Number of observations	-
P_{ef}	Effective rainfall	mm
PWP	Permanent wilting point	mm

$R_{i,j}$	Slant range position	-
Rg	Global radiation	kW/m^2
R^2	Coefficient of determination	-
Rg	Global radiation	-
RAW	Ready available amount of water	%
TWC	Total water content	mm
WUE	Water use efficiency	$kg\ m^{-3}$

List of acronyms

ABHOER	Agence du Bassin Hydraulique d'Oum Er Rbia
AGR	Arrondissement de Gestion du Réseau
ADC	Agricultural Development Center
CIS	CSL InSAR Suite
C.P.C.S	French soil classification
CSL	Centre Spatial de Liège
CV	Coefficient of variation
dB	decibels
DGRID	Département de la Gestion du Réseau d'irrigation et de drainage
DN	Digital number
DTM	Digital terrain model
ERS	European Remote Sensing Satellite
FAO	Food and Agriculture Organization
FLAASH	Fast Line-of-sight Atmospheric Analysis of Spectral Hypercubes
GDP	Gross domestic product
GIS	Geographic information system
GPS	Global positioning system
GVMI	the global vegetation moisture index
GY	Final grain yield
Ha	Hectare

HI	Harvest index
HRV	High-Resolution Visible
INRA	Institut National de la Recherche Agronomique
ISIS	Incentive for the Scientific use of Images from the Spot system
JM	Jeffries-Matusita
K-fold CV	*K*-fold cross-validation
KU Leuven	Universiteit Leuven
LAI	Leaf area index
LOOCV	Leave-one-out cross-validation
MAX	Maximum
M	Mean of the observed variable
MAPM	Ministère de l'Agriculture et de la Pêche Maritime
MBE	Mean bias error
MIN	Minimum
MLC	Maximum-likelihood classification
MPDI	the modified perpendicular drought index
MSI	Moisture stress index
MSPSI	the modified shortwave infrared perpendicular water stress index
NDVI	Normalized difference vegetation index
$NDWI_{Rog}$	Rogers's normalized difference water index
$NDWI_{Gao}$	Gao's normalized difference water index

NIR	Near Infrared
NPK	Nitrogen, phosphorous, potassium
nRMSE	Normalized root mean square error
OA	Overall accuracy
Oi	Observed value
ONCA	Office National du Conseil Agricole
ORMVAT	Office de Mise en Valeur Agricole de Tadla
p	Probability
PA	Producer’s accuracy
PDI	the perpendicular drought index
R	Red
RADAR	RAdio Detection And Ranging
RGB	Red, green, blue
RMSE	Root mean square error
ROI	Region of Interest
SAR	Synthetic aperture radar
SGDB	Spatial geo-database
Si	Simulated value
SPOT	Système probatoire d'observation de la Terre ou Satellite pour l'observation de la Terre
STD DEV	Standard deviation
SWCI	the surface water content index
SWIR	Shortwave Infrared

ULg	Université de Liège
VSDI	visible and shortwave infrared drought index

Table content

List of figures

List of tables

Chapter 1

Introduction and thesis outline

1. Context

Irrigated areas produce more than half of all foodstuffs in the world and therefore contribute significantly to food security. This activity, however, consumes about 72% of available water resources (Geerts and Raes, 2009; Seckler et al., 1999). In Morocco, water availability is one of the main limiting factors in achieving good yields. Irrigated agriculture occupies only 15% of the cultivated area (about 1.5 million ha) in the country, but accounts for about 45% of the agricultural Gross Domestic Product and 75% of agricultural exports, depending on the season. This contribution is greater during dry seasons when production in rainfed areas is severely affected (MAPM, 2012). The challenge for stakeholders and managers in the irrigated perimeter is to increase production, control water management and rationalize irrigation. In order to save water and help farmers meet this challenge, they are given technical supervision and coaching, as well as subsidies for irrigation equipment, and legislation governing the mobilization and rational use of water resources has been enacted (Conseil Supérieur de l'Eau et du Climat, Law No. 10-95).

2. Water resources in the study area

Created in the 1940s, the Tadla irrigated perimeter was among the first large irrigation schemes in the country. It is on a plain in central Morocco (32°23′ N latitude; 6°31′ W longitude; 445 m above sea level) that covers about 100,000 hectares (ha) and is characterized by a flat topography. The plain has a semi-arid climate, with about 300 mm average annual precipitation over the 1970-2010 period and a high inter-annual variation, ranging from 130 to 600 mm over the same period.

The Tadla irrigated perimeter is divided into two sub-schemes by the Oum-Er-Rbia river, which flows from the Middle-Atlas Mountains (east) to the Atlantic Ocean (west) (Figure 1).

The irrigation water used in the Tadla perimeter comes mainly from surface water (87.1% of the total amount of irrigation water consumed in 2009/2010). Two dams, Ahmed-Al-Hansali (capacity of 750 million m^3) and Bin-El-Ouidane (1.5 billion m^3), supply irrigation water to the Tadla perimeter, in addition to groundwater pumping.

The over-exploitation of groundwater has led to reduced piezometric levels (FAO, 2011). The proportion of groundwater, however, has increased in recent years due to frequent droughts. Groundwater used for agricultural purposes in the Tadla comes from Beni-Moussa and Beni Amir groundwater and the Turonian deep water table. The total amount groundwater used by the Tadla perimeter was 12.9% (120 million m^3 per year) of the total amount of irrigated water used in the 2009-2010 cropping season.

The irrigation scheduling program is based on the amount of water reserves in dams at the beginning of the cropping season and the estimated need for irrigation water. In drought years, restrictions on the water allocation to the Tadla perimeter are set by the Agence du Bassin Hydraulique d'Oum Er Rbia (ABHOER), which is responsible for the assessment and management of water resources in the Oum Er Rbia watershed area.

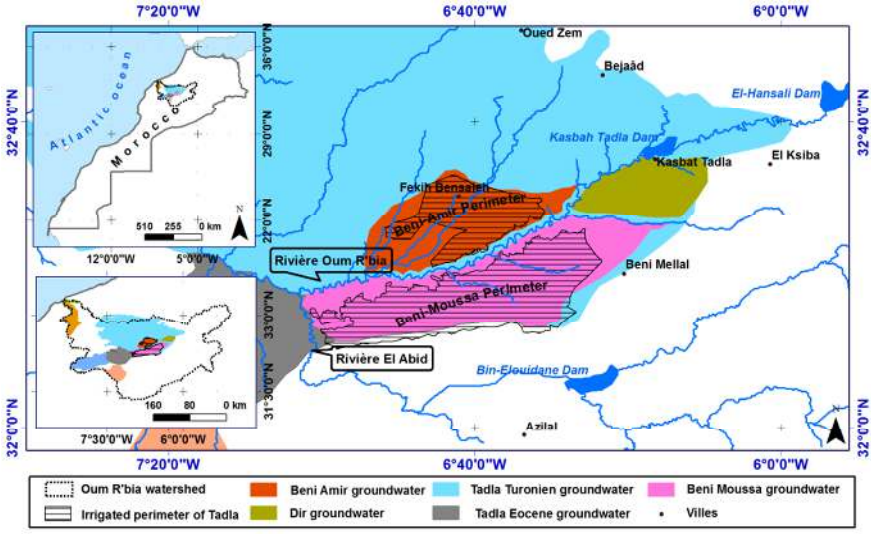

***Figure 1**: Location of the Tadla irrigated perimeter.*

The Tadla irrigated perimeter is managed by the Regional Office for Agricultural Development of Tadla (ORMVAT), a public sector institution within the Ministry of Agriculture that is responsible for organizing the distribution of the water in the perimeter to more than 27,000 farmers.

The Département de la Gestion du Réseau d'irrigation et de drainage (DGRID), which is responsible for managing the irrigation and drainage network, establishes the provisional distribution program in the irrigated perimeter, covering 100,000 ha. This program is sent to the district-level network management agency, Arrondissement de Gestion du Réseau (AGR), for implementation. The AGR receives applications from farmers for their weekly water requirements per block and, based on these applications and within the context of the provisional DGRID program, sets the water rotational turns for irrigation blocks of 25-40 ha and then releases the water.

The irrigation water is supplied via a canal system consisting of a network of main canals (212 km), primary and secondary canals (742 km) and tertiary canals (2,166 km). Distribution agents and valve guards are responsible for

implementing and controlling the distribution of the irrigation water. This system involves many field staff and agents at the local level, but lacks the ability to monitor and optimize control of the entire irrigated area.

Since the 1980s, several studies of the Tadla perimeter (Table 1) have been carried out by national and regional stakeholders in partnership with international institutions and development bodies. They have focused on identifying periods of likely water scarcity and improving irrigation management across the perimeter, but have not provided a spatio-temporal approach for the monitoring and control of the main production parameters. Such an approach, however, is essential for decision-making on large-scale schemes, such as Tadla. Our research sought to contribute to improving the spatio-temporal monitoring and control of irrigation in the Tadla irrigated perimeter.

Table 1: *Studies and projects on the Tadla irrigated perimeter*

Project	Project title	Project period
SID	Soil monitoring under Irrigation and drainage	1983-1985
RAB	Improving irrigation management at farm level	1991-1993
PAGI-1 & PAGI-2	Improvement of the irrigation management	1994-1995
MRT	Ressource management of Tadla	1996-1998
PGRE	Water resource management	1999-2001
PSIRMA	Water saving in irrigated systems in the Maghreb	2004-2009

3. Wheat production

Wheat is the main crop in the Tadla irrigated perimeter, covering more than 36% (40,000 ha) of the total irrigated area. Despite the large amounts of irrigation water used, wheat yields remain low, with high inter-seasonal variations due to fluctuating water availability and poor management practices. The average yield in the 1994-2010 period was 32 quintals/ha, with a coefficient of variation of 9.84% (ORMVAT, 2009). Water is one of the main factors limiting wheat production in the Tadla perimeter, and good management of irrigation water on a large-scale is required in order to address this challenge.

The volume of irrigation water used by wheat in the 1994-2002 period in Tadla rose to 136 million m^3/year, on average. This is equivalent to 18% of all irrigation water used across the irrigated perimeter (ORMVAT, 2009).

The wheat-growing cycle in the region runs from November-December to June. During this period, wheat is irrigated following traditional flood irrigation practice, from two to five times, depending on rainfall availability in the autumn and the volume of water accumulated in dams during winter and spring.

Traditional flood irrigation practice (Robta) involves compartmentalizing land into elementary basins with an average size of 50-60 m² and supplying water to these basins, one by one. This technique results in irrigation efficiency losses of about 50% (ORMVAT, 2002).

The spatio-temporal monitoring of wheat development, irrigation supplies and surface water content could be an interesting basis for improving irrigation scheduling and preventing water stress from adversely affecting yield (Duchemin et al., 2006).

4. Thesis outline

The objective of the research described here was to improve irrigation management and plot surface water content monitoring for wheat crop throughout a large perimeter, based on remote sensing and crop modeling in the semi-arid area of Morocco (figure 2). The research was aimed primarily at decision-makers and managers of large-scale irrigated perimeters. The development and application of decision-support tools are presented. The chapters (2-4) are based on scientific papers published in, or submitted to, peer-reviewed international journals.

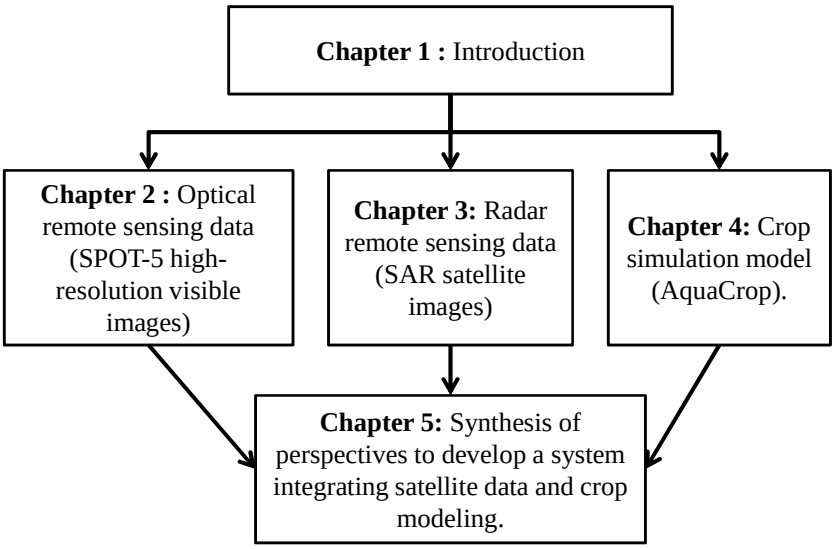

Figure 2: *Schematic diagram illustrating the thesis outline*

Chapter 2 aims to evaluate the potential of two spectral indices, Roger's normalized difference water index ($NDWI_{Rog}$) and the moisture stress index (MSI), to assess surface water content in wheat fields in order to detect irrigation water supplies in the irrigated perimeter. The indices were computed using red, near infrared (NIR) and shortwave infrared (SWIR) spectral bands from SPOT-5 high-resolution visible (HRV) images. These satellite images covered the main growth stages of wheat.

These indices were compared with corresponding *in situ* measurements of soil moisture and vegetation water content in 30 wheat fields in the Tadla irrigated perimeter in the 2012-2013 and 2013-2014 cropping seasons.

The results obtained were validated using a k-fold cross validation method. $NDWI_{Rog}$ was identified as an operative index for monitoring irrigation and estimating and mapping surface water content changes at the main crop growth stages.

Chapter 3 assesses the potential of *synthetic aperture radar* (SAR) satellite images for detecting irrigation supplies and analyzes the radar backscattering coefficient as a function of the changes of wheat water content and soil moisture

throughout the cropping season in irrigated semi-arid areas. The analysis was performed using SAR images acquired between 31 March and 12 April 2011 and the irrigation water invoices database (invoices submitted to farmers for irrigated water use). A reference level of 1 dB was set for differentiating between irrigated (recently, up to 2 days) and non-irrigated plots. SAR backscattering signal analysis showed the potential for improving irrigation monitoring and detecting irrigation supplies at the field and perimeter levels.

Chapter 4 addresses the management of irrigation water in plots throughout the cropping season using a soil-plant-atmosphere model (i.e., the AquaCrop model developed by the Land and Water Division of Food and Agriculture Organization of the United Nations, FAO). The experiment was conducted on 15 fields between 2009 and 2012. AquaCrop v. 4.0 was adjusted and tested for durum wheat plots under semi-arid conditions. Grain yield, biomass and the evolution of soil water content (0-90 cm layer) in an irrigated perimeter were simulated. Chapter 4 also describes the analysis of irrigation scenarios used to test the ability of the model to schedule irrigation water and identify the relationship between grain yield and irrigation water scheduling in order to improve grain yield and increase water-use efficiency.

Chapter 2

Monitoring surface water content using visible and shortwave infrared SPOT-5 data of wheat plots in irrigated semi-arid regions [1]

[1] Adapted from: Benabdelouahab T, Balaghi R, Hadria R, Lionboui H, Minet J, Tychon B. 2015. Monitoring surface water content using visible and short-wave infrared SPOT-5 data of wheat plots in irrigated semi-arid regions. International Journal of Remote Sensing 36: 4018-4036. DOI:10.1080/01431161.2015.1072650.

Irrigated agriculture is an important component of the agricultural sector, in arid and semi-arid regions. Given the large spatial coverage of irrigated areas, operational tools based on satellite remote sensing can contribute to optimal irrigation management. The objective of this study consisted in detecting irrigation supplies and in estimating surface water content of cereal fields using two spectral indices, the normalized difference water index (NDWI) and the moisture stress index (MSI) derived from SPOT-5 high-resolution visible (HRV) data. , These two indices were correlated to observed soil moisture and vegetation water content in 30 wheat fields located in an irrigated area of Morocco, for two consecutive seasons, in 2012-2013 and 2013-2014. $NDWI_{Rog}$ and MSI were highly correlated with *in situ* measurements at both the beginning of the growing season (sowing) and at full vegetation cover (grain filling). From sowing to grain filling, the best correlation (R^2=0.86; p<0.01) was found for the relationship between $NDWI_{Rog}$ values and observed soil moisture values. $NDWI_{Rog}$ can be used operationally for monitoring irrigation, such as detecting irrigation supplies and mitigating wheat water stress at field and regional levels in semi-arid areas.

1. Introduction

Half of the world's food supply comes from irrigated areas that use about 72% of the available water resources (Geerts and Raes, 2009; Seckler et al., 1999). In Morocco, water availability is the main limiting factor for crop production, and it is becoming a national priority for the agricultural sector (Lionboui et al., 2014). This situation has led to work on developing optimum strategies for planning and managing available water resources. Cereal (wheat and barley) production is strongly linked to the amount and distribution of rainfall in rainfed areas (Balaghi et al., 2013b) and to the amount of groundwater and water stored in dams for irrigated areas. A set of irrigated areas in the country was equipped with the means to improve and secure crop production. Despite the large amounts of consumed irrigation water, wheat yields in irrigated areas remain low and fluctuate from one season to another due to fluctuating water availability and non-

optimal management practices (Balaghi et al., 2010). In the current context of climate change, water scarcity and population growth, managing irrigation water has become a critical issue.

In Morocco, the Tadla irrigated area is managed by the Regional Office for Agricultural Development of Tadla (ORMVAT). The main cultivated crop in this area is wheat, covering more than 40,000 hectares (ha), which represent more than 36% of the total irrigated area (ORMVAT, 2009). ORMVAT is seeking a spatio-temporal methodology for monitoring surface water content in order to improve irrigation scheduling and preventing agricultural water stress (Er-Raki et al., 2010; Ozdogan et al., 2010). In addition, this could also be profitable for detecting uncontrolled irrigation and illegal water pumping.

Remotely sensed reflectance has been used to estimate soil and vegetation water content for various crops and to monitor water irrigation per surface unit (Ben-Gal et al., 2010; Ceccato et al., 2002a; Cheng et al., 2012; Hadria et al., 2010; Penuelas et al., 1997; Tian et al., 2001; Trombetti et al., 2008), drawing on the high temporal and spatial resolution of satellite images. Several indices based on wavelengths ranging between 400 and 2,500 nm have been developed to describe land-surface moisture conditions (Kogan, 2000). Estimation of surface water content values from remote sensing data is usually based on reflectance in the red (R; 610-680 nm), Near Infrared (NIR; 780-890 nm) and Shortwave Infrared (SWIR; 1,580-1,750 nm) regions of the spectrum (Lobell et al., 2003; Moreno et al., 2014; Muller and Décamps, 2000; Skidmore et al., 1975).

During wheat development cycle, crop water stress can be deduced from both vegetation and soil water content (Feng et al., 2013; Ghulam et al., 2007; Ning et al., 2013). Water stress indices used for crop management should therefore be based on the spectral bands that are sensitive to both soil moisture and vegetation water content.

Many indices for the simultaneous estimation of vegetation water content and soil moisture have been proposed for different land surfaces, from bare soils to

vegetated areas, among which are the visible and shortwave infrared drought index (VSDI) (Ning et al., 2013), the modified shortwave infrared perpendicular water stress index (MSPSI) (Feng et al., 2013), the modified perpendicular drought index (MPDI) (Ghulam et al., 2007), the normalized difference water index ($NDWI_{Rog}$) (Rogers and Kearney, 2004) and the moisture stress index (MSI) (Hunt Jr and Rock, 1989).

Indices specifically designed for vegetation water content monitoring have been developed using NIR and SWIR bands, including the normalized difference infrared index (NDII) (Hardisky et al., 1983), the global vegetation moisture index (GVMI) (Ceccato et al., 2002a; Ceccato et al., 2002b) and the normalized difference water index ($NDWI_{Gao}$) (Gao, 1996). Although this last index has been given the same name as the $NDWI_{Rog}$ developed by Rogers and Kearney (2004), it is based on a different formula. Gao's $NDWI_{Gao}$ is calculated as the normalized difference of NIR and SWIR bands, whereas Rogers and Kearney (2004) use red and SWIR bands to compute the $NDWI_{Rog}$ (Lei et al., 2009). In our study, we used the $NDWI_{Rog}$ definition given by Rogers and Kearney (2004).

In the literature, many indices based on NIR spectral reflectance have been developed to monitor soil moisture, such as the perpendicular drought index (PDI) (Ghulam et al., 2007), the distance drought index (DDI) (Yang et al., 2008), the surface water content index (SWCI) (Zhang et al., 2008) and the surface water capacity index (SWCI) (Du et al., 2013). These indices have proved to be efficient over bare soil surfaces (Ghulam et al., 2008; Qin et al., 2008; Zhang et al., 2008).

An operational index for simultaneously measuring surface water content of bare soil, mixed bare and covered soil has become crucial for irrigation management, especially in arid and semi-arid regions. This is required, especially for large irrigated areas and throughout the cropping season, when the vegetation cover is continuously changing. An operational tool adapted to this context, and that combines simplicity and robustness still deserves to be explored.

The main objective of this study was to explore the potential of $NDWI_{Rog}$ and MSI for comparing, quantifying and mapping the surface water content of wheat plots, from bare soil to completely covered soil. This index could lead to an operational tool for monitoring surface water content and managing irrigation, at least for the study area.

2. Materials and methods

2.1 Study area

The study area is located in central Morocco (32°23′ north ; 6°31′ west; 445 m above sea level), within the irrigation perimeter of the Tadla region. The area is characterized by a semi-arid climate: the annual average temperature is about 19°C, with large inter-seasonal variation. The average cropping season precipitation is about 300 mm (average over the 1970-2010 period), with significant inter-annual variation ranging from 130 to 600 mm. The area covers about 100,000 (ha) and is characterized by a flat topography. The groundwater depth varies from 31 to 117 m (Bouchaou et al., 2009; Najine et al., 2006). Wheat is one of the main cultivated crops, covering 36% of the total cultivated land. As in the rest of Morocco, traditional flood irrigation is the dominant practice used in cereal plots. Generally, the wheat-growing cycle in the region starts in November and ends in June of the following calendar year, overlapping the rainy season. Wheat is irrigated from two to five times, depending on water availability in autumn and winter and on amount of stored water in dams during the rainy season.

The area is divided into several hundred irrigation plots. For this study, 30 wheat plots were selected, with size varying from 1.7 to 24.5 ha (total area 117 ha). The diversity of crop management and irrigation schedules in these plots was representative of the general agricultural practices in the area.

Figure 3 shows the location of studied area and illustrates the location of the selected plots. The plots were labeled from P1 to P26 and divided into 348 sub-

plots of about 0.5 ha each. The plots P8, P9, P11 and P16 were monitored for two successive cropping seasons (2012-2013 and 2013-2014). The irrigation was managed by farmers. The irrigation duration ranged from 1 to 2 days per ha.

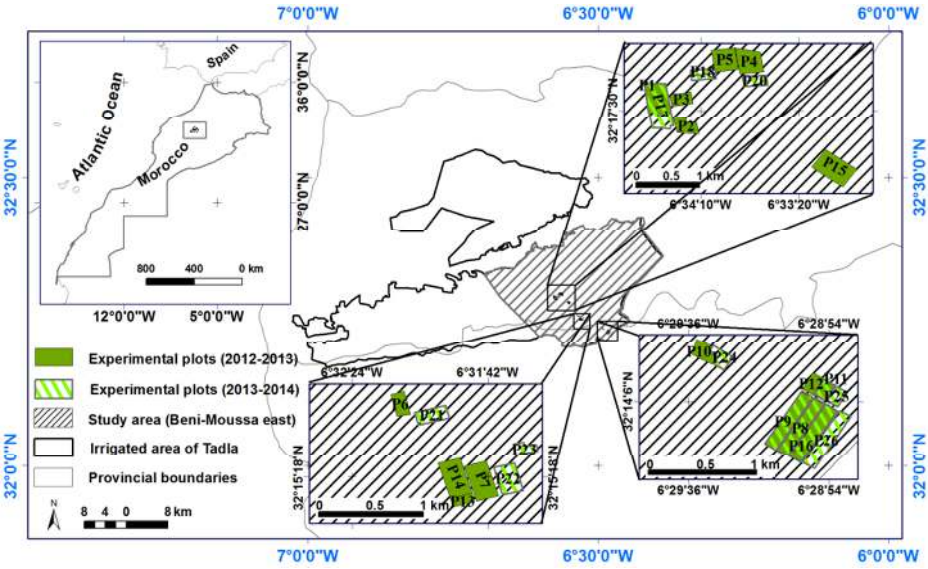

Figure 3: *Location of the irrigated area (upper left inset shows a map of Morocco; the study area is indicated by diagonal lines and the experimental plots are in grey)*

2.2 Soil data

At the study area, soil physics analyses were performed from 30 soil samples (Table 2) (Benabdelouahab, 2009). These samples were collected from several sites providing coverage of the entire study area. Water content at permanent wilting point (PWP) and field capacity (FC) were measured using a pressure plate extractor. Soil reached PWP and FC when the water potential was at -1.5 MPa and -0.033 MPa, respectively (Kirkham, 2005).

On the basis of these analyses (Table 2), the soils are mainly homogeneous with fine texture which is characterized by a high water holding capacity. The proportions of clay, silt and sand, which determine together the soil textural class, present a high homogeneity, with a standard deviation of 3.40%, 2.69% and 1.27%, respectively. The bulk density value is 1.21 (g.cm-3), with a standard

deviation of 0.14. The small variability of the bulk density permits us to consider this parameter as constant value. This result justifies the use of the gravimetric soil moisture.

Table 2: *Soil physics properties in Tadla, Morocco*

Soil properties	Depth 0-30		Depth 30-60		Depth 60-90	
	Value	STD DEV	Value	STD DEV	Value	STD DEV
Sand (%)	25.4	2.7	24.5	1.9	24	0.3
Silt (%)	41	1.3	35.5	1.65	39.7	1.3
Clay (%)	33.6	3.4	40	1.3	36.3	1.5
Bulk density ($g.cm^{-3}$)	1.2	0.1	1.5	0.1	1.5	0.1
Field capacity (mm)	78.7	11.6	95.2	8.2	96	12.1
Saturation (mm)	106	4.2	118	4.8	125	5.5
Permanent wilting point (mm)	36.2	3.1	39.4	6.2	39.7	8.8
Hydraulic conductivity ($cm.h^{-1}$)	5.1	1.9	3.5	1.7	3.5	1.9

2.3 Field data

The experiments were conducted during the 2012-2013 and 2013-2014 wheat cropping seasons to assess changes in soil moisture and vegetation. Dates and amounts of irrigation water supply and physiological crop data were collected.

Soil moisture was measured weekly for all 30 plots during the two cropping seasons, starting from sowing until grain filling, at 0-10 cm depth, with three random replications per plot. Soil moisture was measured using gravimetric methodology (dried in an oven at 105°C for 24 hours). Vegetation water content was also measured weekly, starting from tillering until wheat grain filling (January to May 2013). In each plot, the vegetation water content was measured in four randomly selected quadrats (i.e., an area of 0.5 * 0.5 m). From each quadrat, sub-samples were used to measure the weight of the fresh and dry above-ground biomass in order to quantify vegetation water content (dried in an oven at

65°C for 48 h). Soil and vegetation water content were quantified on a gravimetric basis (i.e., grams water/grams soil or biomass), expressed as a percentage (%). These measurements were used to establish a relationship between vegetation water content and covered soil moisture.

The collected field data (soil moisture and vegetation water content) were vectorized as points and the experimental plots as polygons, in a Geographical Information System. Polygons were drawn so as to remove pixels falling along plots boundaries. The experimental plots were subdivided into sub-plot units of identical size (0.5 ha) and an identifier code was assigned to each of these units. Polygons of these sub-plot units served as a way of extracting pixel images that were close and directly linked to ground measurements.

As far as possible, field data were collected in a regular and timely manner to ensure that ground measurements were acquired synchronously with satellite passes so as to obtain a good comparison between field measurements and remote sensing data. Field measurements collected within a maximum of 3 days before or after a satellite pass were used for the analysis. We also ensured that during this period (between the field observation and the image acquisition date) there was no precipitation event or irrigation water supply.

2.4 Satellite images and their processing

Ten SPOT-5 HRV satellite images were acquired between December (at wheat emergence) and April (at grain filling) for the 2012-2013 and 2013-2014 cropping seasons (Table 3). They covered temporal changes in surface water content during the main wheat growth stages, except for the final senescent stage. The processing level of the acquired images was 1B, which included radiometric and geometric corrections. Atmospheric corrections were performed from radiance images, using the Fast Line-of-sight Atmospheric Analysis of Spectral Hypercubes (FLAASH) model available in the ENVI software. FLAASH is an atmospheric correction tool that corrects the wavelengths between 400 and 2,500 nm by eliminating the effects of water vapor and aerosols in the atmosphere. This

model is considered to be more accurate for SPOT-5 images than other models (Guo and Zeng, 2012).

The NDVI threshold method (Momeni and Saradjian, 2007; Ning et al., 2013) was used to classify the land surface into three land cover categories (Tables 5 and 6): bare soil (beginning of cropping season) with NDVI < 0.2; partly vegetated soil (mixed cover) with $0.2 \leq NDVI \leq 0.5$; and full vegetation cover with NDVI > 0.5.

The 12 December 2012 and 2 December 2013 images were acquired at the beginning of the growing season, when the soil was bare, whereas the 21 March 2013, 26 March 2013, 11 April 2013, 26 March 2014 and 15 April 2014 images were acquired when the soil was completely covered. The 2 February 2013, 6 January 2014 and 1 February 2014 images were acquired in the middle of the cropping season when the surface was partly covered by vegetation.

Table 3: *List of acquired SPOT-5 HRV images and their characteristics*

Acquisition date	Cropping season	Sensor	Wavelength (nm)	Resolution (meters)
12 December 2012	2012/2013	SPOT-5 HRV	Green: 500-590 Red: 610-680 NIR: 780-890 SWIR:1580-1750	Red: 10 Green: 10 NIR: 10 SWIR: 20
02 February 2013				
21 March 2013				
26 March 2013				
11 April 2013				
02 December 2013	2013/2014			
06 January 2014				
01 February 2014				
26 March 2014				
15 April 2014				

The visible spectrum (400-740 nm) is sensitive to vegetation water stress (Jensen, 2005), with a more significant reflectance change in the red band (580-680 nm). The NIR band serves as a moisture-reference band, whereas the SWIR band is used as the moisture-measuring band. Reflectance in the NIR spectrum (740-

1,300 nm) is most sensitive to leaf internal structure changes (Jacquemoud and Baret, 1990) and is insensitive to moisture variation (Elvidge and Lyon, 1985), except in conditions leading to leaf dehydration which therefore affects leaf structure (Girard and Girard, 2010; Jensen, 2007). Recent studies confirmed the high sensitivity of the SWIR band to moisture variation in vegetation and soil (Ceccato et al., 2001; Cheng et al., 2013; Cheng et al., 2011; Hunt Jr et al., 2011; Hunt Jr and Rock, 1989; Liu et al., 2012; Yilmaz et al., 2008a; Yilmaz et al., 2008b).

The first step of images post-processing involved computing two spectral indices, the $NDWI_{Rog}$ (Lasaponara and Masini, 2012; Rogers and Kearney, 2004) and the MSI (Ceccato et al., 2001; Ceccato et al., 2002b; Hunt Jr and Rock, 1989) (Table 4), using the spectral reflectance in the Red, NIR and SWIR bands for each SPOT-5 HRV image.

Table 4: *Spectral indices derived from the SPOT-5 sensor (Red, NIR and SWIR refer to the spectral reflectance bands of SPOT-5 image)*

Indices	Equation	Properties	References
Normalised Difference Water Index ($NDWI_{Rog}$)	(Red – SWIR)/(Red + SWIR)	Vegetation water content and soil moisture content	Rogers and Kearney, 2004; Lei, Li, and Bruce 2009; Lasaponara and Masini, 2012
Moisture Stress Index (MSI)	(SWIR/NIR)	Vegetation water content	Ceccato et al. 2001; Ceccato et al. 2002; Hunt Jr and Rock 1989

The second step involved delineating the region of interest (ROI) used as a mask of wheat sub-plots. The average values of the $NDWI_{Rog}$ and MSI spectral indices were then computed for each corresponding sub-plot (7×7 pixels) where field measurements were conducted (Figure 4).

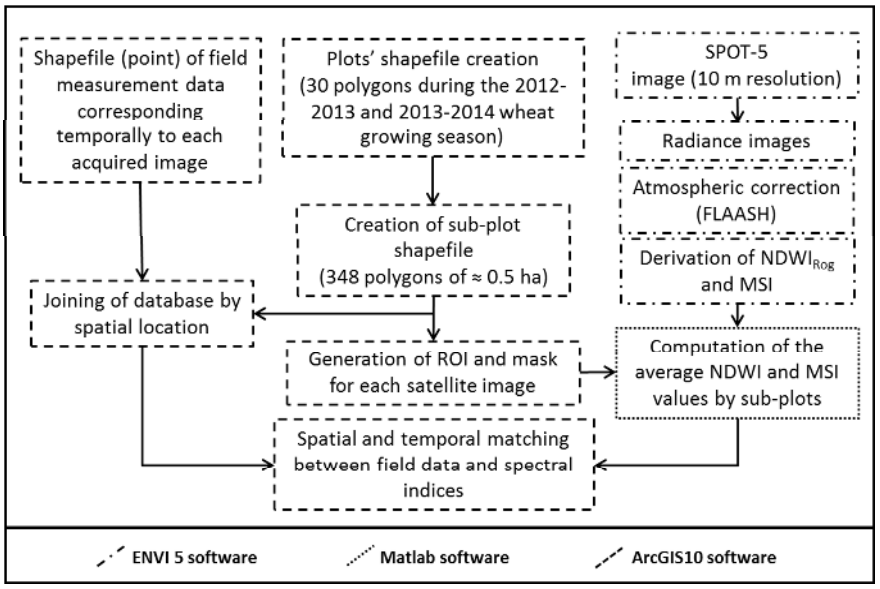

***Figure 4**: Schematic diagram illustrating field data and satellite image processing*

2.5 Model calibration and evaluation

The average MSI and $NDWI_{Rog}$ values of the sub-plots and the corresponding ground measurements were compared using linear regression analysis. The regression coefficients *a* and *b*, reported in Tables 5 and 7, stand for the slope and intercept of the regression line, respectively.

The statistics used for evaluating the regression models were: the coefficient of determination (R^2), the root mean square error (RMSE) which is one of the most widely used as error assessment indices), and the normalized RMSE (nRMSE) expressed as a percentage of the RMSE divided by the mean of observed values (Richter et al., 2012):

$$RMSE = [\sum_{i=1}^{n} (Si-Oi)^2/n]^{0.5} \quad (1)$$

$$nRMSE = [\sum_{i=1}^{n} (Si-Oi)^2/n]^{0.5} \times 100/M \quad (2)$$

where Si and Oi refer to simulated and observed values of the studied variable, respectively; n is the number of observations; and M is the mean of the observed variable.

nRMSE indicates the accuracy of the model and the dispersion around the mean of the observed values.

The accuracy of the regression models was evaluated using the k-fold cross validation (k-fold CV) approach (Cassel, 2007). Cross validation is a resampling method that offers a different approach to model evaluation. It uses k replicate samples of observation data, builds models with (k-1)/k of data and tests with the remaining 1/k. The random k-fold CV takes k independent samples of size N*(k-1)/k (Cassel, 2007). In our study, it involved 33.3% of the observations as the validation data, with the remaining 66.6% of the observations being the training data, with 10 repetitions (N = 10).

2.6 Mapping soil moisture

Soil moisture was mapped using relationships of the validated linear regression models between satellite indices and ground measurements. The maps display surface soil moisture at plot level for each acquired satellite image. The same approach could be used to map vegetation water content (see the Appendix 1).

3. Results and discussion

3.1 Soil moisture assessment at the beginning of wheat cropping season

The relationship between observed soil moisture and the MSI and $NDWI_{Rog}$ values was assessed in 47 sub-plots at the beginning of the wheat cropping season (NDVI<0.2), using images acquired on 12 December 2012 and 2 December 2013.

The reduced number of data used for this analysis is explained by the infrequent measurements collected with a lag time of maximum 3 days between field measurements and dates of satellite pass.

As shown in Table 5, the R^2 and RMSE were 0.84 ($p<0.01$) and 1.03% for the $NDWI_{Rog}$ and 0.79 ($p<0.01$) and 1.18% for the MSI, respectively.

We compared the soil moisture values predicted using the k-fold CV method and those measured in situ (Table 6). The statistical indicators obtained from this comparison were $R^2 = 0.81$ ($p<0.01$) and RMSE = 1.09% for $NDWI_{Rog}$ and $R^2 = 0.76$ ($p<0.01$) and RMSE = 1.24% for MSI. This comparison showed that errors were acceptable for both the MSI and $NDWI_{Rog}$, confirming the ability of these indices to accurately explain soil moisture variability for bare soil. Ghulam et al. (2007) reported similar results using the PDI and MPDI, with an R^2 of 0.56 and 0.55, respectively, over bare surfaces.

Table 5: *Linear regression analysis of the relationship between observed soil moisture and selected spectral indices*

			Statistical indicators				
		Samples	**R^2**	**a**	**b**	**RMSE**	**nRMSE**
NDWI Rog	Bare soil (NDVI<0,3)	47	0.84	-22.74	1.18	1.03	10.69
	Mixed Cover (0,3<NDVI<0,7)	65	0.75	-13.9	8.3	1.38	7.22
	Covered Soil (NDVI>0,7)	100	0.83	-20.1	4.57	1.05	6.17
	All types of cover	212	0.86	-20.5	3.42	1.62	10.1
MSI	Bare soil (NDVI<0,3)	47	0.79	-2.04	1.26	1.18	12.23
	Mixed Cover (0,3<NDVI<0,7)	65	0.38	2.4	21.75	-	-
	Covered Soil (NDVI>0,7)	100	0.68	-20.4	31.9	1.44	8.48
	All types of cover	212	0.49	-0.32	6.97	10.19	64.11

Table 6: *The k-fold CV of the linear regression analysis of the relationship between observed soil moisture and selected spectral indices*

		K-fold cross validation indicators			
		Samples	**R^2**	**RMSE**	**nRMSE**
NDWI Rog	Bare soil (NDVI<0,3)	150	0.81	1.09	10.82
	Mixed Cover (0,3<NDVI<0,7)	210	0.74	1.41	7.24
	Covered Soil (NDVI>0,7)	330	0.84	1.08	6.34
	All types of cover	700	0.87	1.61	10.01
MSI	Bare soil (NDVI<0,3)	150	0.76	1.238	12.3
	Mixed Cover (0,3<NDVI<0,7)	210	0.37	-	-
	Covered Soil (NDVI>0,7)	330	0.68	1.51	8.88
	All types of cover	700	0.40	3.27	20.61

3.2 Vegetation water content and soil moisture assessment at full vegetation cover

The relationship between observed vegetation water content and MSI and $NDWI_{Rog}$ was assessed in 62 sub-plots, when the soil was completely covered by vegetation (NDVI > 0.5). The statistical indicators obtained are presented in Table 7. The two spectral indices were strongly related to vegetation water content. The statistical indicators R^2 and RMSE were 0.77 ($p<0.01$), 2.49% for $NDWI_{Rog}$ and 0.55 ($p<0.01$), 3.47% for MSI, respectively.

Table 7: *Linear regression analysis of the relationship between observed vegetation water content and selected spectral indices*

		Statistical indicators				
	Samples	R^2	a	b	RMSE	nRMSE
NDWI Rog	62	0.77	-47.75	43.90	2.49	3.48
Vegetation						
MSI		0.55	-34.98	97.57	3.47	4.85

Table 8: *The k-fold CV of the linear regression analysis of the relationship between observed vegetation water content and the spectral indices*

	K-fold cross validation indicators			
	Samples	R^2	RMSE	nRMSE
NDWI Rog	200	0.78	2.62	3.64
Vegetation				
MSI		0.57	3.69	5.13

In order to validate these results, we compared observed vegetation water content values with those predicted using the k-fold CV method. As shown in Table 8, the errors were low for both $NDWI_{Rog}$ and MSI. The evaluation model indicators obtained for predicted vegetation water content from $NDWI_{Rog}$ were: RMSE=2.62% and R^2=0.72 ($p<0.01$). For MSI, the values were RMSE=3.69% and R^2=0.47 ($p<0.01$). These results confirmed the ability of $NDWI_{Rog}$ to estimate the vegetation water content for wheat, whereas the MSI values were less in agreement with the observed values. Similar results were reported for MSI by QiuXiang et al. (2012) and Hunt Jr and Rock (1989).

Ning et al. (2013) reported the ability of the VSDI to simulate both soil moisture and vegetation water content, obtaining an R^2=0.51 and 0.42, respectively.

In areas with limited water availability, the critical period for wheat is during rapid growth, from the end of tillering to full stem elongation. In our study area, this corresponds to the period that usually begins in mid-March. Figure 5 compares measured soil moisture and wheat vegetation water content during the critical tillering to grain filling period. The figure shows a strong relationship between these two variables, with an R^2=0.82 (*$p<0.01$*). During the development stages of healthy wheat, from tillering to grain filling, and under the soil moisture conditions of the study area, the relationship was linear between FC (24.3%) and PWP (9.8%), which accorded with the findings reported by Girard and Girard (2010). This shows that surface soil moisture can be estimated using vegetation water content and vice-versa.

$NDWI_{Rog}$ and MSI performed well in assessing top 10 cm soil moisture, when the soil was completely covered by vegetation. As shown in Table 5, R^2 and RMSE were equal to 0.83 ($p<0.01$) and 1.05% for the $NDWI_{Rog}$ and 0.68 ($p<0.01$) and 1.44% for the MSI, respectively.

These results show the capacity of both $NDWI_{Rog}$ and MSI to simultaneously estimate both vegetation water content and soil moisture, even when the soil is completely covered by the canopy, as confirmed by the k-fold validation results in Table 6.

Table 5 shows that change in land-cover type induced an MSI with opposing trends. As MSI uses NIR band that behave differently according to type of cover (Ning et al., 2013), this index is not suitable for comparing different land-cover types simultaneously.

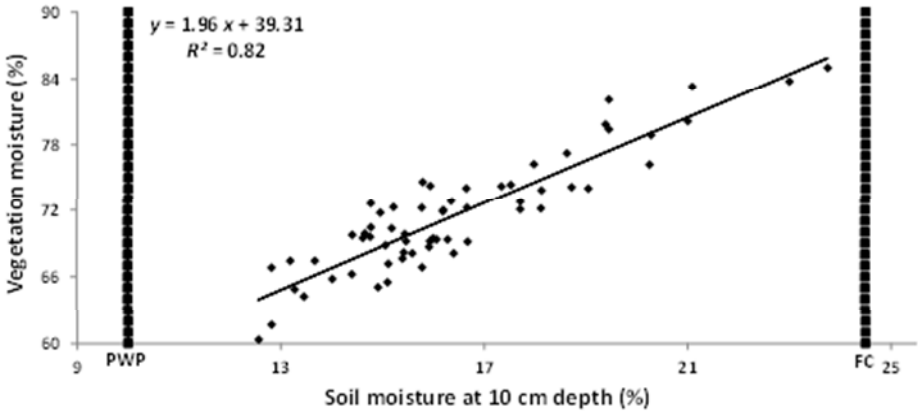

Figure 5: *Relationship between vegetation and soil moisture measurements (FC: Field capacity and PWP: Permanent wilting point). Data were acquired on 21 March 2013, 26 March 2013, 11 April 2013, 26 March 2014 and 15 April 2014*

3.3 Soil moisture assessment during the main growth stages of wheat

Following the strong ability of $NDWI_{Rog}$ and MSI to estimate soil moisture separately for bare soil and full vegetation cover, we tested the capacity of these spectral indices to estimate this parameter throughout wheat cropping season, apart from the senescent stage which was not studied, since no irrigation is applied during this stage of wheat development. Figures 6 and 9 show the comparison between observed soil moisture values and those derived using the spectral indices for the 10 acquisition dates.

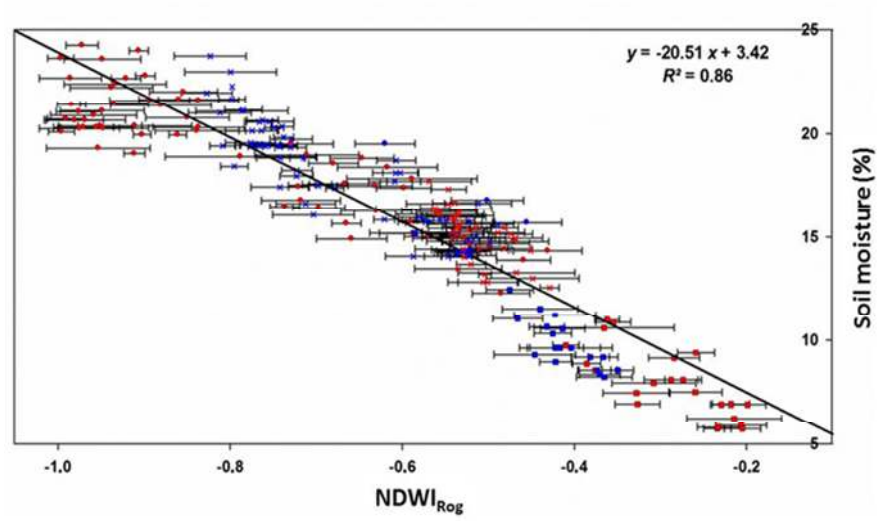

Figure 6: *Relationship between soil moisture (at 10 cm depth) and the $NDWI_{Rog}$ values derived from all the acquired images (cropping season 2012/2013 in blue and cropping season 2013/2014 in Red: squares = bare soil; cross = covered soil; circles = mixed cover). Error bars (based on standard deviation) show the range of $NDWI_{Rog}$ values in each sub-plot*

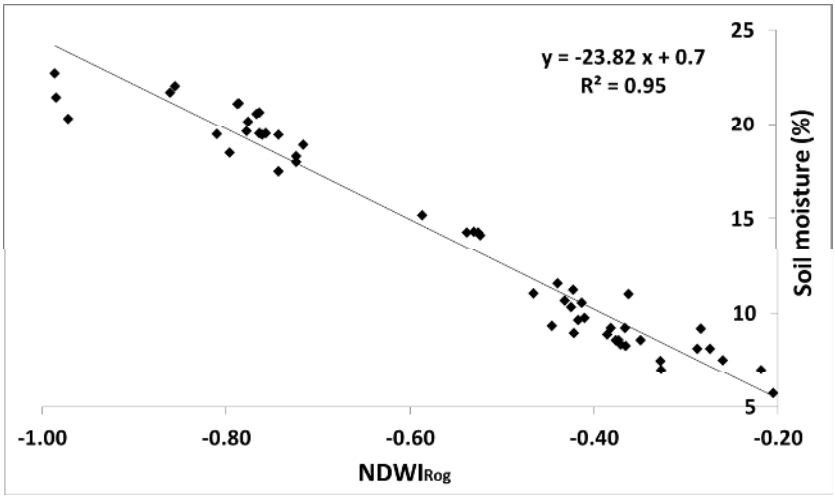

Figure 7: *Relationship between soil moisture (at 10 cm depth) and the $NDWI_{Rog}$ values derived from all the acquired images (lag time of maximum 2 days between field measurements and dates of satellite pass)*

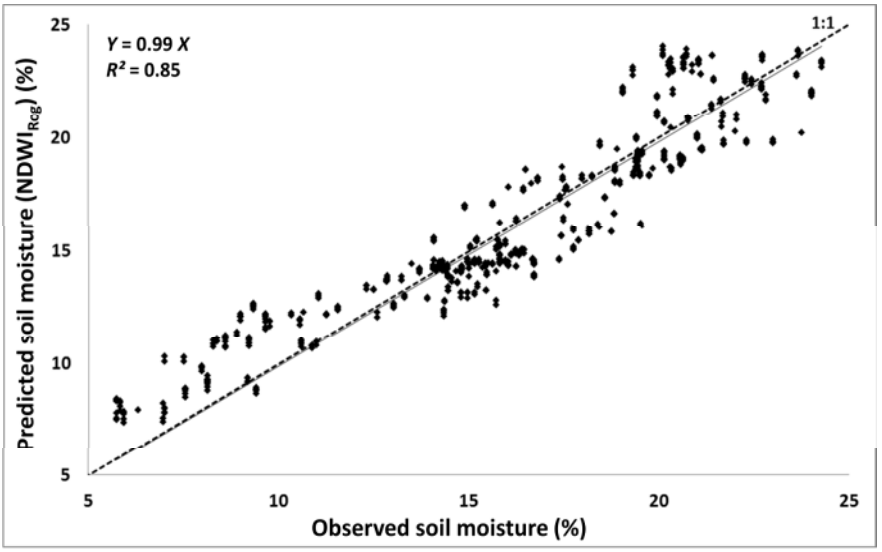

Figure 8: *Comparison between observed and predicted soil moisture using the k-fold CV of all acquired images*

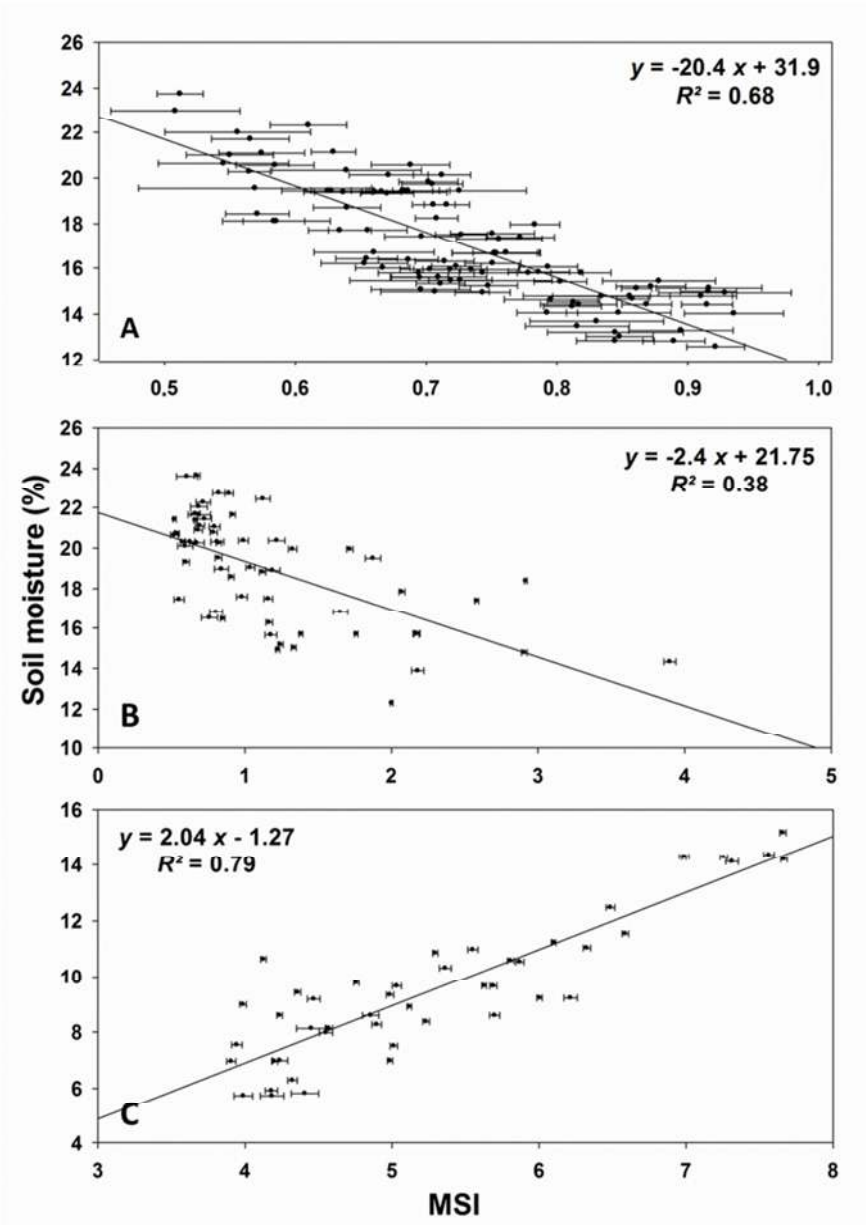

***Figure 9**: Relationship between soil moisture (at 10 cm depth) and the MSI values derived from all the acquired images: (A) covered soil; (B) mixed cover; and (C) bare soil. Error bars (based on standard deviation) show the range of MSI values in each sub-plot*

The statistical indicators R^2 and RMSE were 0.86 ($p<0.01$) and 1.62 % for $NDWI_{Rog}$, respectively (Table 5). The point clouds for MSI, representing different kinds of cover, show opposite trends according to the main growth stages of wheat (Figure 9). This indicated that there was no unique linear relationship between MSI and surface soil moisture, for the entire wheat crop cycle (apart from the senescent stage). The standard deviation of this index varies between 0.009 and 0.1 (Figure 9). The ratio between MSI values and the standard deviation expressed as a percentage varies between 0.23% and 11.88%.

In contrast, there was good agreement between $NDWI_{Rog}$ and soil moisture, whatever the wheat growth stage with a standard deviation values ranging between 0.007 and 0.087 (Figure 6). The ratio between $NDWI_{Rog}$ values and the standard deviation as a percentage ranges between 1.12% and 12.87%. The relationship was maintained from one year to the other (cf. figure 6). The dispersion of the observed cloud points was mainly due to the spatial heterogeneity which characterized soil moisture at plot level (Bi et al., 2009; Song et al., 2009; Wang et al., 2013), and the variable time lags ranging from 0 to 3 days between field measurement and satellite pass.

With a two-day lag time, 75% of the overall observed points were discarded. In this case, the selected points corresponded to only five of the acquired images. As shown in Figure 7, R^2 and RMSE were 0.95 ($p<0.01$) and 1.16% for the $NDWI_{Rog}$, respectively. The observed point clouds dispersion was significantly reduced (figure 7).

As shown in Table 5, the slope values (a) of the different types of cover for $NDWI_{Rog}$ were relatively similar. For mixed cover, the slope was slightly steeper, indicating the stability of $NDWI_{Rog}$ at different stages of crop cover (from emergence to grain filling) and its ability to quantify soil moisture throughout crop growth.

This finding was confirmed when comparing estimated and observed soil moisture using the k-fold CV approach (Figure 8). The statistics obtained for $NDWI_{Rog}$ were RMSE = 1.61% and $R^2 = 0.85$ ($p<0.01$).

In Figure 8, it is important to note that the model may overestimate the dry soil moisture (lower than 12%). Further analysis, with a larger dataset, should be performed to check a possible nonlinear relationship between $NDWI_{Rog}$ and soil moisture.

With regard to MSI, the statistical analysis showed that this index is not suitable for estimating soil moisture throughout crop growing period, although it can accurately estimate bare soil moisture and vegetation water content separately (Figure 9). The NIR reflectance of covered soil is significantly higher than that of bare soil (Ning et al., 2013). As MSI uses NIR as the reference band, the values of this index are much higher for bare soil than for covered soil, which means that MSI cannot be used to compare dissimilar land-cover types.

Feng et al. (2013) simulated soil moisture using the MSPSI model and obtained an R^2 of 0.66. They also obtained R2 values of 0.54, 0.48 and 0.60 for the PDI, MPDI and SPSI models, respectively, for both bare and covered surfaces.

Ning et al. (2013) proposed using the VSDI for monitoring soil and vegetation moisture simultaneously over different land-cover types. This index is based on exploiting the SWIR and red bands. In a comparison between VSDI and the fractional water index over different land-cover types, they obtained an R^2 of 0.54.

3.4 Mapping soil moisture

Figures 10 and 11 show the soil moisture maps derived from the 10 SPOT-5 dates based on $NDWI_{Rog}$ for the first (2012-2013) and second (2013-2014) cropping season, respectively. These maps were generated using a regression model (soil moisture = -20.51 * $NDWI_{Rog}$ + 3.42) obtained by comparing the 10 available images and field measurements (see Figure 6). Soil

moisture ranged from 6% (red) to 24% (blue). Figures 10(f) and 11(f) show the location of the plots.

The maps display change and variability of soil moisture between and within the plots, showing in particular differences between dry and wet plots. Such results could be very useful for monitoring water stress on a large scale for wheat, and for detecting irrigation supplies.

In Figure 10(a), plots P1, P2, P3, P4 and P5 have a higher moisture contents than other plots. This variation is caused by the first irrigation being applied before 12 December 2012, the date when satellite image was acquired.

Some plots (P6, P7, P8 and P9) in Figure 10(b) show internal heterogeneity of the surface water content. The drying process is apparent in these plots, indicating the onset of water stress in the crop. This figure also shows heterogeneity among different plots, mainly due to irrigation supplies not being provided at the same time.

Figure 10(b) shows high soil moisture values, exceeding 16%, for plots P1, P2, P3, P4 and P15 in the red square and P10 in the blue square. These plots were irrigated during the last 10 days of January 2013. This was the second irrigation applied by farmers in the study area. Plot P4 did not appear to be completely irrigated at this time, indicating that irrigation was in progress on the image acquisition date. The other plots were irrigated in January or after 2 February 2013, the date of the satellite pass.

Figures 10(c) and 10(d) show significant homogeneity and a dominance of blue, indicating that soil moisture was high (20-24%). This is explained by rainfall that occurred between 14 and 18 March 2013 (31.3 mm) and on 24 March 2013 (14 mm). These dates correspond to the dates when images were acquired (i.e., 21 and 26 March 2013). Figure 10(e) shows that after 2 weeks of rainfall, there was a homogeneous drying of the plots, with soil moisture ranging from 14 to 16%. The drying process was somewhat attenuated for plots (P4 and P5) which were irrigated by the end of March.

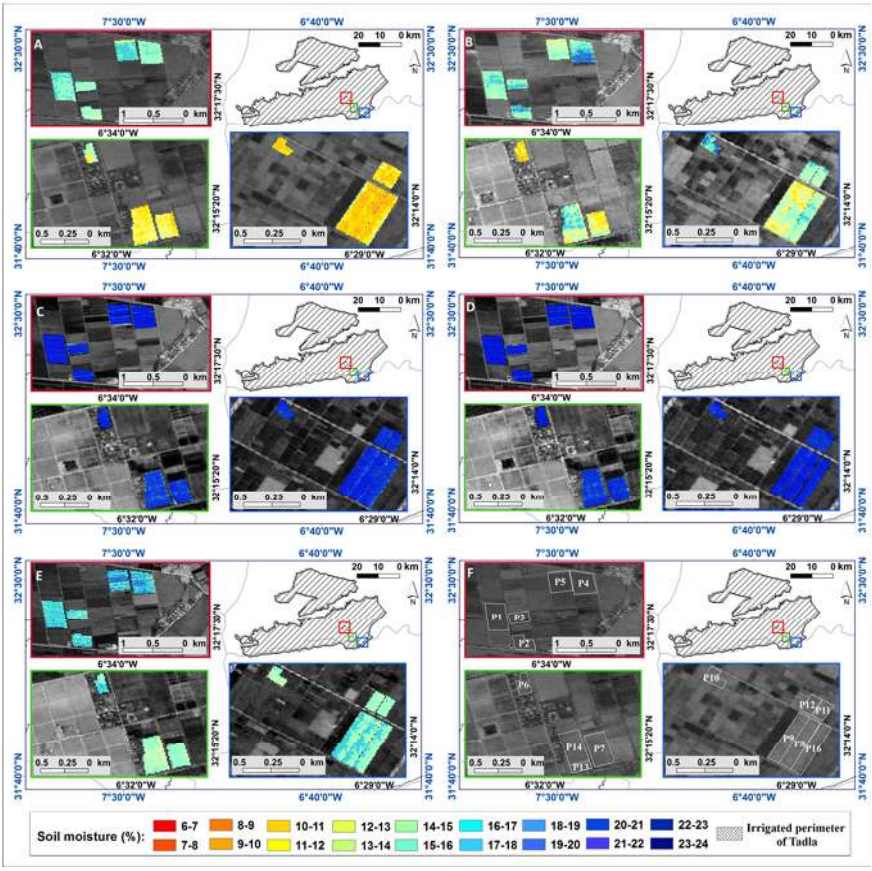

Figure 10: *Soil moisture maps derived from the* $NDWI_{Rog}$ *data: (a) 12 December 2012; (b) 2 February 2013; (c) 21 March 2013; (d) 26 March 2013; (e) 11 April 2013; and (f) codes for the experimental plots*

In Figure 11(a), some pixels in P24 displayed quite a high surface water content level (16-18%), explained by the first irrigation. In wheat fields, irrigation water is supplied straight after sowing. Thus, the detection of the first irrigation can generally indicate the sowing date.

In Figure 11(b), it is interesting to note that plot P17 appears to be partly irrigated, indicating that irrigation was in progress. Plots P8, P9, P11, P16, P18, P19, P20,

P24 and P25 were irrigated a few days before acquisition of the satellite image on 6 January 2014.

Figure 11(c), derived from the satellite image acquired on 1 February 2014, shows high and homogeneous surface water content (20-24%). This is explained by significant rainfall that occurred between 30 and 31 January 2014 (36.5 mm).

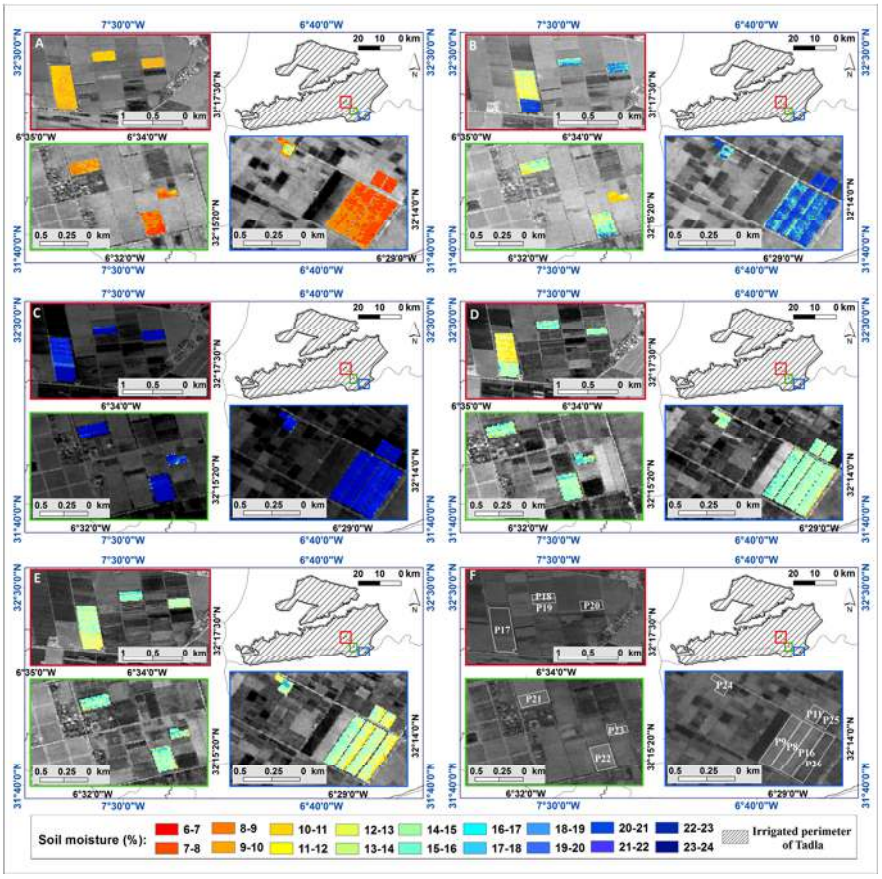

Figure 11: *Soil moisture maps derived from the $NDWI_{Rog}$ data: (a) 2 December 2013; (b) 6 January 2014; (c) 1 February 2014; (d) 26 March 2014; (e) 15 April 2014; and (f) codes for the experimental plots*

Both Figures 11(d) and 11(e), derived from images acquired on 26 March 2014 and 15 April 2014, show relatively low humidity, ranging from 12 to 15%. This can be explained by irrigation that was scheduled at the beginning of March and after mid-April, in addition to lack of rainfall for the period of 12 days before the date of image acquisition. These figures portray the process of drying and the start of water stress of wheat crop.

The developed method can be used as an operational tool for managing irrigation and crops and monitoring the evolution of surface water content at the plot scale, as well as on a larger scale across the irrigated area.

The practical aspects of this method that could improve irrigation water management in an irrigated perimeter include the following:

- The method combined to a calibrated crop model can be used for triggering irrigation supplies in water stress situations and otherwise prevent contributions in excess of irrigation water. Such information could be valuable for decision-makers in charge of irrigation and crop management in irrigated areas.
- It could also be useful for detecting illegal irrigation and pumping. This is relevant in irrigated areas where irrigation has not been scheduled and uncontrolled water pumping is prohibited.
- It could also be used for detecting the date of sowing, which is usually concomitant with the first irrigation.

4. Conclusions

This study sought to assess the ability of two spectral indices, $NDWI_{Rog}$ and MSI derived from SPOT-5 HRV satellite images, to estimate surface water content from bare soil to completely covered soil throughout the cropping season in irrigated semi-arid areas.

The comparison between $NDWI_{Rog}$, using the Red and SWIR bands, and soil moisture measurements at a depth of 0-10 cm throughout the cropping season showed good agreement, with an R^2 of 0.86. MSI appeared to be less suitable for quantifying and comparing soil moisture content at different stages during wheat

cycle. This index could be used, however, to estimate bare soil moisture, covered soil moisture and vegetation water content separately. The derived soil moisture maps showed interesting spatial patterns that could be related to the dates of irrigation and rainfall events in the irrigated perimeter of Tadla.

$NDWI_{Rog}$ can be used to compare, quantify and map surface water content, at different stages of crop cover (from sowing to grain filling) over years. It shows potential for improving irrigation monitoring, detecting irrigation supplies, wheat stress management and our understanding of surface water content changes at field and regional levels in the study area. The performance of the methodology should be checked in other contexts before judging its suitability for application in other areas.

Chapter 3

Detecting wheat irrigation supply using SAR data in semi-arid regions [2]

[2] Submitted 13.07.2015 (under review): Benabdelouahab, T., Derauw, D., Tychon, B., Balaghi, R., Wellens, J., Barbier, C., 2015. Detecting wheat irrigation supply using SAR data in semi-arid regions. Remote Sensing Applications: Society and Environment.

The objective of this study was to use SAR data to detect the supply of irrigation water during the anthesis and grain-filling phenological stages of wheat in the irrigated Tadla perimeter of Morocco. Backscattering coefficients were derived from four ERS-1 images acquired between 31 March and 12 April 2011 and were compared with the irrigation water invoices database in order to assess their sensitivity to surface moisture (vegetation water content and soil moisture). The analysis showed that there were significant changes in backscattering values caused by irrigation, with values ranging between 0.11 and 3.11 dB. A reference level of 1 dB was established for differentiating between (recently; up to 2 days) irrigated and non-irrigated plots. We also select available images with an interval of 3 days for the acquisition of SAR images in order to ensure continuous monitoring of the irrigated wheat plots over time. The study showed that radar data contain important information for the assessment of irrigation supplies during the cropping season, which could help regional decision-support systems to monitor and control irrigation supplies over large areas.

1. Introduction:

Irrigated areas throughout the world are facing increasing pressure due mainly to erratic precipitation regimes (Dore, 2005), long dry periods and rapidly growing population demands. In this context, the effective management and monitoring of irrigated areas require a good understanding of the spatial and temporal processes governing agricultural systems.

Managing and monitoring an irrigated area effectively can be done by analyzing these processes over an entire crop cycle and a large agricultural area where the surface is heterogeneous (various types of crops, classes of soil and management approaches) in order to assess the overall impact of crop management practices.

In Morocco, cereals are one of the major grain crops grown and they hold an important place in the agricultural production systems, occupying 75% of the cultivated area and accounting for 10-20% of the agricultural Gross Domestic Product (GDP). Nevertheless, yields remain low and fluctuate from one area to

another and one season to another because of varying water management, field management and weather conditions (Balaghi et al., 2010).

Given the importance of wheat production in semi-arid areas where water is the main limiting factor, large-scale irrigation of wheat is common practice. There is therefore a need for good management of irrigation supplies in order to improve irrigation scheduling and prevent water stress from adversely affecting yield. Remote sensing satellites can be used for monitoring land surface changes because of their extensive coverage capacity and frequent revisits (Fieuzal et al., 2011; Kalluri et al., 2003; Moran et al., 1997; Ozdogan et al., 2010).

Several studies have investigated the sensitivity of Synthetic Aperture Radar (SAR) imagery to surface parameters (soil cover, surface water content and roughness) (Baghdadi et al., 2009; Dabrowska-Zielinska et al., 2007; Feng et al., 2013; Moran et al., 1997; Ulaby et al., 1986; Zribi et al., 2005). SAR sensitivity is linked to the sensor characteristics (frequency, incidence and polarization). Many authors (Beriaux, 2012; Hadria et al., 2009; Mattia et al., 2003; McNairn et al., 2012) have demonstrated the potential of SAR for monitoring agricultural factors that have a significant influence on backscatter coefficients.

The recent launch of Sentinel-1, which offers both good spatial resolution and high revisit time, could be interesting (Aulard-Macler, 2011; Snoeij et al., 2008). It is still difficult, however, to acquire synchronous multi-sensor time series in order to analyze satellite data sensitivity over comparable surface conditions. C-band data are available from the ERS-1/2, EnviSat, Radarsat-1/2 and Sentinel-1 systems.

For wheat canopies and topsoil moisture, the sensitivity of radar backscattering coefficients was demonstrated by Mattia et al. (2003) and Picard et al. (2003). Some attempts have been made to use simplified relationships between SAR backscattering coefficients and wheat canopy characteristics (Dente et al., 2008; Mattia et al., 2003). Few authors, however, have tried to apply the radar on a large scale and in a representative context (Fieuzal et al., 2013).

At C-band frequency, the temporal behavior of wheat in different studies (Mattia et al., 2003; Saich and Borgeaud, 2000) shows similar global trends for the same study site. Recent studies have proposed multi-sensor approaches for irrigation management purposes by combining optical and radar images (Fieuzal et al., 2011; Hadria et al., 2009; Hadria et al., 2010).

In irrigation monitoring, it is Clearly expected that the backscattering signal generated from SAR images and interferometric coherence reacts to changes in surface moisture (Hadria et al., 2009), which could be important indicator to detect irrigation inputs and monitoring surface moisture on a large scale and in a realistic context during the anthesis and grain-filling phenological stages of wheat. In this case study, the change in backscattering values and coherence is expected to be related primarily to changes in water content of the cover and the ground since the roughness parameter is assumed to be constant, since it is wheat at the same development stage for all parcels. This information could be very useful in improving national grain yield forecast models that currently do not take into account production from irrigated areas, despite the fact that they occupy over 1million ha. Irrigation water supply data (time, duration and irrigated area) could be integrated into yield forecast models in order to improve their accuracy.

In this context, we conducted an analysis of a large number of agricultural plots using time series of SAR images in order to assess their sensitivity to surface moisture. This was done by evaluating the values of the backscatter signal compared with the variability of the surface moisture that is closely related to the irrigation supply program at wheat plot level (databases of irrigation dates). With respect to the use of temporal coherence as an indicator, no conclusive results were derived due to the lack of adequate SAR data.

2. Methodology

Previous studies using SAR images have shown the potential of using backscattering signals to monitor vegetation water content and surface soil moisture via a simple linear relationship and one incidence-angle data (De Zan et

al., 2014; Fieuzal et al., 2011; Le Hegarat-Mascle et al., 2002; Mattia et al., 2003; Ulaby et al., 1986; Zribi et al., 2005; Zwieback et al., 2015). Drawing on these studies, the methodology adopted in our study sought to detect irrigation water supplies to the wheat crop using SAR data.

2.1 Study Site

The irrigated Tadla perimeter (Figure 12) is in central Morocco, between the Atlantic coast in the north-west and the Atlas Mountains in the south-east (32°23′N latitude; 6°31′W longitude; 445 m above sea level). The studied area is characterized by a semi-arid climate; the annual average temperature is about 19°C, with a large inter-seasonal variation (max = 38°C in August and min = 3.5°C in January). The average annual precipitation is about 300 mm (average over the 1970-2010 period), with significant inter-annual variation (from 130 mm to 600 mm).

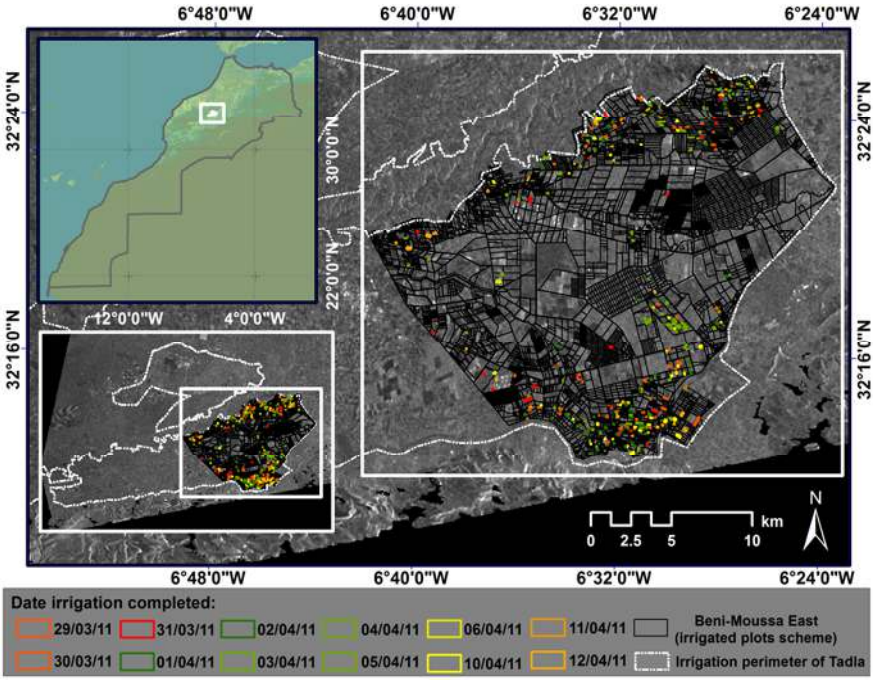

Figure 12: *Location of the irrigated area (upper left inset shows a map of Morocco; the plot plan is indicated by black lines and the studied irrigated plots are multicolored according to the date the irrigation was completed)*

The irrigated Tadla perimeter is managed by the Regional Office for the Agricultural Development of Tadla (ORMVAT). The studied area is in Beni-Moussa East, covers 40,000 ha and is characterized by flat topography.

Cereal crops are one of the main crops in the study area. In the 2010-2011 cropping season, wheat occupied about 17% (6,730 ha) of the total cultivated area of Beni-Moussa East. It is usually sown between mid-November and December, depending on when the first significant precipitation occurs, and is harvested between May and June.

We studied those wheat plots that were irrigated between 29/03/2011 and 12/04/2011. The studied plots represented 3.5% (235.5 ha) of the total area under wheat in Beni-Moussa East. Irrigation is applied here using the traditional surface

flood method. During the growing season, wheat is irrigated between two and five times, depending on rainfall conditions.

2.2 Ground and Satellite Data

2.2.1 Ground Data

We used the available invoices of irrigation water database intended for farmers for the period between 28/03/2011 and 15/04/2011 corresponding to the period when images were acquired in the 2010/2011 cropping season. This database is organized and managed by ORMVAT, which is in charge of irrigation water management in the area. The database holds data on periods of irrigation (start and end), plots and the amount of water used by farmers across the studied area. During the crop development stages of anthesis and grain filling, plot conditions (phenological stages, irrigation techniques) were fairly homogeneous.

2.2.2 Climate Data

Daily meteorological data was obtained from the Affourer station, which is part of the Moroccan National Weather network and is located in the study area (Figure 13). Rainfall was measured with tipping bucket rain gauges. The collected data showed that there was no precipitation between 16/03/2011 and 21/04/2011. The change in backscattering values of SAR images was therefore due only to irrigation water supplies to the wheat crop in the study area.

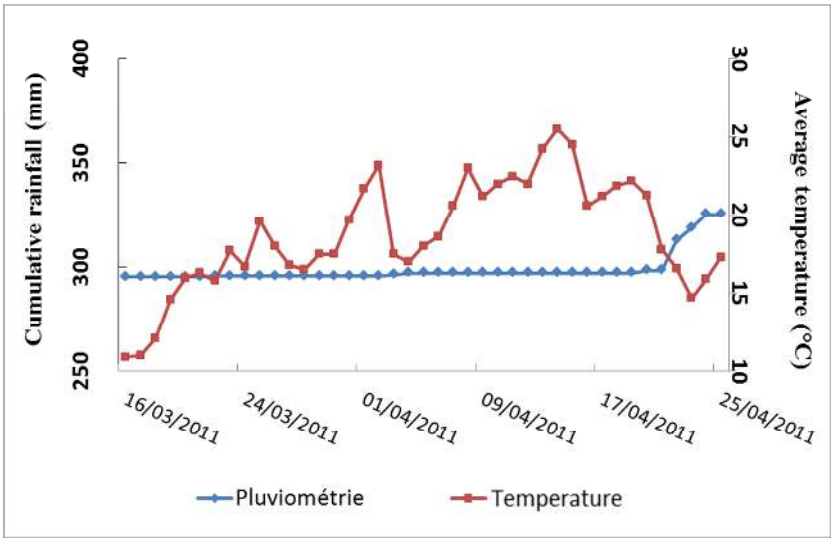

Figure 13: *Daily meteorological data for the study area*

2.2.3 Radar Data: Time Series of SAR Images

We selected all ERS images available in the archives. The ERS-1 ERS-2 satellite are SAR instruments operating at C-band (f = 5.3 GHz, $\lambda \approx 5.6$ cm). SAR images were acquired, all in the descending pass. The images were acquired in VV polarizations at medium incidence angles (23.3°) (Table 9). Figure 12 gives an example of a SAR image of the study area.

Between 1995 and 1996, ERS-1 and ERS-2 were flying in Tandem, i.e. ERS-2 was following ERS-1 with a one day delay. The Tandem ERS images were used to evaluate the Tandem coherence on the area. But, no ground data were available for this period. Four ERS2 acquired in 2008 were also made available. They were acquired with a 35-day repeated cycle.

In 2011, at end of its life, ERS2 orbit was adapted to offer a 3-day repeat interval. Four images of our zone were acquired during this period allowing us to have a short but good time series of SAR data for which ground data were available.

Table 9*: *SAR images selected covering the study area

Sensor	Date d'acquisition d'image	Polarisation
ERS	11/08/2008	VV
ERS	15/09/2008	VV
ERS	24/11/2008	VV
ERS	29/12/2008	VV
ERS	31/03/2011	VV
ERS	03/04/2011	VV
ERS	06/04/2011	VV
ERS	12/04/2011	VV
ERS1	01/01/1996	VV
ERS2	02/01/1996	VV
ERS1	03/09/1995	VV
ERS2	04/09/1995	VV
ERS1	17/12/1995	VV
ERS2	18/12/1995	VV

2.2.4 Amplitude Images

Time series of backscattering amplitude images were generated over the study area based on Single-Look Complex images from the ERS-1/2 archives. Using the CSL InSAR Suite (CIS) developed by the Centre Spatial de Liège (Derauw, 1999), an amplitude image and coherence image were computed and geoprojected with a final ground sampling of 30*30 m (Grandchamp and Cavassilas, 1997). The step-by-step process was as follows:

- Amplitude image reduction: Amplitude was computed before geoprojection using box averaging to reduce the speckle noise by the incoherent summation of backscattering values.

- Coregistration: In order to generate usable time series, we performed coarse and then fine coregistration in relation to a global master acquisition. The chosen global master acquisition was the one from 31 March 2011. Coarse coregistration

(about 2.5 pixels) is performed by correlating the amplitude windows centered on target anchor points regularly distributed on the master image. Fine coregistration (about 0.5 pixel), when applicable, is performed through local coherence maximization.

- **Interpolation:** Slave images were interpolated with regard to the computed transform in order to superimpose them on the master one and allow the SAR products to be computed. After these steps, the CIS tool computed the amplitude images, the interferogram and the coherence image, in addition to the geoprojection of these products.

Once amplitude images and tandem coherence time series were generated, temporal evolution of coherence and amplitude were analyzed to detect irrigation water supplies to the wheat crop. Then indicators of irrigation evidences were sought crossing with available archives data provided from irrigation water management services.

2.2.5 Backscatter Coefficient Calculation and Georeferencing

Amplitude images are not calibrated and do not provide information on the backscattering coefficient. Image calibration was performed using equations 1 and 2, below (Laur et al., 2002). This step allows the amplitude digital number (DN) to be converted into the backscattering coefficient in decibels (dB) for each pixel.

Following radiometric calibration, all images are then georeferenced using ENVI 5 software.

$$\sigma^0_{i,j} = \frac{DN^2_{i,j}}{K} \frac{1}{G(\theta_{i,j})^2} \left(\frac{R_{i,j}}{R_{ref}}\right)^3 sin(\alpha_{i,j}) \quad (1)$$

$$\sigma^0(\text{dB}) = 10 \log \sigma^0_{i,j} \quad (2)$$

In equation 1, backscattering coefficients (σ^0) are derived from the digital number (DN) of the pixels (i, j) and from the parameters of the images, such as the local incidence angle ($\alpha_{i,j}$), the slant range position ($R_{i,j}$) and the look angle corresponding to pixel 'i,j' ($\theta_{i,j}$), and the constant parameters come from the ERS SAR calibration document (the calibration factor) [K], the gain [$G(\theta_{i,j})^2$)] (Laur et al., 2002).

2.3 Delimitation of the Cereal Area

2.3.1. Satellite Images and Their Processing

One SPOT-5 HRV satellite image was acquired on 15 April 2011 (Table 10), when the soil was completely covered by vegetation. It spanned the period between anthesis (March) and grain filling (April) in the 2010-2011 cropping season.

Table 10: *List of acquired SPOT-5 HRV images and their characteristics*

Acquisition date	Cropping season	Sensor	Wavelength (nm)	Resolution (meters)
15/04/2011	2010/2011	SPOT-5 HRV	Green: 500-590 Red: 610-680 NIR: 780-890	Red: 5 Green: 5 NIR: 5

The processing level of the acquired images was (1B), which included radiometric and geometric corrections.

2.3.2 Supervised Classification

In order to define the cereal area, we used a maximum likelihood classification method that is a widely used supervised pixel-based method (Ouyang et al., 2011).

Training areas representative of the land cover classes were selected in order to develop class signature files. For each image, training areas were defined based on a field survey, expert field knowledge and ancillary data (tree crops mask and irrigation canals). Two thirds of the training areas were used in the classification process, the remaining one third in the accuracy assessment. The main classes were: cereals; bare soil; industrial crops; perennial crops; and arboriculture.

For the wheat class, we selected a sufficient number of pixels representing 1.08% of the total pixels (500,123 pixels) (Yang et al., 2011). We performed the separability analysis, using the Jeffries-Matusita distance, for training samples in the final classification scheme with values of separability between 1.99 and 2, indicating good class separation.

The contingency matrix was used to evaluate the percentage of sampled pixels classified as expected. User accuracy and producer accuracy regarding the wheat class were 97.8% and 96.73%, respectively. The overall accuracy assessment and Kappa values were 95.7% and 0.94, respectively, indicating good classification.

2.4 Integration and Intersection of Ground and Satellite Data

From the SAR data we obtained an amplitude time series. We also analyzed archival data of the irrigation supply schedule used by farmers in the irrigated Tadla perimeter at the plot level. The archival data was provided by ORMVAT.

The backscatter parameter from the ERS-2 images was averaged for each of the 341 training plots. This was followed by crossing all the information layers to monitor and analyze the spatiotemporal evolution of backscattering intensity, depending on irrigation water supplies used by farmers for their wheat plots. Figure 14 summarizes these steps.

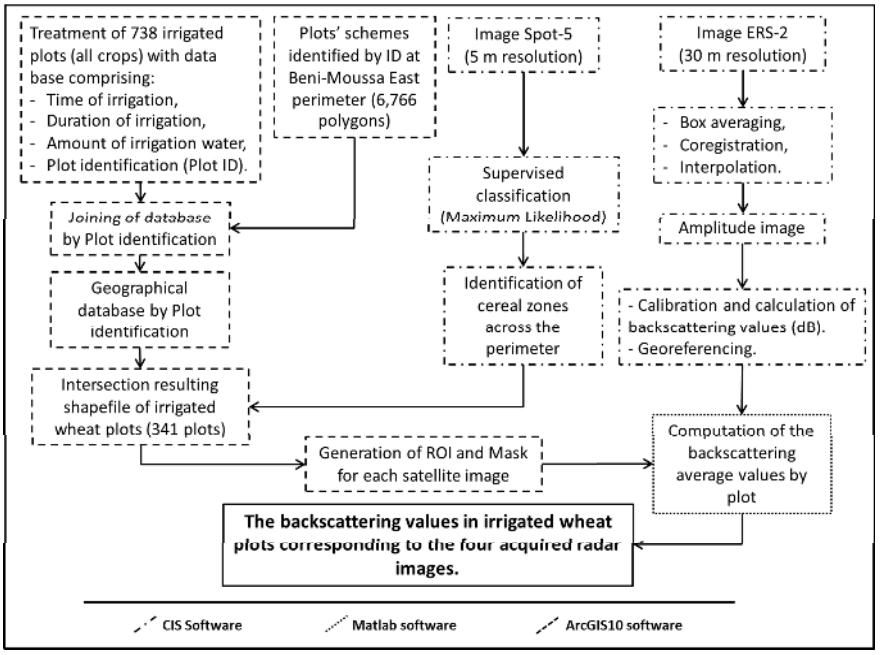

Figure 14: *Schematic diagram illustrating field data and SAR data processing*

3. Results and Discussion

Amplitude and coherence images were derived from the ERS-2 acquired images. However, for images acquired on 2008 and 2011 a loss of coherence was observed. This general de-correlation is due to the prolonged lag time (about 1 month) separating the acquired images on 2008, and to the attitude of ERS-2 that was badly controlled at the end of satellite life leading to the angular yaw instability for the images acquired on 2011 (Figure 15). Inversely a good coherence was found for ERS tandem images acquired in 1995 and 1996 (Figure 16).

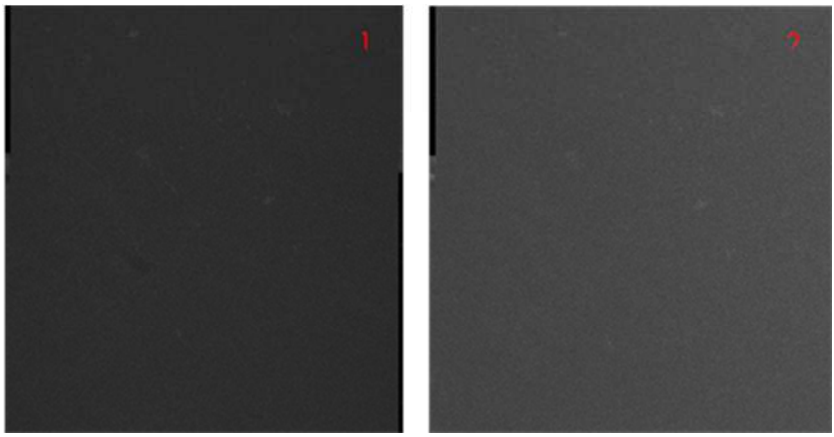

Figure 15: *Coherence image (1) between acquired images on 31/03/11 and 03/04/11 and (2) between acquired images on 31/03/11 and 12/04/11*

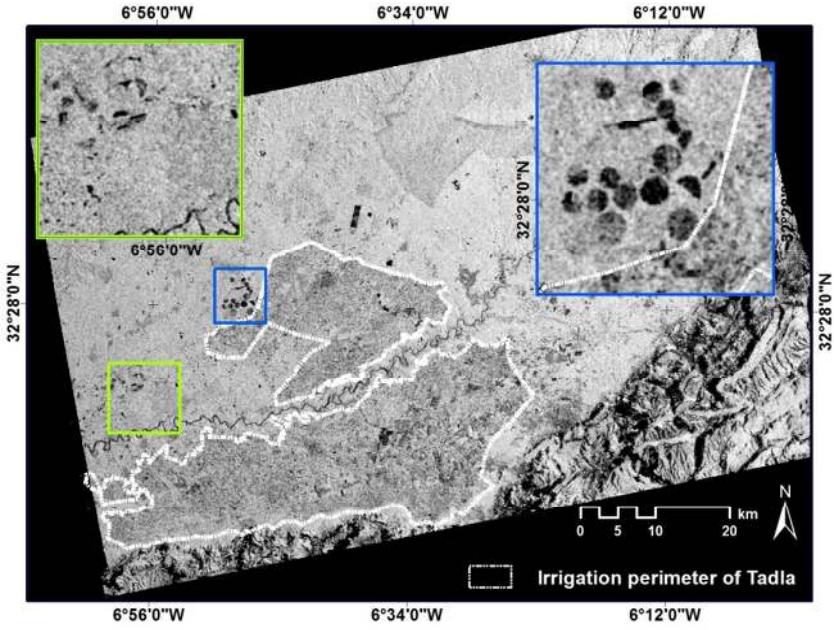

Figure 16: Coherence image between ERS 1 and ERS 2 acquired respectively on 01/01/1996 and 02/01/1996

The available invoices of irrigation water database only covered the period between 28/03/2011 and 15/04/2011 corresponding to ERS-2 images acquired in the 2010/2011 cropping season. Amplitude images were derived from the ERS-2 images acquired on 31/03/11, 03/04/11, 06/04/11 and 12/04/11.

These data were used to assess the potential of SAR data for detecting irrigation and to analyze the radar backscattering as a function of changes in wheat water content and soil moisture.

The lack of ground data during the Tandem acquisition period on one side and the lack of coherence due to the ERS2 aging in 2011 on the other side prevent us to perform the expected study using interferometric coherence as an indicator.

Table 11 shows the measured backscattering values for all plots for which irrigation dates were made available. For each SAR acquisition date, backscattering values are ordered and classified according to the known date of irrigation completion. Clear changes and trends in backscattering values can be seen. These changes are subsequent to irrigation water applied to the plots and to the heterogeneity of their moisture condition. As shown in Table 11, the backscattering values for all plots varied between 0.11 to 3.11 dB. In this case, roughness is considered as constant, since all parcels were homogeneous in term of the cultivated crop and the development stage.

As shown in Figure 17, the highest backscatter values occurred when the SAR acquisition date corresponded with the irrigation completion date. In this case, the average backscattering values of plots smaller than 1 ha (Figure 17-B) and plots larger than 1 ha (Figure 17-C) varied between 2.99 and 3.18 dB and between 1.97 and 3.14, respectively. The average backscattering values for all plots, whatever their size, varied between 2.79 and 3.11 dB (Figure 17-A). It is important to note that the total number of plots was 341, of which 282 were smaller than 1 ha and 59 were larger than 1 ha.

The variation was more important for plots with an area between 1.01 and 4.42 ha, exhibiting a standard deviation of 1.11 dB, unlike plots smaller than 1 ha

which had a small deviation of 0.19 dB. This large variation was due to the duration of irrigation and the timing of the start of irrigation, which affected the response of backscatter plots and the fall in backscattering values in already irrigated plots, given that the flood irrigation takes 1-2 days ha^{-1}.

Table 11: *The average backscattering values for irrigated wheat plots as a function of date of completion of irrigation and date of acquired images (no gap means that irrigation time is the date of satellite pass and a gap indicates the difference in days between irrigation and satellite pass (negative gap: irrigated plots; positive gap: non-irrigated plots)*

			SAR Acquisition data											
			All plots				Plots ≤ 1 ha				Plots > 1 ha			
			31/3/11	3/4/11	6/4/11	12/4/11	31/3/11	3/4/11	6/4/11	12/4/11	31/3/11	3/4/11	6/4/11	12/4/11
Completion of irrigation	29/3/11	σ° average (dB)	1.34	0.22	0.48	0.47	1.36	0.16	0.45	0.46	1.16	0.88	0.79	0.55
		Std σ° (dB)	0.32	0.69	0.60	0.59	0.32	0.68	0.62	0.61	0.25	0.45	0.13	0.08
		Gap (Days)	-2	-5	-8	-11	-2	-5	-8	-11	-2	-5	-8	-11
		Number of plots	24	24	24	24	22	22	22	22	2	2	2	2
	30/3/11	σ° average (dB)	1.79	0.37	0.70	0.75	1.79	0.37	0.70	0.75	1.88	-0.12	0.50	0.97
		Std σ° (dB)	0.56	0.59	0.57	0.55	0.56	0.59	0.57	0.55	0.86	1.29	0.39	0.47
		Gap (Days)	-1	-4	-7	-10	-1	-4	-7	-10	-1	-4	-7	-10
		Number of plots	26	26	26	26	23	23	23	23	3	3	3	3
	31/3/11	σ° average (dB)	2.86	0.68	0.59	0.91	3.12	0.84	0.65	0.98	2.46	0.45	0.48	0.78
		Std σ° (dB)	0.75	0.64	0.50	0.71	0.73	0.39	0.33	0.80	0.62	0.88	0.67	0.59
		Gap (Days)	0	-3	-6	-9	0	-3	-6	-9	0	-3	-6	-9
		Number of plots	28	28	28	28	17	17	17	17	11	11	11	11
	1/4/11	σ° average (dB)	0.23	1.68	0.78	0.62	0.29	1.72	0.82	0.71	-0.34	1.32	0.43	-0.15
		Std σ° (dB)	0.70	0.28	0.55	0.63	0.71	0.23	0.56	0.60	0.15	0.55	0.34	0.28
		Gap (Days)	1	-2	-5	-8	1	-2	-5	-8	1	-2	-5	-8
		Number of plots	31	31	31	31	28	28	28	28	3	3	3	3
	2/4/11	σ° average (dB)	0.51	2.14	0.94	0.88	0.52	2.15	0.98	0.93	0.35	1.89	0.35	0.13
		Std σ° (dB)	0.65	0.49	0.63	0.50	0.65	0.50	0.61	0.42	0.75	0.12	0.80	1.20
		Gap (Days)	2	-1	-4	-7	2	-1	-4	-7	2	-1	-4	-7
		Number of plots	32	32	32	32	30	30	30	30	2	2	2	2
	3/4/11	σ° average (dB)	0.44	3.11	1.10	0.95	0.48	3.11	1.14	0.95	0.16	3.14	0.77	0.90
		Std σ° (dB)	0.72	0.73	0.48	0.52	0.69	0.72	0.43	0.53	1.08	0.98	0.83	0.47
		Gap (Days)	3	0	-3	-6	3	0	-3	-6	3	0	-3	-6
		Number of plots	27	27	27	27	24	24	24	24	3	3	3	3
	4/4/11	σ° average (dB)	-0.07	0.14	1.59	0.39	0.08	0.20	1.65	0.51	-0.70	-0.12	1.35	-0.16
		Std σ° (dB)	0.87	0.71	0.53	0.72	0.85	0.74	0.57	0.71	0.66	0.57	0.27	0.48
		Gap (Days)	4	1	-2	-5	4	1	-2	-5	4	1	-2	-5
		Number of plots	59	59	59	59	48	48	48	48	11	11	11	11
	5/4/11	σ° average (dB)	0.35	0.14	2.22	0.77	0.42	0.07	2.24	0.77	0.03	0.46	2.13	0.79
		Std σ° (dB)	0.84	0.97	0.66	0.79	0.85	0.97	0.73	0.83	0.84	1.07	0.34	0.78
		Gap (Days)	5	2	-1	-4	5	2	-1	-4	5	2	-1	-4
		Number of plots	16	16	16	16	13	13	13	13	3	3	3	3
	6/4/11	σ° average (dB)	0.22	0.22	2.93	0.63	0.52	0.42	3.18	1.00	0.46	-0.18	2.44	0.31
		Std σ° (dB)	0.88	0.88	0.90	0.58	0.35	0.70	0.92	0.46	0.52	1.17	0.69	0.66
		Gap (Days)	6	3	0	-3	6	3	0	-3	6	3	0	-3
		Number of plots	12	12	12	12	7	7	7	7	4	4	4	4
	10/4/11	σ° average (dB)	0.35	0.32	0.73	1.74	0.42	0.46	0.84	1.76	-0.05	-0.55	0.04	1.56
		Std σ° (dB)	0.82	0.76	0.81	0.52	0.83	0.69	0.78	0.49	0.63	0.53	0.64	0.74
		Gap (Days)	7	4	1	-2	7	4	1	-2	7	4	1	-2
		Number of plots	36	36	36	36	31	31	31	31	5	5	5	5
	11/4/11	σ° average (dB)	0.22	0.09	0.64	2.14	0.25	0.30	0.66	2.29	0.12	-0.53	0.39	1.66
		Std σ° (dB)	0.66	0.67	0.94	0.67	0.69	0.60	0.59	0.68	0.62	0.46	1.32	0.37
		Gap (Days)	8	5	2	-1	8	5	2	-1	8	5	2	-1
		Number of plots	24	24	24	24	18	18	18	18	6	6	6	6
	12/4/11	σ° average (dB)	0.28	0.44	0.56	2.79	0.41	0.58	0.59	2.99	-0.25	-0.17	0.41	1.97
		Std σ° (dB)	0.84	0.89	0.80	1.21	0.77	0.85	0.62	1.19	1.01	0.88	1.21	1.03
		Gap (Days)	9	6	3	0	9	6	3	0	9	6	3	0
		Number of plots	26	26	26	26	21	21	21	21	5	5	5	5

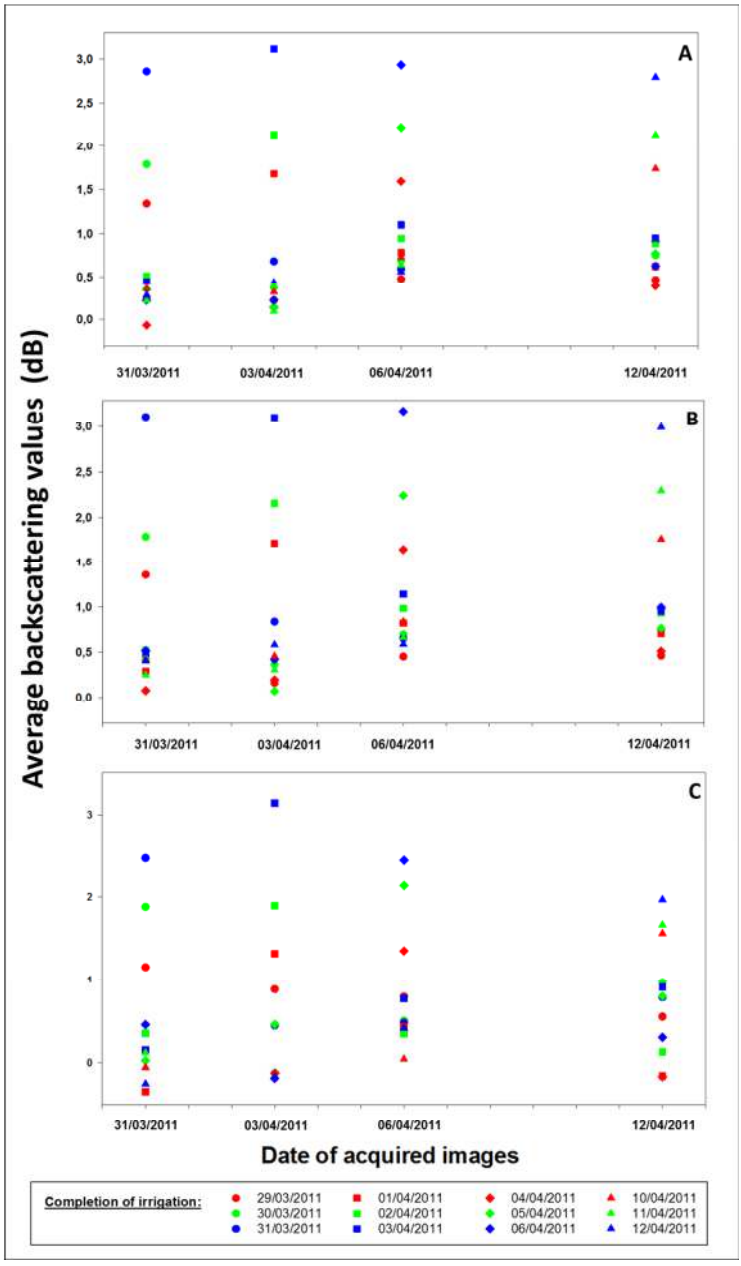

Figure 17: *Potential of SAR data to detect irrigated plots (A: All plots; B: Plots ≤ 1 ha and C: Plot > 1 ha)*

For plots with a gap of 1-2 days between the date of the end of irrigation and the date of image acquisition, the backscattering levels ranged from 1.79 and 2.22 dB and from 1.34 to 1.74 dB for gaps of 1 and 2 days, respectively. Non-irrigated plots or plots irrigated more than 2 days before SAR acquisition showed backscattering values that were generally lower than 1 dB.

This analysis confirms the clear relationship between σ^0 VV and irrigation water supplies. The variation in radar backscattering coefficients can therefore be related mainly to changes in wheat water content and soil moisture induced, in our case, by irrigation. These results were confirmed by Mattia et al. (2003), who found a linear correlation between backscattering coefficients and fresh biomass not exceeding 2,500 g/m^2. A study conducted by Baghdadi et al. (2012) showed that the error (RMSE) in retrieved soil moisture observed at C-band was about 6% for a single incidence angle of 20°.

As shown in Figure 18, backscattering values can also be ordered with regard to the time gap between the SAR acquisition date and the irrigation completion date. This figure shows the responses of backscatter wheat plots to moisture changes in the vegetation cover and soil after an irrigation event. If the gap is zero (i.e., when irrigation ends on the SAR acquisition date), the backscattering values are high. This is true whatever the plot size. Plots smaller or equal than 1 ha or larger than 1 ha had average backscattering values of 3.08 and 2.44, respectively. The average backscattering value for all plots, whatever their size, was 2.92 dB.

There was a discrepancy in average backscattering values between irrigated plots smaller than 1 ha and those larger than 1 ha of 0.6 dB. The difference between the average backscattering value when there was no gap time and when there was a lag of 1 day was 0.6 dB for plots larger than 1 ha and about 1dB for plots smaller than 1 ha. This result tends to confirm the effect of plot non-uniformity on backscatter values.

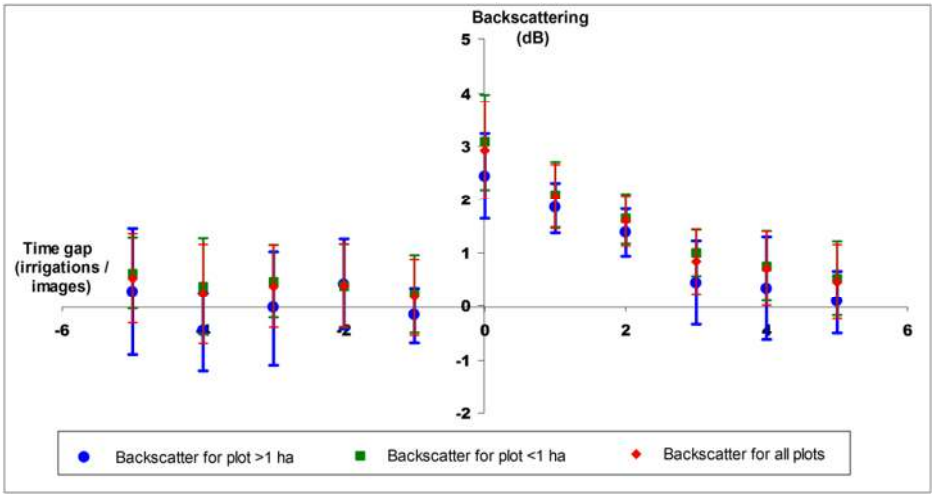

***Figure 18**: Evolution of backscattering values with regard to the time gap between irrigation time and satellite image acquisition. No gap means that irrigation time is the date of the satellite pass and a gap indicates the difference in days between irrigation and satellite pass (negative gap: irrigated plots; positive gap: non-irrigated plots)*

Where the time gap was 1 day or more, there was a decrease in average backscatter values from irrigated wheat plots, varying between 1.34 and 2.22 dB for all plots.

From the third day of the irrigation, backscatter values fell below 1 dB, which was close or equivalent to non-irrigated plots. The value of 1 dB can therefore be considered as a reference threshold that distinguishes between, on the one hand, irrigated plots and, on the other, non-irrigated plots and plots irrigated for more than 2 days. These results can be generalized at the regional level for the studied period, especially where wheat plot conditions are fairly homogeneous.

The time resolution proved to be a limiting factor for the continuous monitoring of the irrigated wheat plots, in that it was no longer possible to detect irrigation from the fourth day onwards (gap = 3), as shown in Figure 18. SAR images therefore need to be acquired at a maximum interval of 3 days (time resolution = 3).

The results showed that SAR technology has great potential for irrigation management and could have an important agricultural-economic impact, if acquisition frequency can be increased and the prices of SAR images can be reduced. In the future, with the possibilities offered by the Sentinel 1A/B missions the use of SAR satellites looks promising. Since the launch of other satellites is expected in the coming years in band C and L on all polarization. The band C and L in all polarization (HH, HV and VV) provide several options to ensure crop monitoring (Dabrowska-Zielinska et al., 2007; Fieuzal et al., 2013). These bands should be deeply studied and tested in order to develop robust and simple approaches for monitoring irrigation.

In general, remote sensing tools are one of the best ways to monitor large agricultural areas, and research should be done on improving the mastery and application of SAR remote sensing in agriculture. In the case of irrigated areas, SAR images offer great potential for detecting changes and monitoring the water content of the surface and biomass in irrigated areas, whatever the plot size.

4. Conclusion

This study sought to assess the potential of SAR data for detecting irrigation supplies and to analyze the radar backscattering coefficients as a function of changes in wheat water content and soil moisture throughout the cropping season in irrigated semi-arid areas. The measured backscattering values showed a clear decreasing trend with regard to the time gap between irrigation completion date and image acquisition date. After 3 or more days between irrigation completion and SAR acquisition, a backscattering value of 1 dB or lower was observed, the same as the value observed for non-irrigated plots. A reference level of 1 dB could therefore be set for differentiating between irrigated and non-irrigated plots.

The study showed that in order to ensure continuous monitoring over time of irrigated wheat plots, an interval 3 days between the acquisitions of SAR images is required. This parameter could be used to compare and map vegetation water content and surface moisture at local and regional level in the irrigated Tadla

perimeter. These results show that radar signal behavior can be generalized, especially where wheat plot conditions are fairly homogeneous.

SAR backscattering signal analysis shows potential for improving irrigation monitoring, detecting irrigation supplies and understanding surface water content changes at the field and regional levels in the study area.

Our findings need to be applied to other crops and other areas in order to test the validity of the proposed methodology.

Chapter 4

Testing AquaCrop to simulate Durum wheat yield and schedule irrigation in semi-arid irrigated perimeter in Morocco [3]

[3] Adapted from: Benabdelouahab, T., Balaghi, R., Hadria, R., Lionboui, H., Djaby, B., Tychon, B., 2015. Testing AquaCrop to simulate Durum wheat yield and schedule irrigation in semi-arid irrigated perimeter in Morocco. Irrigation and Drainage (Accepted for publication / in production).

The aim of this study was twofold: in the first part, we adjusted and tested AquaCrop (4.0 version) parameters for durum wheat under semi-arid conditions. Grain yield, biomass and the evolution of soil water content (0-90 cm layer) in an irrigated perimeter were simulated. The experiment was conducted in the Tadla region, between 2009 and 2012, using 15 fields. The comparison between observed and simulated grain yield and aboveground biomass using a leave-one-out cross-validation (LOOCV) approach gave a normalized root mean square error of 4.1% (0.2 $t.ha^{-1}$) and 5.7% (0.8 t.ha-1), respectively. Similarly, the difference between observed and modeled soil water content has, on average, a nRMSE of 8.2%. In the second part, the analysis of irrigation scenarios showed the potential of crop modeling to schedule irrigation water according to a threshold for water deficit. It also displayed logical trends in the relationship between grain yield and the amount, frequency and timing of irrigation water. Scheduling irrigations during the cropping season improved significantly the grain yield and increased water-use efficiency. We concluded that AquaCrop could be a suitable tool for forecasting yield under semi-arid conditions and to improve crop and irrigation management.

1. Introduction

Currently, durum wheat is among the crops which occupies the largest area of land and continues to be one of the main sources of food grains to humans. World wheat production reached 656 million tons in 2011/2012, with durum wheat accounting for 6% of this amount according to the Food and Agriculture Organization (FAO) (FAO, 2013). Half of the world's food comes from irrigated and drained lands (Bastiaanssen et al., 2000; Lobell et al., 2003). In Morocco, water availability is considered as the main limiting factor for crop growth. Cereal (mainly wheat and barley) production is strongly related to the amount and distribution of annual rainfall in rainfed areas (Balaghi et al., 2010) and to the amount of groundwater and water stored in dams in irrigated areas. Irrigated agriculture in arid and semi-arid regions now plays an important role in food

security, with the availability of large amounts of irrigation water having led to an increase in production.

In Morocco, cereals occupy 75% of the cultivated area and account for 10-20% of the agricultural Gross Domestic Product (GDP). Durum wheat (*Triticum turgidum*) is one of the major grain crops grown in the country and holds an important place in the agricultural production systems. It is cultivated mainly in the south-western plains of Morocco, in semi-arid areas (Balaghi et al., 2010).

In the irrigated perimeter of Tadla, cereal production has exceeded 2 million quintals. The area under wheat exceeds 40,000 hectares (ha) and represents more than 36% of the total irrigated area (ORMVAT). Durum wheat represents around 13,000 ha of the total cultivated cereals in the irrigated plain of Tadla. Flooding irrigation is used for more than 96% of the total area of the perimeter and mobilizes large volumes of water. Despite these large amounts of used water, crop yields remain low and fluctuate from one area to another and one season to another because of varying water management, field management and weather conditions (Balaghi et al., 2010).

Given the importance of wheat production in semi-arid irrigated areas where water is the main limiting production factor, large-scale good management of irrigation water is required (Lionboui et al., 2014). Crops in arid and semi-arid regions, such as those in Morocco, regularly face water stress, considered as the main limiting factor for crop growth. There is therefore a need for assessing soil water availability in order to improve irrigation scheduling and prevent water stress adversely affecting yield.

Simulation models, based on crop physiological processes and crop response to water stress, can contribute to better irrigation management, especially during the critical wheat growth period. The accurate information they provide in terms of crop forecasting and total soil water content can help to improve productivity and

water management through establishing irrigation schemes and planning inputs of irrigation water (quantity and timing).

In this regard, the scientific community is paying increasing attention to approaches based on agro-ecological process models. Many process-based crop models have been developed in the recent years (Eitzinger et al., 2004; Jamieson et al., 1998) and many studies of these models have been conducted to evaluate their performance under arid and semi-arid conditions (Ben Nouna et al., 2000; Duchemin et al., 2008; Hadria et al., 2007). The level of complexity of these models can be high, but when working on a large scale and in operational conditions, robust models with few parameters are usually preferred (Mkhabela and Bullock, 2012; Steduto et al., 2009; Wellens et al., 2013).

AquaCrop is a crop water productivity simulation model developed by the Food and Agriculture Organization (FAO) of the United Nations (Hsiao et al., 2009; Raes et al., 2009a; Raes et al., 2009b; Steduto et al., 2009). The model simulates crop yield response to irrigation, soil and climate conditions. It is based on the concepts of crop yield response to water (Doorenbos and Kassam, 1979; Doorenbos and Pruitt, 1977) and is suitable for areas where the water is a limiting factor for agricultural production. Aimed at balancing precision and simplicity, it uses a small number of explicit and mostly intuitive parameters and input variables that require simple methods for their estimation (Hsiao et al., 2009; Steduto et al., 2009). Simulations of crop growth and development are performed on the basis of daily time steps. The model simulates crop growth using growing degree days (GDDs) or calendar days. Several researchers have tested AquaCrop, under water-limiting conditions, for predicting crop biomass and yield, water requirement, water-use efficiency and soil water dynamics in various weather conditions and environments and have reported satisfactory results. The model has been tested for barley (Araya et al., 2010), cotton (Farahani et al., 2009), maize (Abedinpour et al., 2012; Hsiao et al., 2009; Steduto et al., 2009; Stricevic et al., 2011), durum wheat (Soddu et al., 2013), soft wheat (Andarzian et al.,

2011; Iqbal et al., 2014; Jin et al., 2014; Mkhabela and Bullock, 2012) and cabbage (Wellens et al., 2013).

The research of (Soddu et al., 2013) is quite different from what we done, where they focused on the simulations of future durum wheat yields under climate change scenarios in a rainfed area at regional scale. In addition to crop yield simulation, the model also predicts soil water dynamics and water supply using soil physics parameters and weather data (Geerts et al., 2010; Iqbal et al., 2014; Mkhabela and Bullock, 2012; Xiangxiang et al., 2013).

Designing and implementing operational tools that can provide accurate estimates of crop water needs and the impact on production, and can quantify crop water consumption and production, would facilitate the monitoring of irrigation efficiency and crop water use. The main objective of this study was to test the ability of AquaCrop to simulate durum wheat (*Triticum turgidum*) biomass production, grain yield and the soil water content profile (0-90 cm layer) in an irrigated area, on the one hand, and on the other hand to study the capacity of the model to manage the irrigation water and optimize a timely application of irrigation supply to increase water use efficiency.

2. Materials and methods

2.1 Study area

The study area (Figure 19) is situated in the center of Morocco, between the Atlantic coast in the north-west and the Atlas Mountains in the south-east (32°23´ north latitude; 6°31´west longitude; 445 m above sea level).

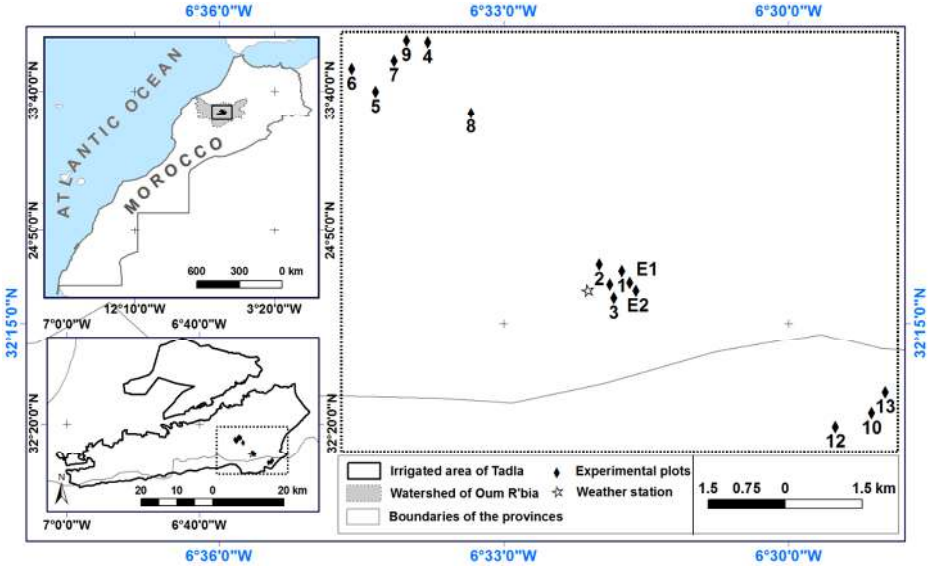

Figure 19: *Location of the Tadla irrigated perimeter (upper left window represents Morocco map; in the upper right window, the experimental plots in black diamond)*

The area is characterized by a semi-arid climate; the annual average temperature is about 19°C, with large inter-seasonal variation (maximum = 38°C in August and minimum = 3.5°C in January). The average annual precipitation is about 300 mm (average over the 1970-2010 period), with significant inter-annual variation (from 130 mm to 600 mm).

Created in the 1940s, the Tadla perimeter was among the first large irrigation schemes in the country and was aimed at benefiting small farmers and introducing modern farming techniques and industrial crops (Préfol, 1986). This irrigated perimeter is managed by the Regional Office for Agricultural Development of Tadla (ORMVAT). The irrigated area covers 100,000 hectares (ha) and is characterized by a flat topography. The groundwater depth in the area varies from 31 to 117 m (Bouchaou et al., 2009; Najine et al., 2006). Durum wheat is one of the main crops in this perimeter (12% of total cultivated area). It is usually sown between mid-November and mid-January, depending when the

first significant precipitation occurs, and is harvested between May and June, depending on temperature conditions. Irrigation is applied using the traditional surface flood method. During the growing season, wheat is irrigated between two and five times, depending on rainfall.

2.2 Field experiments

The experimental sites are located across the eastern Beni-Moussa municipality in the 2009-2010, 2010-2011 and 2011-2012 cropping seasons. Data were collected from 15 fields of durum wheat, located at Tadla's Regional Agricultural Research or belonging to farmers (Table 12), thus providing a valid representation of the soil-plant relationship in the study area. The field data related to Marzak and Karim cultivars, which are widely cultivated in the study region.

The average seeding rate was 350-400 seeds/m² throughout the study area. The nutrient requirements were adequately met by fertilizer applications applied before seeding and at the stem elongation stage. The nutrient doses applied were 0.18 t.ha-1 of triple superphosphate, 0.2 t.ha-1 of ammonitrate and 0.1 t.ha-1 of urea. Weeds and diseases were controlled by the use of herbicides and a preventive fungicide, and no disease infections or pests were detected.

For each studied field, dates of emergence, anthesis and maturity were recorded. Observations of phenological development stages and senescence of durum wheat were made every 7-10 days.

All the studied plots were harvested 10-15 days after physiological maturity, and the grain yield was measured. Aboveground biomass quadrats of 1 m² were cut at ground level with three replicates per plot. The collected samples were placed in the oven at a temperature of 65 °C for 48 hours to get the dry aboveground biomass (Iqbal et al., 2014).

We quantified the water provided at plot level for each irrigation supply. This quantification was done by multiplying the flow rate at the plot by the duration of irrigation. At the irrigated perimeter, the flow was fixed according to the size of

the irrigation canals of large-scale irrigation. By applying the technique of surface irrigation, the farmers consider that this operation is performed once the entire plot is completely submerged. Soil moisture and infiltration rate influence the amount of water supplied, which does not allow the farmers to control the irrigation depth unlike other irrigation methods (drip irrigation and sprinkler irrigation).

Soil moisture was measured using gravimetric methodology in two of the fifteen fields, E1 and E2. The measurements were dried in an oven at 105°C for 24 h and made every 10-15 days and at depths of 0-30, 30-60 and 60-90 cm, during the 2009-2010 growing season for E1 and during the 2010-2011 growing season for E2. The measurements were performed in three replications by sampling.

Table 12: *Main management characteristics of experimental fields of durum wheat*

No.	Year	Area (ha)	Cultivar	Sowing day	Harvesting date	Number of irrigations	Total irrigation (mm)
1	2009	2.3	Marzak	06/12/2009	14/06/2010	1	141
2	2010	1.5	Karim	07/11/2010	13/06/2011	3	421
3	2010	2	Karim	11/12/2010	28/06/2011	3	424
4	2010	0.6	Marzak	07/12/2010	24/06/2011	2	268
5	2010	1.6	Karim	09/12/2010	24/06/2011	2	273
6	2011	2	Karim	10/12/2011	28/06/2012	3	454
7	2011	0.8	Marzak	15/11/2011	16/06/2012	4	491
8	2011	1	Marzak	14/11/2011	17/06/2012	4	543
9	2011	2.6	Karim	18/12/2011	25/06/2012	3	415
10	2011	2.3	Marzak	11/12/2011	25/06/2012	3	410
11	2011	2.5	Marzak	08/12/2011	28/06/2012	3	411
12	2011	0.8	Karim	08/12/2011	28/06/2012	3	361
13	2011	0.8	Karim	06/12/2011	27/06/2012	3	413
E1	2009	0.5	Karim	05/12/2009	23/06/2010	2	329
E2	2010	1.1	Marzak	02/11/2010	07/06/2011	3	398

2.3 Soil data

At the study area, the soils are classified as isohumic mainly based on French soil classification (C.P.C.S) (Badraoui and Stitou, 2001; Massoni et al., 1967). From 30 soil samples collected from several sites providing coverage of the entire study area, soil physics properties were measured (Benabdelouahab, 2009). For three depths (0-30cm), (30-60cm) and (60-90cm), permanent wilting point (PWP) and field capacity (FC) were determined using a pressure plate extractor. The soil reached PWP and FC when the water potential was at -1.5 MPa and -0.033 MPa, respectively (Kirkham, 2005). Hydraulic conductivity was determined by using a Guelph kit at varying depths (Table 13).

Table 13: *Soil physics properties in Tadla, Morocco*

Soil properties	Depth 0-30		Depth 30-60		Depth 60-90	
	Value	STD DEV	Value	STD DEV	Value	STD DEV
Texture	Clay loam		Clay loam		Clay loam	
Sand (%)	25.4	2.7	24.5	1.9	24	0.3
Silt (%)	41	1.3	35.5	1.65	39.7	1.3
Clay (%)	33.6	3.4	40	1.3	36.3	1.5
Bulk density ($g.cm^{-3}$)	1.2	0.1	1.5	0.1	1.5	0.1
Field capacity (mm)	78.7	11.6	95.2	8.2	96	12.1
Saturation (mm)	106	4.2	118	4.8	125	5.5
Permanent wilting point (mm)	36.2	3.1	39.4	6.2	39.7	8.8
Hydraulic conductivity ($cm.h^{-1}$)	5.1	1.9	3.5	1.7	3.5	1.9

2.4 Meteorological data

Meteorological data were measured during wheat growing season by an automated weather station belonging to the Moroccan National Weather Service located near studied plots (32.347° north latitude; -6.382° west longitude;

493 meters (m) above mean sea level) (Table 14). Available data were daily maximum and minimum air temperatures, rainfall, wind speed, relative humidity, and solar radiation. Air temperature and relative humidity were measured at a height of 1.8 m using a radiation shielded probe. Wind speed was measured at a height of 10 m using a cup anemometer and converted to a 2 m elevation using a logarithmic wind speed profile as described by Allen et al. (1998).

Rainfall was measured with tipping bucket rain gauges. Incoming solar radiation (Rs) was measured at 2 m with a pyranometer (CES180). Reference evapotranspiration (ETo) was calculated using the Penman-Monteith equation (Allen, 2000; Allen et al., 1998). Data were measured by each sensor at 10 s intervals and recorded as daily averages, sums, maximum and minimum values.

Table 14: *Monthly average weather conditions over the experimental plots (3 cropping seasons, from 2009-2010 to 2011-2012)*

Month	Temperature min (°C)		Temperature max (°C)		Rainfall (mm)		ET0 (mm/month)	
	Average	STD	Average	STD	Average	STD	Average	STD
November	3.7	1.2	27.9	4.9	22.5	26.8	63.4	10.9
December	0.4	1.8	24.2	1.5	109.8	0.0	48.4	2.2
January	-1.0	1.9	24.0	3.3	76.0	45.0	51.9	6.9
February	-1.7	2.4	24.9	6.3	73.6	61.2	63.0	3.1
March	-0.5	2.6	28.3	5.6	43.6	36.2	96.0	4.2
April	6.0	2.8	31.2	5.1	1.5	2.2	132.8	23.9
May	6.3	1.3	37.0	5.7	5.9	5.2	165.7	10.8
June	12.7	0.3	40.3	3.0	10.8	17.0	200.5	13.1

2.5 AquaCrop: presentation and parameterization

AquaCrop is a FAO crop model (Steduto et al., 2009) that simulates crop and soil response to water stress under various climatic, soil and crop management conditions. Crop yield is estimated as the product of dry biomass by the harvest index (HI). At the flowering stage, HI increases linearly as a function

of time after a latent phase, up to near physiological maturity. Transpiration is calculated and then translated into biomass using biomass water productivity, evaporative demand and air CO2 concentration data (Allen et al., 1998; Steduto et al., 2009).

AquaCrop (v4.0), used in this study, is structured so as to integrate the soil-plant-atmosphere continuum. It consists of five components: i) weather component, which requires five types of data input – daily maximum and minimum air temperatures (T), daily rainfall, daily reference evapotranspiration and the mean annual CO2 concentration in the atmosphere; ii) crop input parameters (planting dates, plant density, growth phenology and aerial canopy); iii) soil component, which is configured as an independent system of variable depth, with one or several horizons of varying texture compositions, and the hydraulic characteristics including hydraulic conductivity at saturation (Ks) and volumetric water content at saturation, FC and PWP; iv) field management conditions (fertilizer application and field-surface practices); and v) irrigation management (irrigation method, percentage of wetted surface, date and amount of water applied). AquaCrop provides default values, called conservative parameters, that are related to the crops being studied (Raes et al., 2009a). The non-conservative parameters depend on crop management and environmental conditions. In this study, these parameters were estimated using measured data from all three cropping seasons.

Default settings proposed by the model was used to estimate initial canopy cover (CCo) from sowing rate, seed weight, seed number and estimated germination rate. The canopy expansion rates were automatically estimated by the model after we provided phenological dates, i.e. (date of emergence, maximum canopy cover, senescence and maturity. The flowering date, length of flowering stage, HI reference and HI build-up period were specified in order to calculate grain yield production. AquaCrop was run on the basis of calendar days.

2.6 Testing AquaCrop

In order to validate and calibrate the model for durum wheat (Triticum turgidum), we used the results of the experiments conducted from 2009-2010 to 2011-2012. Initially, the parameters were established using the whole dataset from 15 fields for the simulation of grain yield and biomass; for soil water content we used only the soil moisture measurements carried out in the E1 and E2 fields. Accuracy of the model was evaluated using the k-fold cross validation (k-fold CV) approach, given the small size of our dataset (< 30 observations). This approach uses k replicate samples of observation data, builds model with (k-1)/k of data and tests with the remaining 1/k. Where the number of observations was reduced, leave-one-out cross validation (LOOCV), which is a k-fold CV taken to its extreme, with K equal to the number of systematic repetitions, was used (Cassel, 2007). LOOCV is an effective and widely used method (Cawley and Talbot, 2003; Cawley and Talbot, 2004). In our study, it involved using a single observation from the 15 observations as the validation data, and the other observations as the training data. This was repeated such that each observation in the sample was used once for validation (Stone, 1974).

The conservative parameters of crop growth in winter soft wheat and durum wheat are presumed to be close as they display quite similar physiological behavior (El Hafid et al., 1996). On this basis, we initially used the conservative parameters of soft wheat following the AquaCrop manual annexes (Raes et al., 2009b) to derive the conservative parameters of durum wheat. This approach led us to adjust only parameters known to be very sensitive for wheat in AquaCrop, i.e. the maximum root water extraction in the top and bottom quarters of the root zone in order to calibrate the model so that it could predict durum wheat yields under semi-arid irrigated conditions. The AquaCrop durum wheat parameters are presented in Table 15.

Table 15: *Crop parameters used for durum wheat*

Parameters description	Value	STD DEV	Unit or meaning	Assessment method
Conservative Parameters				
Base temperature	0	-	◦ C	(Raes et al., 2009b)
Upper temperature	26	-	◦ C	(Raes et al., 2009b)
Canopy cover per seeding at 90% emergence (CC0)	1.5	-	cm²	(Raes et al., 2009b)
Canopy growth coefficient (CGC)	0.05	-	Increase in canopy cover (fraction soil cover per day)	(Raes et al., 2009b)
Crop coefficient for transpiration at CC = 100%	1.1	-	Full canopy transpiration relative to ET0	(Raes et al., 2009b)
Decline in crop coefficient after reaching CCx	0.15	-	% Decline per day due to leaf aging	(Raes et al., 2009b)
Canopy decline coefficient (CDC)	0.072	-	Decrease in canopy cover (in fraction per day)	(Raes et al., 2009b)
Water productivity	15	-	g (biomass) m-²	(Raes et al., 2009b)
Leaf growth threshold p-upper	0.2	-	Above this leaf growth is inhibited	(Raes et al., 2009b)
Leaf growth threshold p-lower	0.65	-	Leaf growth stops completely as this p	(Raes et al., 2009b)
Maximum root water extraction in top quarter of root zone	0.038		(m3 water/m3 soil/day)	Adjusted
Maximum root water extraction in top quarter of root zone	0.018		(m3 water/m3 soil/day)	Adjusted
Leaf growth stress coefficient curve shape	5	-	Moderately convex curve	(Raes et al., 2009b)
Stomatal conductance threshold p-upper	0.65	-	Above this stomata begin to close	(Raes et al., 2009b)
Stomata stress coefficient curve shape	2.5	-	Highly convex curve	(Raes et al., 2009b)
Senescence stress coefficient p-upper	0.7	-	Above this early canopy senescence begins	(Raes et al., 2009b)
Non-conservative parameters				
Plant density	2250000	200000	Plant/ha	Measured
Sowing to emergence	12	0.8	Day	Measured
Sowing to maximum rooting	103	9	Day	Measured
Sowing to senescence	192	11	Day	Measured
Sowing to maturity	172	10	Day	Measured
Sowing to flowering	120	12	Day	Measured
Length of the flowering stage	15	0.71	Day	Measured
Building up of HI	48	-	%	Measured
Maximum rooting depth	0.8	-	m	Measured

2.7 Model evaluation

For evaluating the performance of the AquaCrop, field measurements (observed data) were compared with outputs generated by the model (simulated data) in terms of crop yield, biomass and soil moisture in the root zone.

Different statistical indices were used to compare modeled with observed values. These indices were the coefficient of determination (R^2), the root mean square error (RMSE), the normalized RMSE (nRMSE; expressed as a percentage; Loague and Green (1991) and the mean bias error (MBE).

$$\mathrm{RMSE} = \left[\sum_{i=1}^{n} \frac{(Si-Oi)^2}{n}\right]^{0.5} \quad (1)$$

$$\mathrm{nRMSE} = \left[\sum_{i=1}^{n} \frac{(Si-Oi)^2}{n}\right]^{0.5} \times \frac{100}{M} \quad (2)$$

Si and Oi refer to simulated and observed values of the studied variable, respectively; n is the number of observations; and M is the mean of the observed variable. The nRMSE indicates the accuracy of the model and the dispersion around the mean of the observed values. The simulation is considered to be excellent when the nRMSE value is lower than 10%, good if it is higher than 10% but lower than 20%, fair if it is higher than 20% but lower than 30%, and poor if it is higher than 30% (Jamieson et al., 1991).

The MBE is an indicator that assesses whether the model is underestimating or overestimating the observed values, and it also gives the uniformity of error distribution. Positive MBE values indicate overestimation, negative values indicate underestimation and a value of zero indicates equal distribution between negative and positive values. The MBE is calculated as follows:

$$\mathrm{MBE} = \frac{1}{n}\left[\sum_{i=1}^{n}(Si - Oi)\right] \quad (3)$$

2.8 Model application

Adjusted AquaCrop (v4.0) was used to improve irrigation scheduling in the studied irrigated perimeter. We evaluated the effects of various irrigation scenarios (different dates and frequencies of irrigation supplies) on grain yield and water use efficiency (WUE). We took into account periods of crop stress, development stages of wheat and rainfalls.

The crop parameter values and the soil characteristics for the plots E1 and E2 were used for different scenarios. For irrigation supplies, we conserved the same amount of water provided at plot level and we varied the moment of inputs. In case we proposed an additional irrigation supplement, we took 105 mm, which represents the average amount of water commonly brought in the irrigated perimeter of Tadla due to the use of flooding irrigation method, the lack of plots leveling and the presence of deep soil cracks.

WUE is a helpful indicator for evaluating the impact of irrigation scheduling decisions (Liu et al., 2007). In a crop production system, WUE is used to define the relationship between crop production and the amount of water involved in crop production, expressed as crop production per unit volume of water. In this study, WUE (kg.m-3) refers to the ratio between the final grain yields (GY) and cumulative crop evapotranspiration during the whole crop cycle (ET).

$$\mathrm{WUE} = \frac{\mathrm{GY}}{\mathrm{ET}} \quad (4)$$

3. Results and discussions

3.1 Grain yield

Figure 20 presents the relationship between observed and modeled durum wheat grain yields. The simulated and measured yields showed a good correlation, with an R^2 value of 0.97. The calculated model evaluation criteria between the simulated and measured yields were: RMSE = 0.20 $t.ha^{-1}$, nRMSE =

4.1% and MBE = 0.03 $t.ha^{-1}$. The positive MBE value indicates that the model is in average overestimating slightly the observed values.

Using the LOOCV method, we obtained R^2 values of 0.95 (Figure 21). The difference between the values of the linear regression of the dataset and the values of the LOOCV method validation data were minimal, confirming the ability of the model to simulate yields. The differences between the observed and simulated outputs of LOOCV for durum wheat yield were: RMSE = 0.23 $t.ha^{-1}$, nRMSE = 4.7% and MBE = -0.01 $t.ha^{-1}$.

Andarzian et al. (2011) simulated soft wheat grain yield using AquaCrop and obtained a R^2 of 0.95 and a nRMSE of 5%. The difference between the observed and modeled grain yield of soft wheat was 0.14 $t.ha^{-1}$, indicating that the model overestimated the yield by 2.7%. Mkhabela and Bullock (2012) reported that the difference between the modeled and observed grain yield of soft wheat was 0.12 $t.ha^{-1}$, signifying that AquaCrop overestimated the yield by only 3%. Salemi et al. (2011) reported that the model underestimated the grain yield of soft wheat by 1.35%. The model results are comparable with those provided by other models used by Eitzinger et al. (2004) and Rodriguez et al. (2003) to simulate wheat yield and soil water content. These authors simulated soft wheat grain yield using the STICS model for wheat and reported that there was a good agreement between observed and modeled grain yield, with an RMSE of 0.550 $t.ha^{-1}$, an nRMSE of 8.5% and an MBE of 0.29 $t.ha^{-1}$. AquaCrop also appears to be quite efficient in predicting durum wheat grain yield under semi-arid irrigated conditions in a large range of crop conditions, as indicated by our study.

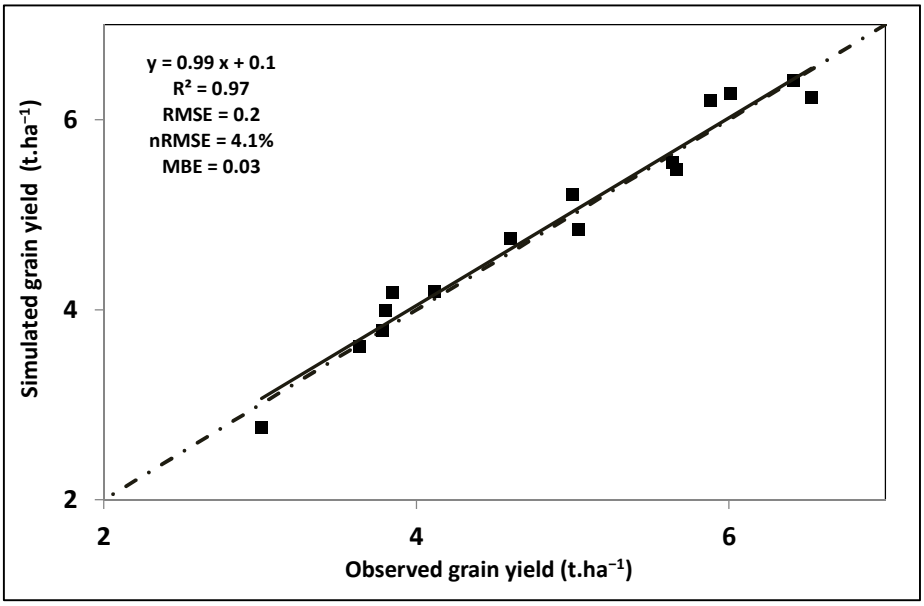

Figure 20: *Relationship between observed and simulated durum wheat grain yield (t.ha^{-1}) using the whole datasets (Calibration)*

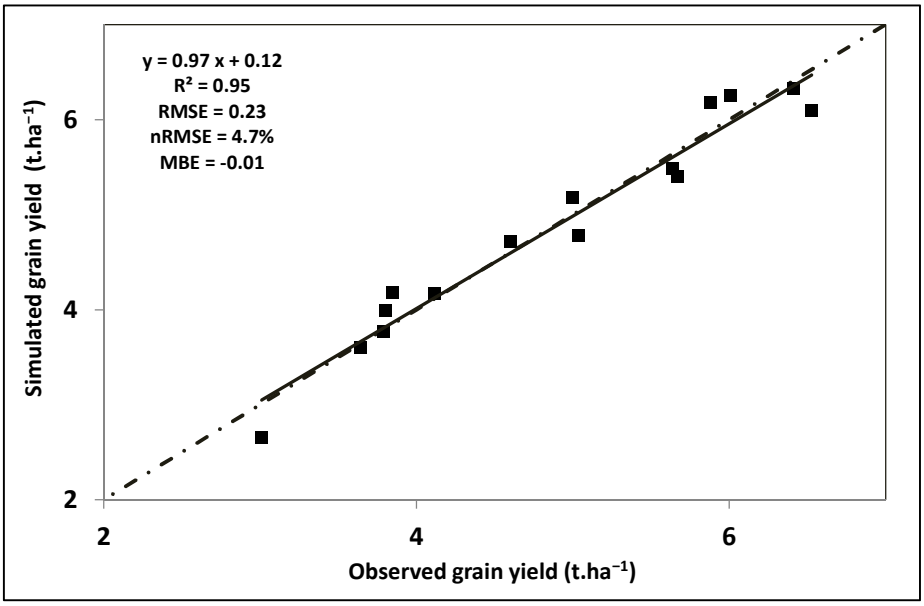

Figure 21: *Relationship between observed and simulated durum wheat grain yield (t.ha^{-1}) using the LOOCV subsets (Validation)*

3.2 Final aboveground biomass

Figure 22 presents the relationship between observed and modeled durum wheat aboveground biomass for the study area. The RMSE, nRMSE and R2 were 0.8 $t.ha^{-1}$, 5.7% and 0.93, respectively. The difference between the values of the linear regression of the observed dataset and the simulated values using the LOOCV method were minimal. The statistical indicators we obtained were: RMSE = 0.7 $t.ha^{-1}$, nRMSE = 4.8%, MBE = 0.01 $t.ha^{-1}$ and R^2=0.92 (Figure 23). These results confirm the capacity of the model to simulate aboveground biomass.

Araya et al. (2010) simulated barley aboveground biomass using AquaCrop and reported an RMSE of 0.36-0.90 $t.ha^{-1}$ and R^2 values higher than 0.8. Similarly, Andarzian et al. (2011) simulated soft wheat aboveground biomass using the model and reported an R^2 value of 0.95 and nRMSE value of 4.4%.

The average difference between simulated and observed biomass of durum wheat was 0.08 $t.ha^{-1}$, indicating that the model slightly underestimated this parameter (by 0.6%). Salemi et al. (2011) reported that the model underestimated the aboveground biomass of soft wheat by 1.42%. In our study, AquaCrop accurately predicted the final aboveground biomass of durum wheat under the conditions in the Tadla area.

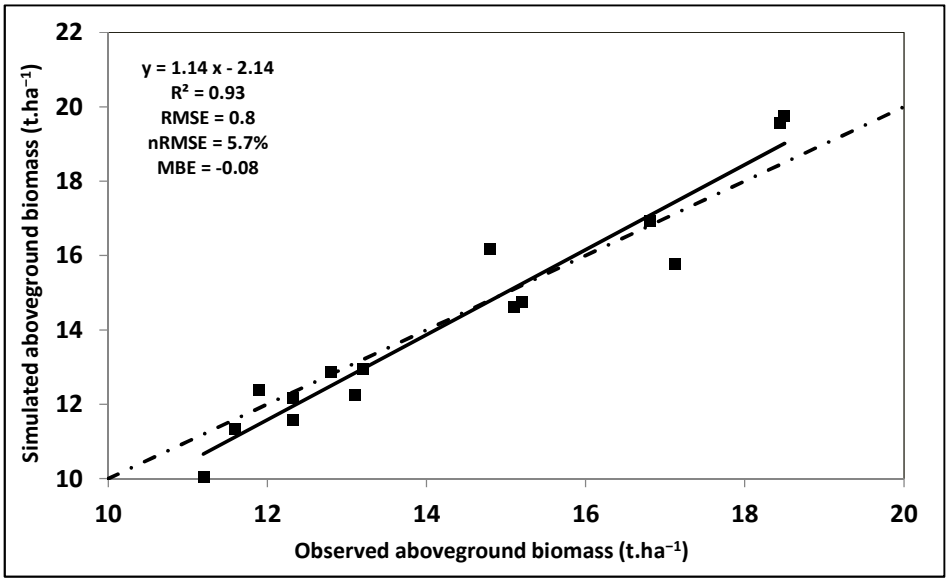

Figure 22: *Relationship between observed and simulated durum wheat biomass ($t.ha^{-1}$) using the whole datasets*

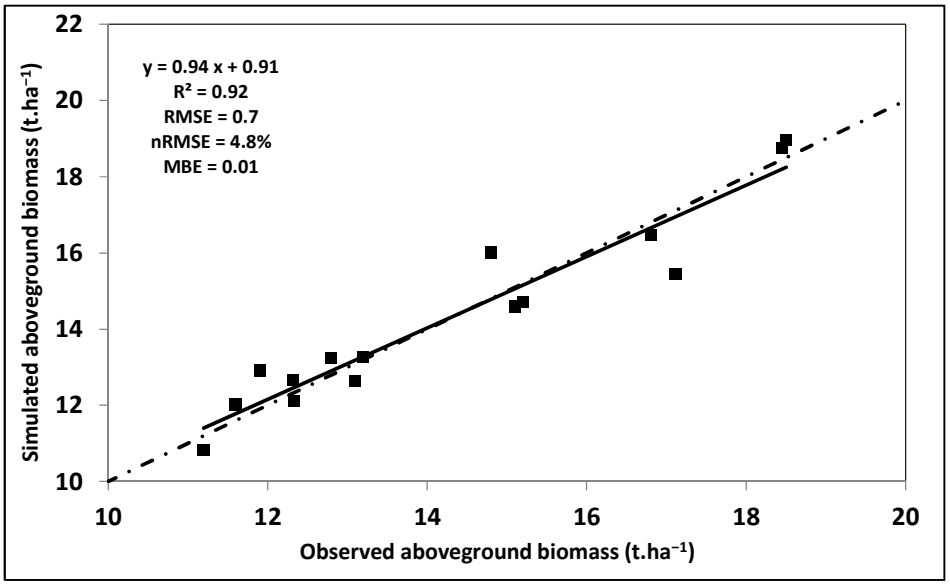

Figure 23: *Relationship between observed and simulated durum wheat biomass ($t.ha^{-1}$) using the LOOCV subsets (Validation)*

3.3 Soil water content

Figures 24 and 25 present the comparison between observed and simulated soil water content of the whole profile for the two fields where this variable was measured. The soils in these plots have similar characteristics. However, when we apply the model at large-scale it advisable to integrate spatial variability of soil data, in order to improve simulation accuracy. An important point arising from these figures is that the variations in simulated soil moisture followed the variation of rainfall and the occurrence of irrigation events exactly, indicating that the model is sensitive enough to be used as an efficient tool to monitor irrigation in real time.

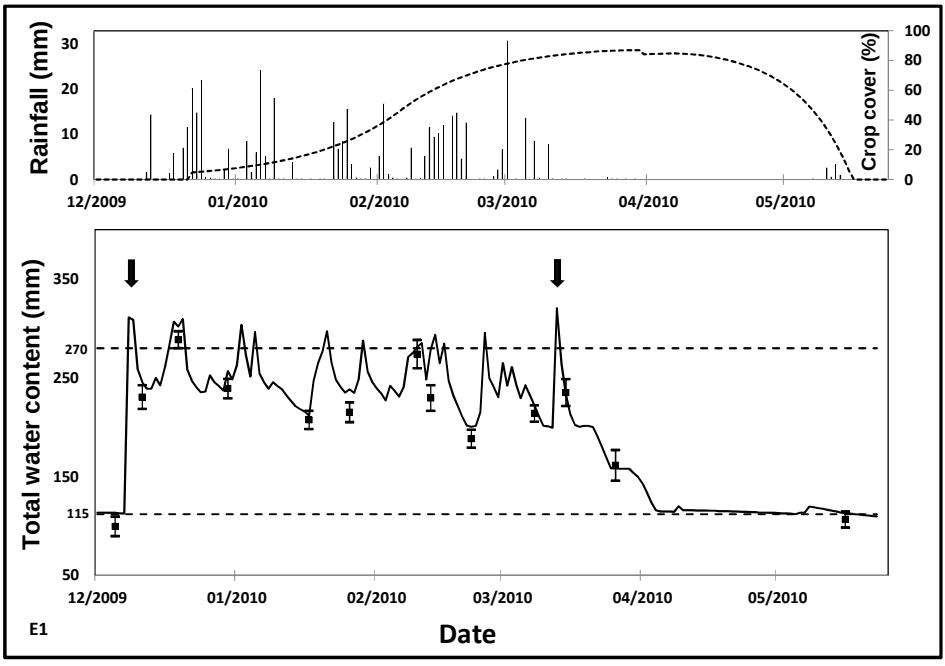

Figure 24: *Comparison between simulated and observed soil moisture measurements at 0-90 cm depth for plot E1 followed during the cropping season 2009/2010. Descendent arrows ⬇ indicate irrigation water supply*

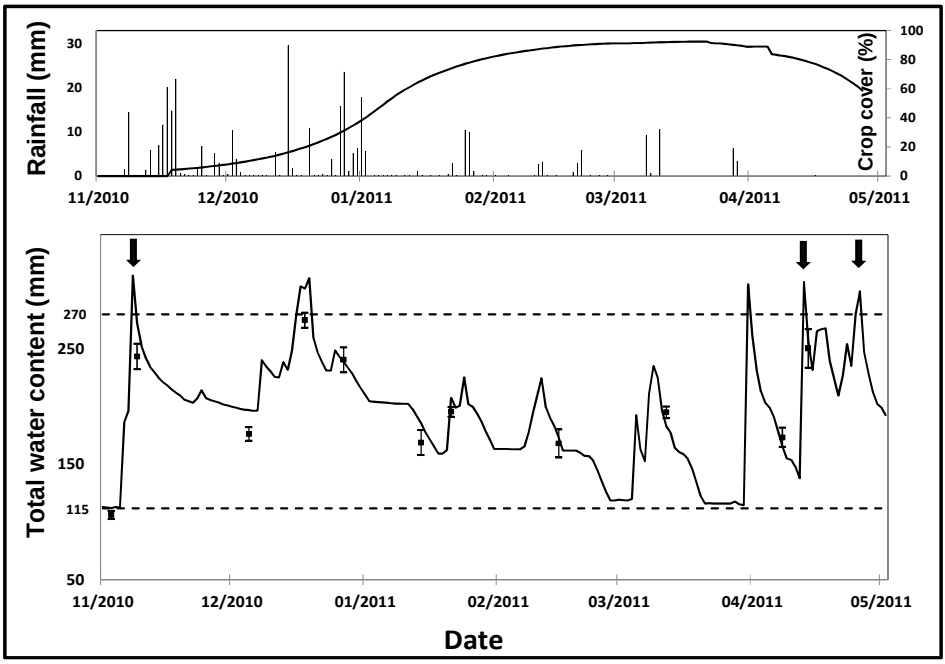

Figure 25: *Comparison between simulated and observed soil moisture measurements at 0-90 cm depth for plot E2 followed during the cropping season 2010/2011. Descendent arrows ⬇ indicate irrigation water supply*

The statistical indices also showed the ability of the model to simulate total soil water content. The RMSE, nRMSE, MBE and R2 values were 17.68 mm, 8.55%, 11.12 mm and 0.95 for the E1 plot and 15.73 mm, 7.90%, 9.47 mm and 0.94 for the E2 plot, respectively. The model simulated well the variation in soil water content in the soil profiles (0-90 cm layer) and captured its tendency to vary. The positive MBE values indicate that the model is overestimating the observed values.

Both Mkhabela and Bullock (2012) and Zeleke et al. (2011) reported that AquaCrop simulated soil water content well and the way it varied in the root zone (0-90 cm layer). Hussein et al. (2011) and Farahani et al. (2009) also reported the

ability of the model to predict wetting and drying events resulting from irrigation and rainfall. Similar results were obtained in our study for the soil moisture profile evolution under durum wheat.

3.4 Model applications for irrigation management scenarios

The results of this part, summarized in tables 16 and 17, showed that grain yields can be improved by 14 to 48% for both studied plots (E1 and E2), depending on the adopted irrigation scenario, and taking into account the availability of water in the root zone and the periods of water stress.

For the 2009/2010 growing season, rainfall provided enough water from the sowing until March unlike the second phase of the season. The non-sufficient quantities of irrigation water supply during the dry phase of the year can drastically affect grain yield. This explains the low yields recorded for the plot E1 (Table 16). In this case study, we suggested to irrigate at grain filling stage (see scenarios E1-S2 to E1-S7 of Table 16) to avoid water stress effect during this stage, since rainfall satisfied water requirements and meet the increasing evaporative demand for the crop during the previous stages. Such situation occurs frequently in studied areas where the high evaporative demand corresponds to the grain filling stage.

Regarding the parcel E2, we achieved good yield (6.2 t/ha) in 2010/2011 because precipitation occurred during grain filling stage (Table 17). However, the scenarios showed, in table 17, that this yield can be improved by scheduling irrigation during the first growing stage of wheat. Indeed, water stress during this period can affect leaf growth that leads to a decrease in biomass production and final grain yield (Hsiao et al., 2009; Steduto et al., 2009).

For the case of double irrigation scenarios, the best yields were achieved when irrigation was applied during the flowering and grain filling stages (E1-S3 and E2-S4). Water stress at grain filling stage leads to a decrease in grain yield which is related to harvest index (Steduto et al., 2009).

In case of low rainfall at early crop growth and grain filling stages, we recommend to farmers to apply an irrigation supply at these stages to improve crops performance and to increase grain weight.

For E1-S2 scenario, we tested the effect of postponing the second irrigation. A delay of ten days caused a decrease in grain yield by about 28% according to the model. In the studied area, the duration to irrigate one hectare is one to two days using the flooding irrigation method. Therefore, plots exceeding 5 ha may be subject to a large heterogeneity of yields due to delayed irrigation. This is not the case for the drip and sprinkler irrigation methods.

One of the problems facing the irrigation management is contributions in excess of the irrigation water that affect saving irrigation water. When analyzing precipitation distribution during the 2010/2011 wheat season, we deduced that we can avoid the first irrigation scheduled initially eight days after sowing. The cancellation of this first irrigation (E2-S8) induced a slight reduction in the estimated yield by only 0.34%.

Water use efficiency was calculated as the ratio of produced wheat grain yield to cumulative evapotranspiration (Table 16 and 17).

Table 16: *Alternative irrigation scenarios implemented in AquaCrop for the plot E1 (Rainfall = 448.6 mm)*

Studied scenarios	Irrigation timing from sowing	Quantity (mm)	Grain Yield (t/ha)	Biomass (t/ha)	Irrigation (mm)	ET (mm)	water-use efficiency (kg/m3)
Baseline scenario*	8; 103	121; 148	3.90	12.42	269	348	1.12
E1-S1	8; 93	121; 148	3.02	11.57	269	321.6	0.94
E1-S2	8; 113	121; 148	4.92	13.57	269	387.5	1.27
E1-S3	111; 142	121; 148	7.63	16.79	269	505	1.51
E1-S4	106; 136	121; 148	7.10	16.03	269	483.1	1.47
E1-S5	111; 142; 160	121; 148; 105	8.93	18.84	374	587.7	1.52
E1-S6	106; 136; 152	121; 148; 105	8.40	17.25	374	564	1.49
E1-S7	6; 111; 142	121; 148; 105	8.30	17.65	374	535.6	1.55
E1-S8	103	148	3.63	12.31	148	346	1.05

*: Reference irrigation scenario which has been applied.

Table 17: *Alternative irrigation scenarios implemented in AquaCrop for the plot E2 (Rainfall = 337 mm)*

Studied scenarios	Irrigation timing from sowing	Quantity (mm)	Grain Yield (t/ha)	Biomass (t/ha)	Irrigation (mm)	ET (mm)	water-use efficiency (kg/m3)
Baseline scenario*	8; 151; 164	128; 150; 120	6.22	15.63	398	395.9	1.57
E2-S1	8; 161; 174	128; 150; 120	5.10	13.47	398	335.5	1.52
E2-S2	8; 141; 154	128; 150; 120	7.27	17.74	398	443.1	1.64
E2-S3	87; 146	150; 120	7.23	17.86	270	443.4	1.63
E2-S4	97; 146	150; 120	7.50	18.47	270	457.6	1.64
E2-S5	87; 141; 154	128; 150; 120	7.90	19.19	398	476	1.66
E2-S6	8; 87; 146	120; 128; 120	7.23	17.85	398	443.4	1.63
E2-S7	97; 141; 154	128; 150; 120	8.19	19.19	536	493.3	1.66
E2-S8	151; 164	150; 120	6.19	15.57	270	394.5	1.57

*: Reference irrigation scenario which has been applied.

The WUE varied in different irrigation scenarios. The highest WUE was found for the scenarios with three irrigations scenario, while the lowest one was found with two irrigations scenario. The WUE generally decreased when water availability decreased (Andarzian et al., 2011).

With the proposed planning based on three irrigations, the values of WUE reached 1.55 for E1-S7 scenario and 1.66 for scenarios E2-S5 and E2-S7 (Table 16 and 17). WUE was lower for the 2009/2011 cropping season compared to 2010/2011. For the first studied cropping season, water stress was so great from the flowering stage. This situation does not meet the high evaporative demand of crops. Scheduling irrigations during the water stress period (the case of scenarios E1-S3, E1-S4, E1-S5, E1-S6 and E1-S7) improved significantly the grain yield, and the WUE increased from 1.12 to 1.55 $kg.m^{-3}$. For the grain yield values, the simulated productions were almost close to the optimal 8 t/ha.

The WUE ranged from 0.94 to 1.66 $kg.m^{-3}$ for the two studied cropping seasons. The highest WUE was observed for three irrigation scenarios (E2-S7), in which it peaked at 1.66 $kg.m^{-3}$ (Table 17).

This application showed the potential of AquaCrop to manage irrigation water and to optimize frequency and timing of the irrigations supplies. This allow to increase WUE by avoiding period of water stress and overwatering, and thus guaranteeing optimal growing conditions throughout the cropping season.

4. Conclusions and perspectives

Irrigated agriculture is an important strategic sector semi-arid region. While irrigation is expected to provide water to crop to prevent water stress, in reality, despite the availability of irrigation water, optimal yields are not often achieved. The stakeholders involved in managing irrigated areas need simulation model tools to help them schedule irrigation and assess its impact on yield.

In this study, the ability of AquaCrop (v4.0) to simulate durum wheat yield, biomass and soil moisture evolution on one hand and to describe the impact of

irrigation water supplies (timing and quantity) on recorded yields on the other hand were shown under semi-arid irrigated conditions.

Required conservative parameters of the model were determined on the basis of predefined parameters for soft wheat. Of the latter, only four had to be adjusted. The use of the statistical LOOCV method provided excellent results for the main model outputs (i.e., soil water content profile evolution, biomass and grain yield).

The analysis of irrigation scenarios showed that the model can optimize frequency and timing of the irrigations supplies. This allow to maintain good grain yields and to increase WUE by avoiding period of water stress and overwatering, and thus guaranteeing optimal growing conditions throughout the cropping season.

Furthermore, new prospects are opening to improve the tool performance by integrating short-term weather forecasts in the process of making decision. This should improve the effectiveness of irrigation scheduling by considering the significant rainfall expected.

This aspect will permit decision-makers and farmers to better schedule irrigation, to insure water saving and to avoid irrigation supplies followed by a significant amount of rainfall. This will be a first step to establish a warning system for irrigation across the whole studied irrigated perimeter.

We concluded that this model is a suitable tool for simulating the effects of water stress on crop productivity in order to improve irrigation management and thereby optimize water-use efficiency under arid and semi-arid conditions.

Chapter 5 Conclusion and perspectives

1. Conclusion

Cereals are by far the most important crops in terms of added value, area covered and food security. In Morocco, water availability is the main limiting factor for cereal production and its management has long been a national priority for the agricultural sector. In terms of agricultural water management, flooding irrigation is practiced on more than 93% of the total area of irrigated perimeters in Morocco and mobilizes large volumes of water. Given the importance of this sector, good management of irrigation water at a large-scale is essential. This has led to work on developing optimum strategies for planning and managing available water resources in order to improve irrigation scheduling and prevent water stress from adversely affecting yield.

In order to address this issue, we focused on two techniques: optical and radar remote sensing; and crop modeling. The approaches developed in this research are intended primarily for decision-makers and managers of large-scale irrigated perimeters (40,000 ha).

Remote sensing was used because of its high potential in monitoring agricultural parameters. We analyzed the ability of two spectral indices ($NDWI_{Rog}$ and MSI) derived from SPOT images and backscattering values derived from SAR images to monitor irrigation. These indices were compared with corresponding *in situ* measurements of soil moisture and vegetation water content in 30 wheat fields. $NDWI_{Rog}$ and MSI were highly correlated with the *in situ* measurements at both the beginning of the growing season (sowing) and at full maturity (grain filling). From sowing to grain filling, the best correlation (R^2=0.86; $p<0.01$) was found for the relationship between $NDWI_{Rog}$ values and observed soil moisture values. $NDWI_{Rog}$ can therefore be used as an operative index for monitoring irrigation in order to estimate and map surface water content changes at the main crop growth stages at the field and regional levels in the Tadla irrigated perimeter.

Backscatter amplitude analysis showed that significant changes in surface states (backscattering values) caused by irrigation could be detected, with values ranging between 0.11 to 3.11 dB.

A reference level was set at 1 dB to differentiate between, on the one hand, irrigated plots and, on the other, non-irrigated plots and plots irrigated for more than 2 days. There was no significant difference between the non-irrigated plots and irrigated plots after more than 2 days.

In order to guarantee continuous irrigation monitoring of the irrigated area over time, it was necessary to ensure that the interval in SAR image acquisition did not exceed 3 days.

This study provided evidence that radar data contain important information for the detection of irrigation water supplies during the studied cropping season period.

The developed approaches, based on remote sensing combined with crop growth models, could be used as an operational tool for managing irrigation and crops, as well as for monitoring the evolution of surface water content at the plot and irrigation scheme levels. The practical aspects of these approaches include: (i) triggering irrigation supplies in water stress situations and otherwise preventing excess supplies of irrigation water; and (ii) detecting illegal irrigation and pumping. This is relevant in irrigated areas where irrigation is not scheduled and uncontrolled water pumping is prohibited.

These approaches will help to improve irrigation monitoring and management in the Tadla irrigation. They will also directly contribute to the sustainability of agricultural production systems and preserve water resources (groundwater and surface).

The performance of the approaches presented need be checked in other contexts before judging their suitability for application in other areas.

The high resolution remote sensing approaches provide a means of synoptic monitoring for agricultural parameters at the time of image acquisition, but do not ensure their temporal monitoring. It is common for there to be more than 10 days between two satellites passes. In order to achieve maximum yield and improve the water-use efficiency in irrigation, it is necessary to control wheat production parameters in time and space. Resorting to crop models is justified mainly by the need to provide temporal monitoring and to assess the impact of the production

parameters monitored on yields with a view to overcoming the limits of remote sensing.

The field crop model (AquaCrop v4.0) developed by FAO was chosen for this research. AquaCrop was adjusted and tested to simulate durum wheat yields and the temporal evolution of soil moisture status, as well as to assess the impact of irrigation water supplies (timing and quantity) on recorded yields. The required conservative parameters of the model were determined on the basis of predefined parameters for soft wheat. Only four of these parameters had to be adjusted. The use of the statistical leave-one-out cross-validation (LOOCV) method gave excellent results for the main model outputs. The comparison between observed and simulated grain yield and above-ground biomass gave a normalized root mean square error (RMSE) of 4.1% (0.2 $t.ha^{-1}$) and 5.7% (0.8 $t.ha^{-1}$), respectively. Similarly, the difference between observed and modeled soil water content was 16.7 mm on average.

The analysis of irrigation scenarios showed that the model can optimize the frequency and timing of irrigation water supplies. It could help to maintain good grain yields and increase water-use efficiency by avoiding periods of water stress and overwatering, thereby guaranteeing optimal growing conditions throughout the cropping season.

New prospects are opening up for improving crop modeling by integrating weather forecasts into the process of decision-making and by adopting spatial modeling that uses data layers on a grid format derived from satellite data. Decision-makers and managers need to be encouraged to adopt spatial and temporal monitoring techniques for better scheduling of irrigation supplies, improving water saving and avoiding supplying irrigation water when rainfall is sufficient. These approaches constitute an important step in establishing an effective irrigation management system across the studied irrigated perimeter.

Our research has provided methods to help stakeholders and policy-makers in their management and decision-making. Each method was applied independently.

2. Perspectives

2.1 Use of recent advances in remote sensing data collection

Remote sensing tools have demonstrated their capabilities to operationally monitor specific farm management practices, including irrigation, over large agricultural areas (Bastiaanssen et al., 2000; Ozdogan et al., 2010; Pinter et al., 2003). The growing interest in satellite imagery is due to the new strategy that enables and encourages the profitable use of high spatial resolution images (10-30 m pixel size). Publicly free remote sensing data has been improved during the last decades, and the potentialities offered are increasing and strengthened with, e.g. the launch of Sentinel 1/2 missions (developed by European Space Agency, ESA, within the Copernicus initiative) and Landsat 8 mission (developed by U.S. Geological Survey and NASA).

Thanks to the Sentinel-1A and Sentinel-2A satellites (launched in April 2014 and April 2015, respectively), and with the Sentinel 1B and 2B satellites (expected to be launched in 2016), high-resolution images of land surface with a temporal frequency of five days (high revisit time) will be available for operational purposes. Complementarity between Sentinel-2 and the US Landsat mission is also expected.

Temporal resolution and spatial coverage of available satellite data can nowadays be improved by using pointable satellites but at high cost. Also, airborne can perform flights on demand and below the clouds to overcome the limitations of satellite sensors instruments (Jones and Vaughan, 2010).

A temporal resolution of about 3–10 days for optic and radar data, can improve significantly irrigation monitoring and crop management throughout the growing season (Vuolo et al., 2015). However, satellites can offer a response with a delay of about one day in data provisions after acquisition. In order to intervene in time, it is compulsory to ensure a short gap between acquisition frequency of satellite images and their processing.

Otherwise, with the current opportunity to acquire good quality satellite data, we think that the main efforts would be devoted, during the coming two decades, to

the development of useful applications in several domains especially in the irrigation management. In this case, the main part of the investment will be allocated for hardware and image processing software as well as personal training.

2.2 Retrieving soil moisture by satellite

The surface soil moisture estimation and irrigation water supply detection can be performed directly using optic, passive and active microwave sensors. As described in Chapters 2 and 3, the potential of remote sensing (optic and radar) to retrieve accurately the surface moisture and detect irrigation supply was demonstrated. The most important consideration is to ensure robust estimation of these two items and to improve irrigation water monitoring and crop management in semi-arid areas. These findings need to be tested and validated with available Landsat-8 and sentinel 1/2 products, so that to add to the knowledge base and improve the mastery and application of satellite imagery in agriculture.

The high sensitivity of the Short Wave Infra-Red (SWIR) band to surface moisture variation was confirmed in Chapter 2. The cloud cover penetration capability constitutes the main limitation for optical remote sensing data use. This limitation is less acute in arid and semi-arid areas where dry periods are more frequent. Optical imagery could be used for water stress warning by detecting plots with under-threshold water content that are probably suffering from water stress.

SAR data in C-band frequency (Chapter 3) has particular advantages since it is largely independent of the time of day or cloud cover, and can also partially penetrate the surface cover. Other wavelengths such as L-band can be explored. Indeed, L-band penetrates deeper into the vegetation cover and soil and provides more relevant information on moisture and water content (Zwieback et al., 2015). These two bands might be explored further in order to develop robust and simple approaches for detecting irrigation schemes for the main crops in irrigated areas.

Moreover, the potential of the studied indices for retrieving surface moisture and backscattering value threshold to detect irrigation supplies for various crops under different irrigation methods can be further investigated. This will help in the

control and monitoring of irrigation water supplies and in assessing surface water content changes.

The discontinuity of remote sensing data heightens the importance of modeling that will simulate the temporal evolution of crop development and soil water content. Combining intermittent remote sensing data with a crop growth modeling approach through assimilation techniques should provide better temporal model outputs than using crop growth models alone.

2.3 Soil water content monitoring at the field-scale

The gravimetric method, used in this research, requires a large data collection effort without ensuring, in most cases, a temporal correspondence with the acquired satellite images or enabling a continuous flow of data. For a temporal synchronization between satellite data and field measurements, it is more appropriate to perform continuous measurement of soil water content in control experimental sites. To achieve this objective, probes can be installed in root zone and connected to data loggers. Measurements data can be automatically recorded in real time and provide detailed time series. A representative set of soil water content stations equipped with electronic probes should ideally be installed on the main irrigation perimeters in order to express the spatial variability of the soil-crop-climate relationship but this requires funds that may not easily be granted.

2.4 Crop models spatialization

AquaCrop model can simulate crop growth and soil water content at a daily time step, based on environmental conditions and under different crop management practices (e.g. irrigation).

As shown in chapter 4at the plot level, AquaCrop could play a key role in optimizing growing conditions throughout the cropping season in order to ensure satisfactory production/yield and improve water-use efficiency, while avoiding water excess or water deficit situations.

The spatialization of the model could give it an added value and serve irrigation perimeters managers to support their management decisions at perimeter scale. This spatialization requires parcel management data (time of seeding, crop type,

fertilizer amounts and time of application, irrigation timing…) for all the parcels of the perimeter (Tadla perimeter is 100000 ha). This large amount of data is often lacking (or provided too late) to perimeter managers to optimize the water supply.

The detection of irrigation supplies timing and the estimation of surface water content in cereal fields using the optical spectral indices and SAR data (chapters 2 and 3) can partially correct this lack and provide very useful information for the perimeter water management.

The combination of the studied crop growth model and remote sensing data (optic and Radar) in an operational system can lead to a significant improvement in crop yield forecasts and soil moisture estimation at local and large scales.

2.5 Development of a system for crop management at large-scale fields

Future research also includes the development of a web interface or user-friendly platform for crop management, based on a system that integrates satellite data and crop modeling (figure 1). This research aimed at providing a scientific and technical approach for monitoring of irrigation supplies and surface water content in a semi-arid irrigated area. The approach could lead to operational management tools for an efficient irrigation at field and regional levels.

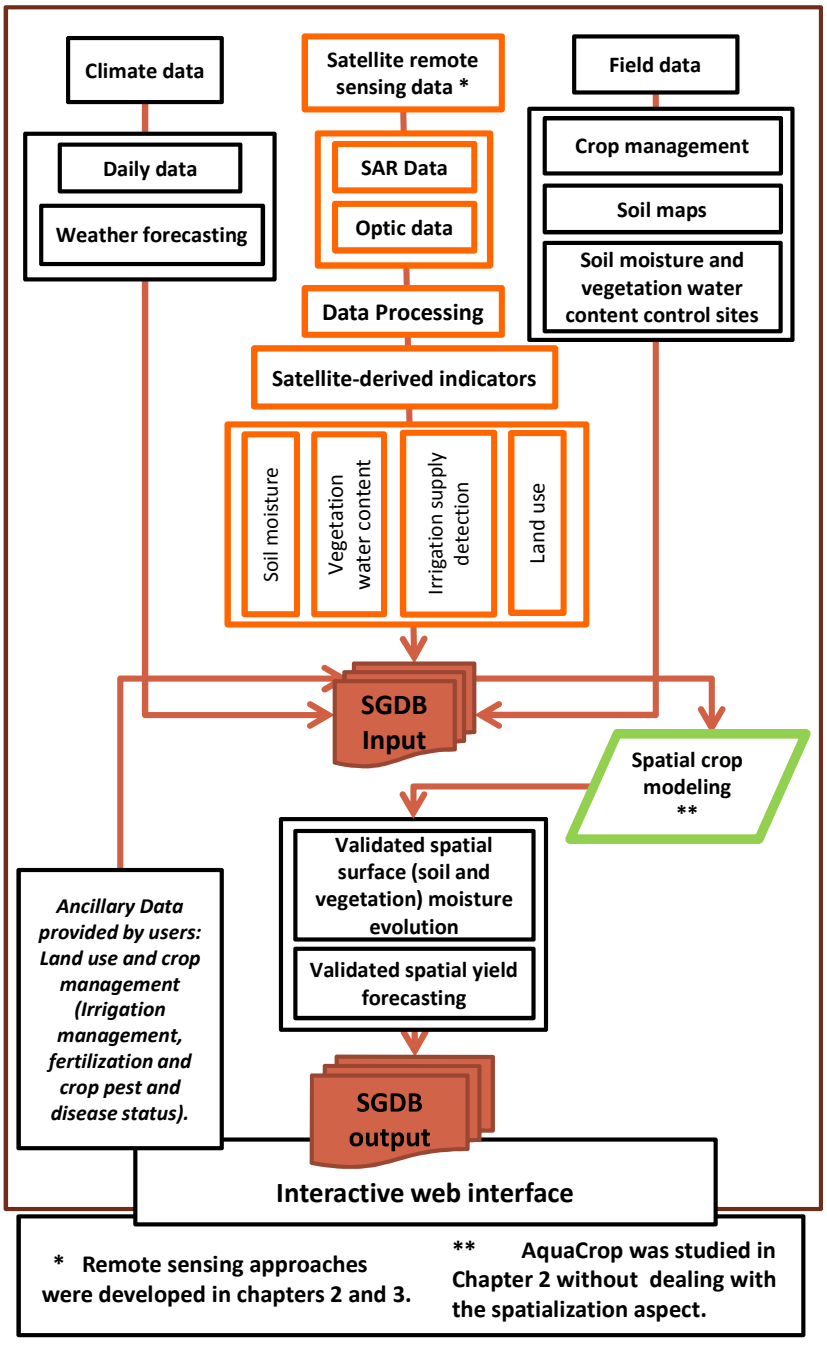

Figure 26: *Workflow of an integrated system for irrigation management and crop growth monitoring in semi-arid regions.*

The proposed system requires three principal components of input data that are satellite remote sensing data (optic and radar), climate data and collected data in the experimental fields. The surface moisture, irrigation supply detection and land use maps are derived from satellite images. The aspects related to remote sensing have been developed for wheat in Chapters 2 and 3 using SPOT-5 and SAR images, respectively. Further studies should be undertaken to test the applicability of this research findings for other crops and using the available Landsat-8 and sentinel 1/2 products.

The proposed operational tool aims to spatialize AquaCrop model by integrating the spatial geo-database (SGDB) in the analysis and simulation process per homogeneous unit or pixel. The SGDB is constituted by the satellite derived indicators, the punctual field data, soil maps, interpolated climate data and weather forecasts.

The data provided by users will also be built at the SGDB for the control of inputs data. The outputs of simulations are integrated in the SGDB and they are available to users. The tool would also provide management and monitoring advices, in real time through a web interface, to meet the requirements of managers and users. On this basis, the irrigation management advice provided is meant to limit excess water application and achieve a better use of irrigation water and cost savings.

For the development of this tool, we intend to exploit the existing platform CGMS Morocco and benefit from the experience of its research team (Balaghi et al., 2013a). As part of INRA's medium-term research project and in partnership with other research institutions, possibilities exist for continuing to develop these tools and test their applicability to any important crops in other irrigated areas with different climatic and edaphic conditions. This tool will be made available to decision-makers and managers of various institutions involved in the management of irrigation water in the region (e.g., ORMVAT, ABOHER).

The proposed system, designed primarily for decision-makers and managers of large irrigated perimeters, requires three principal components of input data that

are satellite remote sensing data (optic and radar), climate data and collected data in the experimental fields. The surface moisture, irrigation supply detection and land use maps are derived from satellite images. The aspects related to remote sensing have been developed for wheat in Chapters 2 and 3 using SPOT-5 and SAR images, respectively. Further studies should be undertaken to test the applicability of this research findings for other crops and using the available Landsat-8 and sentinel 1/2 products.

The proposed operational tool aims to spatialize AquaCrop model by integrating the spatial geo-database (SGDB) in the analysis and simulation process per homogeneous unit or pixel. The SGDB is constituted by the satellite derived indicators, the punctual field data, soil maps, interpolated climate data and weather forecasts.

The managers of large irrigated areas can use the validated spatial surface (soil and vegetation) moisture evolution and spatial yield forecasting provided by the system for crop management and monitoring irrigation. The outputs of simulations are integrated in the SGDB and they are available to users. The tool would also provide management and monitoring advices, in real time through a web interface, to meet the requirements of managers and users. These outputs can be used for: (i) triggering irrigation supplies in water stress situations, (ii) detecting irrigation supplies, (iii) scheduling irrigation and assessing its impact on yield and (iv) detecting illegal irrigation and pumping. In drought years, with the restrictions on the water allocation to the irrigated perimeter, the system could help the managers to prioritize the irrigation of plots and districts depending on the level of water stress and the development stages of crops.

On this basis, the irrigation management advice provided is meant to limit water excess, reduce water shortage and achieve a better use of irrigation water and cost savings. For the development of this tool, we intend to exploit the existing platform CGMS Morocco and benefit from the experience of its research team (Balaghi et al., 2013a). As part of INRA's medium-term research project and in partnership with other research institutions, possibilities exist for continuing to develop these tools and test their applicability to any important crops in other irrigated areas with different climatic and edaphic conditions. This tool will be

made available to decision-makers and managers of various institutions involved in the management of irrigation water in the Tadla region (e.g., ORMVAT, ABOHER) in a first step and may be later transferred to large perimeter managers of all Morocco if it proofs its performance and its usefulness in the Tadla perimeter.

References

Abedinpour M., Sarangi A., Rajput T.B.S., Singh M., Pathak H., Ahmad T. (2012) Performance evaluation of AquaCrop model for maize crop in a semi-arid environment. Agricultural Water Management 110:55-66. DOI: http://dx.doi.org/10.1016/j.agwat.2012.04.001.

Allen R.G. (2000) Using the FAO-56 dual crop coefficient method over an irrigated region as part of an evapotranspiration intercomparison study. Journal of Hydrology 229:27-41. DOI: 10.1016/s0022-1694(99)00194-8.

Allen R.G., Pereira L.S., Raes D., Smith M. (1998) Crop Evapotranspiration-Guidelines for Computing Crop Water Requirements FAO, Rome.

Andarzian B., Bannayan M., Steduto P., Mazraeh H., Barati M.E., Barati M.A., Rahnama A. (2011) Validation and testing of the AquaCrop model under full and deficit irrigated wheat production in Iran. Agricultural Water Management 100:1-8. DOI: http://dx.doi.org/10.1016/j.agwat.2011.08.023.

Araya A., Habtu S., Hadgu K.M., Kebede A., Dejene T. (2010) Test of AquaCrop model in simulating biomass and yield of water deficient and irrigated barley (Hordeum vulgare). Agricultural Water Management 97:1838-1846. DOI: 10.1016/j.agwat.2010.06.021.

Aulard-Macler M. (2011) Sentinel-1 Product Definition ESA. pp. 129.

Badraoui M., Stitou M. (2001) Status of soil survey and soil information system in Morocco, in: C. Lacirignola, et al. (Eds.), Soil resources of Southern and Eastern Mediterranean countries, Bari : CIHEAM. pp. 193-201.

Baghdadi N., Aubert M., Zribi M. (2012) Use of TerraSAR-X data to retrieve soil moisture over bare soils agricultural fields. IEEE Transactions on Geoscience and Remote Sensing Letters 9:512-516.

Baghdadi N., Boyer N., Todoroff P., El Hajj M., Bégué A. (2009) Potential of SAR sensors TerraSAR-X, ASAR/ENVISAT and PALSAR/ALOS for monitoring sugarcane crops on Reunion Island. Remote Sensing of Environment 113:1724-1738. DOI: http://dx.doi.org/10.1016/j.rse.2009.04.005.

Balaghi R., Badjeck M.C., Bakari D., De Pauw E., De Wit A., Defourny P., Donato S., Gommes R., Jlibene M., Ravelo A.C., Sivakumar M.V.K., Telahigue N., Tychon B. (2010) Managing Climatic Risks for Enhanced Food Security: Key Information Capabilities. Procedia Environmental Sciences 1:313-323. DOI: 10.1016/j.proenv.2010.09.020.

Balaghi R., El Hairech T., Tahri M., Lahlou M. (2013a) Manuel d'utilisation de CGMS-Maroc: Système national de suivi grométéorologique de la campagne agricole des rendements céréaliers.

Balaghi R., Jlibene M., Tychon B., Eerens H. (2013b) Agrometeorological Cereal Yield Forecasting in Morocco.

Bastiaanssen W.G.M., Molden D.J., Makin I.W. (2000) Remote sensing for irrigated agriculture: examples from research and possible applications. Agricultural Water Management 46:137-155. DOI: 10.1016/s0378-3774(00)00080-9.

Ben-Gal A., Kool D., Agam N., van Halsema G.E., Yermiyahu U., Yafe A., Presnov E., Erel R., Majdop A., Zipori I., Segal E., Rüger S., Zimmermann U., Cohen Y., Alchanatis V., Dag A. (2010) Whole-tree water balance and indicators for short-term drought stress in non-bearing 'Barnea' olives. Agricultural Water Management 98:124-133. DOI: http://dx.doi.org/10.1016/j.agwat.2010.08.008.

Ben Nouna B., Katerji N., Mastrorilli M. (2000) Using the CERES-Maize model in a semi-arid Mediterranean environment: Evaluation of model performance. European Journal of Agronomy 13:309-322. DOI: http://dx.doi.org/10.1016/S1161-0301(00)00063-0.

Benabdelouahab T. (2009) Spatialisation des paramètres hydrodynamiques des sols du périmètres irrigué du Tadla par les méthodes géostatistiques, INRA research activities report, INRA. pp. 87.

Beriaux E. (2012) Leaf Area Index retrieval from multi-annual and multipolarization SAR time series for crop monitoring, Faculté d'ingénierie biologique, agronomique et environnementale, Université catholique de Louvain, Louvain. pp. 218.

Bi H., Li X., Liu X., Guo M., Li J. (2009) A case study of spatial heterogeneity of soil moisture in the Loess Plateau, western China: A geostatistical approach. International Journal of Sediment Research 24:63-73. DOI: http://dx.doi.org/10.1016/S1001-6279(09)60016-0.

Bouchaou L., Michelot J.L., Qurtobi M., Zine N., Gaye C.B., Aggarwal P.K., Marah H., Zerouali A., Taleb H., Vengosh A. (2009) Origin and residence time of groundwater in the Tadla basin (Morocco) using multiple isotopic and geochemical tools. Journal of Hydrology 379:323-338. DOI: http://dx.doi.org/10.1016/j.jhydrol.2009.10.019.

Cassel D.L. (2007) Re-sampling and simulation, the SAS way, in: Sas (Ed.), Proceedings of the SAS Global Forum 2007 Conference, SAS Institute Inc., Cary, NC.

Cawley G.C., Talbot N.L.C. (2003) Efficient leave-one-out cross-validation of kernel fisher discriminant classifiers. Pattern Recognition 36:2585-2592. DOI: http://dx.doi.org/10.1016/S0031-3203(03)00136-5.

Cawley G.C., Talbot N.L.C. (2004) Fast exact leave-one-out cross-validation of sparse least-squares support vector machines. Neural Networks 17:1467-1475. DOI: http://dx.doi.org/10.1016/j.neunet.2004.07.002.

Ceccato P., Flasse S., Grégoire J.M. (2002a) Designing a spectral index to estimate vegetation water content from remote sensing data: Part 2. Validation and applications. Remote Sensing of Environment 82:198-207. DOI: http://dx.doi.org/10.1016/S0034-4257(02)00036-6.

Ceccato P., Flasse S., Tarantola S., Jacquemoud S., Grégoire J.M. (2001) Detecting vegetation leaf water content using reflectance in the optical domain. Remote Sensing of Environment 77:22-33. DOI: http://dx.doi.org/10.1016/S0034-4257(01)00191-2.

Ceccato P., Gobron N., Flasse S., Pinty B., Tarantola S. (2002b) Designing a spectral index to estimate vegetation water content from remote sensing data: Part 1: Theoretical approach. Remote Sensing of Environment 82:188-197. DOI: http://dx.doi.org/10.1016/S0034-4257(02)00037-8.

Cheng T., Riaño D., Koltunov A., Whiting M.L., Ustin S.L., Rodriguez J.C. (2013) Detection of diurnal variation in orchard canopy water content using MODIS/ASTER airborne simulator (MASTER) data. Remote Sensing of Environment 132:1-12. DOI: http://dx.doi.org/10.1016/j.rse.2012.12.024.

Cheng T., Rivard B., Sánchez-Azofeifa A. (2011) Spectroscopic determination of leaf water content using continuous wavelet analysis. Remote Sensing of Environment 115:659-670. DOI: http://dx.doi.org/10.1016/j.rse.2010.11.001.

Cheng T., Rivard B., Sánchez-Azofeifa A.G., Féret J.B., Jacquemoud S., Ustin S.L. (2012) Predicting leaf gravimetric water content from foliar reflectance across a range of plant species using continuous wavelet analysis. Journal of Plant Physiology 169:1134-1142. DOI: http://dx.doi.org/10.1016/j.jplph.2012.04.006.

Dabrowska-Zielinska K., Inoue Y., Kowalik W., Gruszczynska M. (2007) Inferring the effect of plant and soil variables on C- and L-band SAR backscatter over agricultural fields, based on model analysis. Advances in Space Research 39:139-148. DOI: http://dx.doi.org/10.1016/j.asr.2006.02.032.

de San Celedonio R.P., Abeledo L.G., Miralles D.J. (2014) Identifying the critical period for waterlogging on yield and its components in wheat and barley. Plant and Soil 378:265-277. DOI: 10.1007/s11104-014-2028-6.

De Zan F., Parizzi A., Prats-Iraola P., Lopez-Dekker P. (2014) A SAR Interferometric Model for Soil Moisture. Geoscience and Remote Sensing, IEEE Transactions on 52:418-425. DOI: 10.1109/TGRS.2013.2241069.

Dente L., Satalino G., Mattia F., Rinaldi M. (2008) Assimilation of leaf area index derived from ASAR and MERIS data into CERES-Wheat model to map wheat yield. Remote Sensing of Environment 112:1395-1407. DOI: http://dx.doi.org/10.1016/j.rse.2007.05.023.

Derauw D. (1999) Phasimétrie par Radar à Synthèse d'Ouverture: théorie et applications, Sciences Physiques, Université de LIEGE, Liège. pp. 127.

Doorenbos J., Kassam A.H. (1979) Yield response to water. FAO irrigation and drainage 33:193.

Doorenbos J., Pruitt W.O. (1977) Guidelines for predicting crop water requirements. FAO, Rome.

Dore M.H.I. (2005) Climate change and changes in global precipitation patterns: What do we know? Environment International 31:1167-1181. DOI: http://dx.doi.org/10.1016/j.envint.2005.03.004.

Du L., Tian Q., Yu T., Meng Q., Jancso T., Udvardy P., Huang Y. (2013) A comprehensive drought monitoring method integrating MODIS and TRMM data. International Journal of Applied Earth Observation and Geoinformation 23:245-253. DOI: http://dx.doi.org/10.1016/j.jag.2012.09.010.

Duchemin B., Hadria R., Erraki S., Boulet G., Maisongrande P., Chehbouni A., Escadafal R., Ezzahar J., Hoedjes J.C.B., Kharrou M.H., Khabba S., Mougenot B., Olioso A., Rodriguez J.C., Simonneaux V. (2006) Monitoring wheat phenology and irrigation in Central Morocco: On the use of relationships between evapotranspiration, crops coefficients, leaf area index and remotely-sensed vegetation indices. Agricultural Water Management 79:1-27. DOI: 10.1016/j.agwat.2005.02.013.

Duchemin B., Maisongrande P., Boulet G., Benhadj I. (2008) A simple algorithm for yield estimates: Evaluation for semi-arid irrigated winter wheat monitored with green leaf area index. Environmental Modelling & Software 23:876-892. DOI: http://dx.doi.org/10.1016/j.envsoft.2007.10.003.

Eitzinger J., Trnka M., Hösch J., Žalud Z., Dubrovský M. (2004) Comparison of CERES, WOFOST and SWAP models in simulating soil water content during growing season under different soil conditions. Ecological Modelling 171:223-246. DOI: http://dx.doi.org/10.1016/j.ecolmodel.2003.08.012.

El Hafid R., El Mourid M., Samir K., Bakoulou B. (1996) Caractérisation de certaines variétés de blé, orge et du triticale sous différentes situations hydriques en conditions de champ et simulées. Al awamia 93:7-26.

Elvidge C.D., Lyon R.J.P. (1985) Influence of rock-soil spectral variation on the assessment of green biomass. Remote Sensing of Environment 17:265-279. DOI: http://dx.doi.org/10.1016/0034-4257(85)90099-9.

Er-Raki S., Chehbouni A., Duchemin B. (2010) Combining Satellite Remote Sensing Data with the FAO-56 Dual Approach for Water Use Mapping In Irrigated Wheat Fields of a Semi-Arid Region. Remote Sensing 2:375-387.

FAO. (2013) FAO Cereal Supply and Demand, World food situation.

Farahani H.J., Izzi G., Oweis T.Y. (2009) Parameterization and Evaluation of the AquaCrop Model for Full and Deficit Irrigated Cotton All rights reserved. Agron. J. 101:469-476. DOI: 10.2134/agronj2008.0182s.

Feng H., Chen C., Dong H., Wang J., Meng Q. (2013) Modified Shortwave Infrared Perpendicular Water Stress Index: A Farmland Water Stress Monitoring Method. Journal of Applied Meteorology and Climatology 52:2024-2032. DOI: 10.1175/jamc-d-12-0164.1.

Fieuzal R., Baup F., Marais-Sicre C. (2013) Monitoring Wheat and Rapeseed by Using Synchronous Optical and Radar Satellite Data—From Temporal Signatures to Crop Parameters Estimation. Advances in Remote Sensing 2:162-180. DOI: 10.4236/ars.2013.22020.

Fieuzal R., Duchemin B., Jarlan L., Zribi M., Baup F., Merlin O., Hagolle O., Garatuza-Payan J. (2011) Combined use of optical and radar satellite data for the monitoring of irrigation and soil moisture of wheat crops. Hydrology and Earth System Sciences 15:1117-1129. DOI: 10.5194/hess-15-1117-2011.

Gao B.C. (1996) NDWI - A normalized difference water index for remote sensing of vegetation liquid water from space. Remote Sensing of Environment 58:257-266.

Geerts S., Raes D. (2009) Deficit irrigation as on-farm strategy to maximize crop water productivity in dry areas. Agricultural Water Management 96:1275-1284.

Geerts S., Raes D., Garcia M. (2010) Using AquaCrop to derive deficit irrigation schedules. Agricultural Water Management 98:213-216. DOI: http://dx.doi.org/10.1016/j.agwat.2010.07.003.

Geerts S., Raes D., Garcia M., Miranda R., Cusicanqui J.A., Taboada C., Mendoza J., Huanca R., Mamani A., Condori O., Mamani J., Morales B., Osco V., Steduto P. (2009) Simulating Yield Response of Quinoa to Water Availability with AquaCrop. Agron. J. 101:499-508. DOI: 10.2134/agronj2008.0137s.

Ghulam A., Qin Q., Kuskya T., Li Z. (2008) A Re-Examination of Perpendicular Drought Indices. International Journal of Remote Sensing 29:6037-6044. DOI: doi:10.1080/01431160802235811.

Ghulam A., Qin Q., Teyip T., Li Z.L. (2007) Modified perpendicular drought index (MPDI): a real-time drought monitoring method. ISPRS Journal of Photogrammetry and Remote Sensing 62:150-164. DOI: http://dx.doi.org/10.1016/j.isprsjprs.2007.03.002.

Girard M.C., Girard C.M. (2010) Traitement des données de télédétection: Environnement et ressources naturelles. 2 ed.

Grandchamp M., Cavassilas J.F. (1997) Restauration d'images marines issues d'un radar à ouverture synthétique par filtrage adapté et technique multivues, SEIZIÈME COLLOQUE GRETSI, Gronoble. pp. 789-792.

Guo Y., Zeng F. (2012) Atmospheric correction comparison of SPOT-5 image based on model FLAASH and model QUAC. Int. Arch. Photogramm. Remote Sens. Spatial Inf. Sci. XXXIX-B7:7-11. DOI: 10.5194/isprsarchives-XXXIX-B7-7-2012.

Hadria R., Duchemin B., Baup F., Le Toan T., Bouvet A., Dedieu G., Le Page M. (2009) Combined use of optical and radar satellite data for the detection of tillage and irrigation operations: Case study in Central Morocco. Agricultural Water Management 96:1120-1127. DOI: 10.1016/j.agwat.2009.02.010.

Hadria R., Duchemin B., Jarlan L., Dedieu G., Baup F., Khabba S., Olioso A., Le Toan T. (2010) Potentiality of optical and radar satellite data at high spatio-temporal resolutions for the monitoring of irrigated wheat crops in Morocco. International Journal of Applied Earth Observation and Geoinformation 12, Supplement 1:S32-S37. DOI: 10.1016/j.jag.2009.09.003.

Hadria R., Khabba S., Lahrouni A., Duchemin B., Chehbouni A., Carriou J. (2007) Calibration and validation of the STICS crop model for managing wheat irrigation in the semi-arid Marrakech/Al Haouz Plain. Arabian Journal for Science and Engineering 32:87-101.

Hardisky M.A., Michael S.R., Klemas V. (1983) Growth response and spectral characteristics of a short Spartina alterniflora salt marsh irrigated with freshwater and sewage effluent. Remote Sensing of Environment 13:57-67. DOI: http://dx.doi.org/10.1016/0034-4257(83)90027-5.

Hsiao T.C., Heng L., Steduto P., Rojas-Lara B., Raes D., Fereres E. (2009) AquaCrop: The FAO crop model to simulate yield response to water. III. Parameterization and testing for maize. Agron. J. 101:448–459.

Hunt Jr E.R., Li L., Yilmaz M.T., Jackson T.J. (2011) Comparison of vegetation water contents derived from shortwave-infrared and passive-microwave sensors over central Iowa. Remote Sensing of Environment 115:2376-2383. DOI: http://dx.doi.org/10.1016/j.rse.2011.04.037.

Hunt Jr E.R., Rock B.N. (1989) Detection of changes in leaf water content using Near- and Middle-Infrared reflectances. Remote Sensing of Environment 30:43-54.

Hussein F., Janat M., Yakoub A. (2011) Simulating cotton yield response to deficit irrigation with the FAO AquaCrop model. Spanish Journal of Agricultural Research 9:1319-1330.

Iqbal M.A., Bodner G., Heng L.K., Eitzinger J., Hassan A. (2010) Assessing yield optimization and water reduction potential for summer-sown and spring-sown maize in Pakistan. Agricultural Water Management 97:731-737. DOI: http://dx.doi.org/10.1016/j.agwat.2009.12.017.

Iqbal M.A., Shen Y., Stricevic R., Pei H., Sun H., Amiri E., Penas A., del Rio S. (2014) Evaluation of the FAO AquaCrop model for winter wheat on the North China Plain under deficit irrigation from field experiment to regional yield simulation. Agricultural Water Management 135:61-72. DOI: http://dx.doi.org/10.1016/j.agwat.2013.12.012.

Jacquemoud S., Baret F. (1990) PROSPECT: A model of leaf optical properties spectra. Remote Sensing of Environment 34:75-91. DOI: http://dx.doi.org/10.1016/0034-4257(90)90100-Z.

Jamieson P.D., Porter J.R., Goudriaan J., Ritchie J.T., van Keulen H., Stol W. (1998) A comparison of the models AFRCWHEAT2, CERES-Wheat, Sirius, SUCROS2 and SWHEAT with measurements from wheat grown under drought. Field Crops Research 55:23-44. DOI: http://dx.doi.org/10.1016/S0378-4290(97)00060-9.

Jamieson P.D., Porter J.R., Wilson D.R. (1991) A test of computer simulation model ARC-WHEAT1 on wheat crop grown in New Zealand. Field crops Res. 27:337-350.

Jensen J.R. (2005) Introductory Digital Image Processing: a Remote Sensing Perspective. third ed. Prentice-Hall, Inc.

Jensen J.R. (2007) Remote Sensing of the Environment: An Earth Resource Perspective. 2nd ed. Prentice Hall.

Jin X.L., Feng H.K., Zhu X.K., Li Z.H., Song S.N., Song X.Y., Yang G.J., Xu X.G., Guo W.S. (2014) Assessment of the AquaCrop Model for Use in Simulation of Irrigated Winter Wheat Canopy Cover, Biomass, and Grain Yield in the North China Plain. PLoS ONE 9:e86938. DOI: 10.1371/journal.pone.0086938.

Jones H.G., Vaughan R.A. (2010) Remote Sensing of Vegetation: Principles, Techniques, and Applications OUP Oxford.

Kalluri S., Gilruth P., Bergman R. (2003) The potential of remote sensing data for decision makers at the state, local and tribal level: experiences from NASA's Synergy program. Environmental Science & Policy 6:487-500. DOI: http://dx.doi.org/10.1016/j.envsci.2003.08.002.

Kirkham M.B. (2005) 8 - Field Capacity, Wilting Point, Available Water, and the Nonlimiting Water Range, in: M. B. Kirkham (Ed.), Principles of Soil and Plant Water Relations, Academic Press, Burlington. pp. 101-115.

Kogan F.N. (2000) Contribution of Remote Sensing to Drought Early Warning, in: World Meteorological Organization (Ed.), Early Warning Systems for Drought Preparedness and Drought Management, WMO/TD. pp. 86-100.

Kohavi R. (1995) A study of cross-validation and bootstrap for accuracy estimation and model selection, Fourteenth International Joint Conference on Artificial Intelligence, San Mateo, CA: Morgan Kaufmann. pp. 1137–1143.

Lasaponara R., Masini N. (2012) Satellite Remote Sensing: A New Tool for Archaeology Springer.

Laur H., Bally P., Meadows P., Sanchez J., Schaettler B., Lopinto E., Esteban D. (2002) DERIVATION of the BACKSCATTERING COEFFICIENT σo in ESA ERS SAR PRI PRODUCTS, in: ES-TN-RS-PM-HL09 (Ed.). pp. 56.

Le Hegarat-Mascle S., Zribi M., Alem F., Weisse A., Loumagne C. (2002) Soil moisture estimation from ERS/SAR data: toward an operational methodology. Geoscience and Remote Sensing, IEEE Transactions on 40:2647-2658. DOI: 10.1109/TGRS.2002.806994.

Lei J., Li Z., Bruce W. (2009) Analysis of Dynamic Thresholds for the Normalized Difference Water Index. Photogrammetric Engineering & Remote Sensing 75:1307-1317.

Lionboui H., Fadlaoui A., Elame F., Benabdelouahab T. (2014) Water pricing impact on the economic valuation of water resources. International Journal of Education and Research 2:147-166.

Liu J., Williams J.R., Zehnder A.J.B., Yang H. (2007) GEPIC – modelling wheat yield and crop water productivity with high resolution on a global scale. Agricultural Systems 94:478-493. DOI: http://dx.doi.org/10.1016/j.agsy.2006.11.019.

Liu S., Roberts D.A., Chadwick O.A., Still C.J. (2012) Spectral responses to plant available soil moisture in a Californian grassland. International Journal of Applied Earth Observation and Geoinformation 19:31-44. DOI: http://dx.doi.org/10.1016/j.jag.2012.04.008.

Loague K., Green R.E. (1991) Statistical and graphical methods for evaluating solute transport models: overview and application Journal contam. Hydrol. 7:51-73.

Lobell D.B., Asner G.P., Ortiz-Monasterio J.I., Benning T.L. (2003) Remote sensing of regional crop production in the Yaqui Valley, Mexico: estimates and uncertainties. Agriculture, Ecosystems and Environment 94:205–220.

Massoni C., Missante G., Beaudetm G., Combesh, Etienne P., Ionesco T. (1967) Excursion au Maroc: Description de la pédologie des régions traversées. Les cahiers de la recherche agronomique 24:163-194.

Mattia F., Le Toan T., Picard G., Posa F.I., D'Alessio A., Notarnicola C., Gatti A.M., Rinaldi M., Satalino G., Pasquariello G. (2003) Multitemporal C-band radar measurements on wheat fields. IEEE Transactions on Geoscience and Remote Sensing 41:1551-1560.

McNairn H., Merzouki A., Pacheco A., Fitzmaurice J. (2012) Monitoring Soil Moisture to Support Risk Reduction for the Agriculture Sector Using RADARSAT-2. Selected Topics in Applied Earth Observations and Remote Sensing, IEEE Journal of 5:824-834. DOI: 10.1109/JSTARS.2012.2192416.

Mkhabela M.S., Bullock P.R. (2012) Performance of the FAO AquaCrop model for wheat grain yield and soil moisture simulation in Western Canada. Agricultural Water Management 110:16-24. DOI: http://dx.doi.org/10.1016/j.agwat.2012.03.009.

Momeni M., Saradjian M.R. (2007) Evaluating NDVI-based emissivities of MODIS bands 31 and 32 using emissivities derived by Day/Night LST

algorithm. Remote Sensing of Environment 106:190-198. DOI: http://dx.doi.org/10.1016/j.rse.2006.08.005.

Moran M.S., Inoue Y., Barnes E.M. (1997) Opportunities and limitations for image-based remote sensing in precision crop management. Remote Sensing of Environment 61:319-346. DOI: http://dx.doi.org/10.1016/S0034-4257(97)00045-X.

Moreno A., Maselli F., Chiesi M., Genesio L., Vaccari F., Seufert G., Gilabert M.A. (2014) Monitoring water stress in Mediterranean semi-natural vegetation with satellite and meteorological data. International Journal of Applied Earth Observation and Geoinformation 26:246-255. DOI: http://dx.doi.org/10.1016/j.jag.2013.08.003.

Muller E., Décamps H. (2000) Modeling soil moisture-reflectance. Remote Sensing of Environment 76:173–180.

Najine A., Jaffal M., Khammari K.E., Aïfa T., Khattach D., Himi M., Casas A., Badrane S., Aqil H. (2006) Contribution de la gravimétrie à l'étude de la structure du bassin de Tadla (Maroc) : Implications hydrogéologiques. Comptes Rendus Geoscience 338:676-682. DOI: http://dx.doi.org/10.1016/j.crte.2006.04.015.

Ning Z., Yang H., Qiming Q., Lu L. (2013) VSDI: a visible and shortwave infrared drought index for monitoring soil and vegetation moisture based on optical remote sensing. International Journal of Remote Sensing 34:4585-4609. DOI: doi.org/10.1080/01431161.2013.779046.

ORMVAT. (2009) Rapport annuel de l'Office de la mise en valeur agricole de Tadla.

Ouyang Z.T., Zhang M.Q., Xie X., Shen Q., Guo H.Q., Zhao B. (2011) A comparison of pixel-based and object-oriented approaches to VHR imagery for mapping saltmarsh plants. Ecological Informatics 6:136-146. DOI: http://dx.doi.org/10.1016/j.ecoinf.2011.01.002.

Ozdogan M., Yang Y., Allez G., Cervantes C. (2010) Remote Sensing of Irrigated Agriculture: Opportunities and Challenges. Remote Sensing 2:2274-2304.

Penuelas J., Pinol J., Ogaya R., Filella I. (1997) Estimation of plant water concentration by the reflectance Water Index WI (R900/R970). International Journal of Remote Sensing 18:2869-2875. DOI: 10.1080/014311697217396.

Picard G., Le Toan T., Mattia F. (2003) Understanding C-band radar backscatter from wheat canopy using a multiple-scattering coherent

model. Geoscience and Remote Sensing, IEEE Transactions on 41:1583-1591. DOI: 10.1109/TGRS.2003.813353.

Pinter P.J., Jr., Hatfield J.L.H., Schepers J.S., Barnes E.M., Moran M.S., Daughtry C.S.T., Upchurch D.R. (2003) Remote Sensing for Crop Management. Photogrammetric Engineering & Remote Sensing 69: 647–664.

Préfol P. (1986) Prodige de l'irrigation au Maroc. Le développement exemplaire du Tadla,1936-1985, Nouvelles Editions Latines, Paris, France.

Qin Q., Ghulam A., Zhu L., Wang L., Li J., Nan P. (2008) Evaluation of MODIS Derived Perpendicular Drought Index for Estimation of Surface Dryness Over Northwestern China. International Journal of Remote Sensing 29:1983-1995. DOI: doi:10.1080/01431160701355264.

QiuXiang Y., AnMing B., Yi L., Jin Z. (2012) Measuring cotton water status using water-related vegetation indices at leaf and canopy levels. Journal of Arid Land 4(3):310–319. DOI: doi: 10.3724/SP.J.1227.2012.00310.

Raes D., Steduto P., Hsiao T.C., Fereres E. (2009a) AquaCrop:The FAO Crop Model to Simulate Yield Response to Water: II. Main Algorithms and Software Description. Agron. J. 101:438-447. DOI: 10.2134/agronj2008.0140s.

Raes D., Steduto P., Hsiao T.C., Fereres E. (2009b) AquaCrop:The FAO Crop Model to Simulate Yield Response to Water: Reference Manual Annexes.

Richter K., Atzberger C., Hank T.B., Mauser W. (2012) Derivation of biophysical variables from Earth observation data: validation and statistical measures. Journal of Applied Remote Sensing 6:063557-1-063557-23. DOI: 10.1117/1.jrs.6.063557.

Rodriguez J.C., Duchemin B., Hadria R., Watts C., Garatuza J., Chehbouni A., Khabba S., Boulet G., Palacios E., Lahrouni A. (2003) Wheat yield estimtion using remote sensing and the STICS model in the semiarid Yaqui valley, Mexico. Agronomie 24:295-304. DOI: http://dx.doi.org/10.1016/j.jag.2009.09.003.

Rogers A.S., Kearney M.S. (2004) Reducing signature variability in unmixing coastal marsh Thematic Mapper scenes using spectral indices. International Journal of Remote Sensing 25:2317-2335. DOI: 10.1080/01431160310001618103.

Saich P., Borgeaud M. (2000) Interpreting ERS SAR signatures of agricultural crops in Flevoland, 1993-1996. Geoscience and Remote Sensing, IEEE Transactions on 38:651-657. DOI: 10.1109/36.841995.

Salemi H., Soom M.A.M., Lee T., Mousavi S., Ganji A., Yusoff M.K. (2011) Application of AquaCrop model in deficit irrigation management of Winter wheat in arid region. African Journal of Agricultural Research 610:2204-2215.

Seckler D., Barker R., Amarasinghe U. (1999) Water scarcity in the twenty-first century. Water Resources Development 15:29–42. DOI: 10.1080/07900629948916.

Skidmore E.L., Dickerson J.D., Shimmelpfennig H. (1975) Evaluating surface-soil water content by measuring reflectance. Soil Science Society of American Proceedings 39:238–242.

Snoeij P., Attema E., Davidson M., Floury N., Levrini G., Rosich B., Rommen B. (2008) Sentinel-1, the GMES Radar Mission. IEEE:5.

Soddu A., Deidda R., Marrocu M., Meloni R., Paniconi C., Ludwig R., Sodde M., Mascaro G., Perra E. (2013) Climate Variability and Durum Wheat Adaptation Using the AquaCrop Model in Southern Sardinia. Procedia Environmental Sciences 19:830-835. DOI: http://dx.doi.org/10.1016/j.proenv.2013.06.092.

Song X., Zhou X., Li X., Li X. (2009) Spatial Heterogeneity Analysis of Soil Moisture Based on Geostatistics, Information Science and Engineering (ICISE), 2009 1st International Conference on. pp. 5134-5137.

Steduto P., Hsiao T.C., Raes D., Fereres E. (2009) Aquacrop-the FAO crop model to simulate yield response to water: I. Concepts and underlying principles. Agron. J. 101:426-437.

Stone M. (1974) Cross-Validatory Choice and Assessment of Statistical Predictions. Journal of the Royal Statistical Society. Series B (Methodological) 36:111-147. DOI: citeulike-article-id:6758792 doi: 10.2307/2984809.

Stricevic R., Cosic M., Djurovic N., Pejic B., Maksimovic L. (2011) Assessment of the FAO AquaCrop model in the simulation of rainfed and supplementally irrigated maize, sugar beet and sunflower. Agricultural Water Management 98:1615-1621. DOI: 10.1016/j.agwat.2011.05.011.

Tian Q., Tong Q., Pu R., Guo X., Zhao C. (2001) Spectroscopic determination of wheat water status using 1650-1850 nm spectral absorption

features. International Journal of Remote Sensing 22:2329-2338. DOI: 10.1080/01431160118199.

Trombetti M., Riaño D., Rubio M.A., Cheng Y.B., Ustin S.L. (2008) Multi-temporal vegetation canopy water content retrieval and interpretation using artificial neural networks for the continental USA. Remote Sensing of Environment 112:203-215. DOI: http://dx.doi.org/10.1016/j.rse.2007.04.013.

Ulaby F.T., Ulaby M.K., Moore A., K. F. (1986) Microwave remote sensing active and passive vol. 3Artech House, Norwood, MA

Vuolo F., Essl L., Atzberger C. (2015) Costs and benefits of satellite-based tools for irrigation management. Frontiers in Environmental Science 3. DOI: 10.3389/fenvs.2015.00052.

Wang Y.G., Zhu H., Li Y. (2013) Spatial heterogeneity of soil moisture, microbial biomass carbon and soil respiration at stand scale of an arid scrubland. Environmental Earth Sciences 70:3217-3224. DOI: 10.1007/s12665-013-2386-z.

Wellens J., Raes D., Traore F., Denis A., Djaby B., Tychon B. (2013) Performance assessment of the FAO AquaCrop model for irrigated cabbage on farmer plots in a semi-arid environment. Agricultural Water Management 127:40-47. DOI: http://dx.doi.org/10.1016/j.agwat.2013.05.012.

Xiangxiang W., Quanjiu W., Jun F., Qiuping F. (2013) Evaluation of the AquaCrop model for simulating the impact of water deficits and different irrigation regimes on the biomass and yield of winter wheat grown on China's Loess Plateau. Agricultural Water Management 129:95-104. DOI: http://dx.doi.org/10.1016/j.agwat.2013.07.010.

Yang C., Everitt J.H., Murden D. (2011) Evaluating high resolution SPOT 5 satellite imagery for crop identification. Computers and Electronics in Agriculture 75:347-354. DOI: http://dx.doi.org/10.1016/j.compag.2010.12.012.

Yang N., Qin Q., Jin C., Yao Y. (2008) The Comparison and Application of the Methods for Monitoring Farmland Drought Based on NIR-Red Spectral Space. International Geoscience and Remote Sensing Symposium (IGARSS 2008):III871-III874. DOI: doi: 10.1109/IGARSS.2008.4779488.

Yilmaz M.T., Hunt Jr E.R., Goins L.D., Ustin S.L., Vanderbilt V.C., Jackson T.J. (2008a) Vegetation water content during SMEX04 from ground data and Landsat 5 Thematic Mapper imagery. Remote Sensing of

Environment 112:350-362. DOI: http://dx.doi.org/10.1016/j.rse.2007.03.029.

Yilmaz M.T., Hunt Jr E.R., Jackson T.J. (2008b) Remote sensing of vegetation water content from equivalent water thickness using satellite imagery. Remote Sensing of Environment 112:2514-2522. DOI: http://dx.doi.org/10.1016/j.rse.2007.11.014.

Zeleke K.T., Luckett D., Cowley R. (2011) Calibration and Testing of the FAO AquaCrop Model for Canola. Agron. J. 103:1610-1618. DOI: 10.2134/agronj2011.0150.

Zhang H., Chen H., Shen S., Zhou G., Yu W. (2008) Drought Remote Sensing Monitoring Based on the Surface Water Content Index (SWCI) Method. Remote Sensing Technology and Application 23:624-628.

Zribi M., Baghdadi N., Holah N., Fafin O. (2005) New methodology for soil surface moisture estimation and its application to ENVISAT-ASAR multi-incidence data inversion. Remote Sensing of Environment 96:485-496. DOI: 10.1016/j.rse.2005.04.005.

Zwieback S., Hensley S., Hajnsek I. (2015) Assessment of soil moisture effects on L-band radar interferometry. Remote Sensing of Environment 164:77-89. DOI: http://dx.doi.org/10.1016/j.rse.2015.04.012.

Appendix 1

Assessment of vegetation water content in wheat using near and shortwave infrared spot5 data in an irrigated area [4]

[4] Adapted from: Benabdelouahab, T., Balaghi, R., Hadria, R., Lionboui, H., Tychon, B., 2015. Assessment of vegetation water content in wheat using near and shortwave infrared spot5 data in an irrigated area. Revue de Science de l'Eau (Accepted for publication).

In Morocco, water availability is becoming a national priority for the agricultural sector. In this context, the stakeholders try continuously to improve strategies of water irrigation management, on one hand, and to assess vegetation water content status, on the other hand, in order to improve irrigation scheduling and prevent water stress that affects yield adversely.

The aim of this study was to evaluate the potential of two spectral indices, calculated from SPOT-5 high resolution visible (HRV) data, to retrieve the vegetation water content values of wheat in an irrigated area. These indices were the normalized difference water index ($NDWI_{Gao}$) and the moisture stress index (MSI). The values of these indices were compared with corresponding values of in situ-measured vegetation water content in 16 fields of wheat during the 2012-2013 cropping season.

Good correlations were found between observed vegetation water content values and $NDWI_{Gao}$ and MSI values during the crop growth period from anthesis to grain filling. These results were validated using the K-fold cross validation method and showed a good stability of the proposed regression models with a slight advantage for the $NDWI_{Gao}$. Based on these results, the $NDWI_{Gao}$ was chosen to map the spatial variability of vegetation water content of wheat at the east of Beni-Moussa irrigated perimeter. These results proved that the indices based on near and shortwave infrared band (NIR and SWIR) are able to monitor vegetation water content changes in wheat from anthesis to grain filling stage. These indices could be used to improve irrigation and crop management of wheat at both field and regional levels.

1. Introduction

In the world, irrigated areas produce more than half of all foodstuffs and thus contribute to food security. They are using about 72% of available

water resources (Geerts et al., 2009; Seckler et al., 1999). In Morocco, water availability is considered as the main limiting factor for crop growth. Cereal production is strongly related to the amount and distribution of annual rainfall in rainfed areas and to the amount of groundwater and water stored in dams in irrigated areas. Irrigation water has to be supplied to the plants when the soil water reserves are depleted and are causing plant stress. For instance, in the Tadla irrigated area, the main crop is wheat and represents more than 36% (40.000 ha) of the total irrigated area (ORMVAT, 2009).

The average volume of water consumed by the wheat crop during the period from 1994 to 2002 reached 136 Mm^3 / year in the irrigated perimeter of Tadla. This amount is the equivalent of 18% of all irrigation consumed across the irrigated perimeter (ORMVAT, 2009). In this situation, knowing the vegetation water content could be an interesting basis for improving irrigation scheduling and preventing water stress adversely affecting yield (Duchemin et al., 2006).

In order to estimate the water content of the vegetation for various crops, remote sensing has been used through the spectral indices (Ceccato et al., 2002a; Hadria et al., 2010; Trombetti et al., 2008), taking account of the high temporal and spatial resolution of the recent satellites.

During the wheat development cycle, water stress effects can be directly observed in the vegetation (Feng et al., 2013; Ghulam et al., 2007; Ning et al., 2013). Water stress indices used in irrigation management should therefore be based on the spectral bands that are sensitive to vegetation water content. Many indices designed for vegetation moisture monitoring have been developed using NIR (780-890 nm) and SWIR (1580-1750 nm) bands, including the normalized difference infrared index (NDII) (Hardisky et al., 1983), the global vegetation moisture index (GVMI) (Ceccato et al., 2002a), the moisture stress index (MSI) (Hunt Jr and Rock, 1989) and the normalized difference water index ($NDWI_{Gao}$) (Gao,

1996). For wheat management, the use of these spectral indices for assessing the vegetation water content becomes essential during critical periods (flowering to grain filling) to ensure good yields.

Recent studies have confirmed the high sensitivity of the SWIR band to vegetation water variations (Ceccato et al., 2001; Cheng et al., 2013; Hunt Jr et al., 2011; Liu et al., 2012; Yilmaz et al., 2008b). Otherwise, the reflectance in the NIR spectrum (740–1300 nm) is the most sensitive to leaf internal structure changes (Jacquemoud and Baret, 1990) and is insensitive to vegetation water variation (Elvidge and Lyon, 1985), except in extremely high stress conditions, which cause severe leaf dehydration and thus affect leaf structure (Jensen, 2007). The NIR band serves as a moisture-reference band, whereas the SWIR band is used as the moisture-measuring band. Currently, the spectral indices are widely used to estimate the biophysical properties of the vegetation, including the water content. However, the uses of these indices are often made with empirical methods.

In arid and semi-arid regions, stakeholders and managers of water resources express a strong need for tools that can assess vegetation water content. In this paper, we explored the potential of two spectral indices, the $NDWI_{Gao}$ and MSI, derived from high spatial resolution SWIR and NIR, to assess and map the vegetation water content of wheat in the irrigated area of Tadla, Morocco.

2. Materials and methods

2.1 Study area

The study area (Figure 27) is located in the center of Morocco, between the Atlantic coast in the north-west and the Atlas Mountains in the south-east (32°23´ north latitude; 6°31´west longitude; 445 m above sea level). This irrigated plain of Tadla covers about

100,000 ha and is characterized by a flat topography and composed of a right bank (Beni-Amir) and left bank (Beni-Moussa). This area is characterized by a semi-arid climate: the average annual precipitation is about 300 mm (average over the period 1970-2010), with a significant inter-annual variation ranging from 130 to 600 mm in the same period. This plain is managed by the Regional Office for Agricultural Development of Tadla (ORMVAT).

Wheat is one of the main crops in this area, covering 36% of the total cultivated area. The wheat-growing cycle in the region runs from November-December to June. During this period, wheat is irrigated, using the flooding irrigation technique, between two and five times, depending on the water available in autumn and the volume accumulated in dams during winter and spring seasons.

The area is divided into several hundred irrigation plots. Sixteen wheat plots of them were selected in this study. The size of these plots varied from 1.7 to 14.5 ha (the total area is 77 ha). The combination of crop management and irrigation schedule for these plots was representative of the agricultural practices for wheat in the region. Figure 27 shows the location of studied area and illustrates the position of the selected plots (P1 to P16).

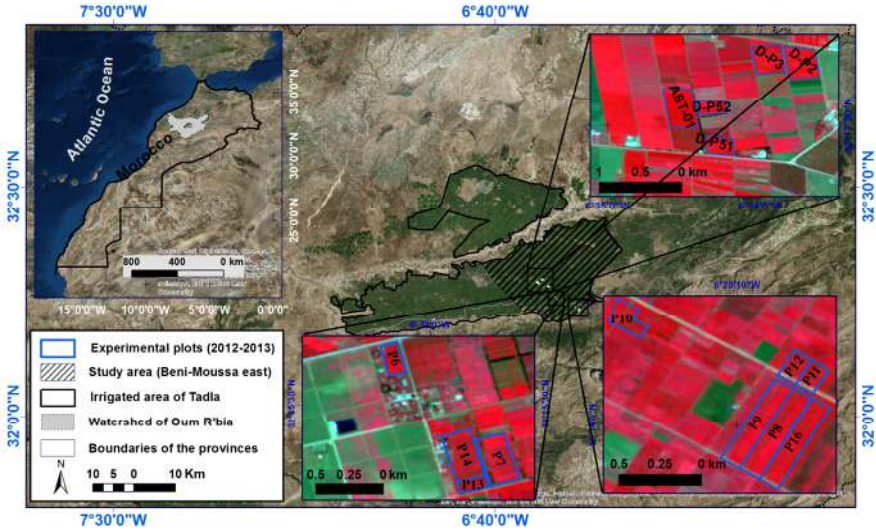

Figure 27: *Location of the Tadla irrigated perimeter (upper left window represents Morocco map; in the lower right window, the study area in dashed line and the experimental plots are in blue)*

2.2 Field experiments

Experiments were conducted during the 2012-2013 wheat growing season to record dates and amounts of irrigated water supplied and to collect crop physiological data. Data were collected from 16 fields of wheat, located at Tadla's Regional Agricultural Research or belonging to farmers, thus providing a valid representation of the soil-plant relationship in the study area. The field data related to Marzak and Achtar cultivars, which are widely cultivated in the study region.

Vegetation water content was measured weekly from anthesis until wheat grain filling (March to May 2013). It was measured in four randomly selected quadrates in each plot (i.e., an area of 0.5 * 0.5 m). From each quadrate, sub-samples were used to measure the weight of the fresh and dry above-ground biomass (dried in an oven at 65°C for 48 h) (Iqbal et al., 2010). Water vegetation content was quantified on a gravimetric (g

water/g vegetation) basis and was expressed in this document as a percentage (%).

We synchronized the field measurements with the planning for acquiring satellite images. In our case study, we only considered field measurements taken within a time lag of three days. We also ensured that during this time lag there was no rainfall event or irrigation supply.

Using geographical information system (GIS) software, we vectorized the collected field data (vegetation water content) as point and the experimental plots delimitations as polygons. We subdivided the experimental plots into units (sub-plots) of the same size and assigning per unit a code to identify and locate in space and time. Then, each sub-plot has been joined to the punctual data of vegetation water content and soil moisture corresponding to it spatially.

2.3 Satellite images and their processing

Three SPOT-5 HRV satellite images were acquired in 21 March 2013, 26 March 2013 and 11 April 2013 when the soil was completely covered by vegetation. They covered the period between anthesis (March) and grain filling (April) in the 2012-2013 cropping season. These wheat growth stages are crucial to ensure good yield (de San Celedonio et al., 2014).

SPOT-5 scenes have 10-m pixel resolution and four spectral bands: B1 (green: 0.50–0.59 μ m), B2 (red: 0.61–0.68 μ m), B3 (near infrared NIR: 0.79–0.89 μ m) and B4 (short-wave infrared SWIR: 1.58–1.75 μ m). One of the big advantages of Spot 5 images compared to other VHR images is the large swath (60 km×60 km) that allows a complete view of our region of interest. We also had the opportunity to program the satellite passes when the vegetation covered completely the soil and to match the critical time for the wheat crop.

The processing level of the acquired images was (1B), which included radiometric and geometric corrections. We conducted an atmospheric correction from the images of radiance, using the FLAASH model (Fast Line-of-sight Atmospheric Analysis of Spectral Hypercubes) included in the ENVI 5 software. The latter model is considered more accurate compared to other models for SPOT-5 image (Guo and Zeng, 2012).

We computed the two spectral indices, NDWIGao (Gao, 1996; Hardisky et al., 1983) and the MSI (Ceccato et al., 2002a; Ceccato et al., 2001; Hunt Jr and Rock, 1989), using the spectral reflectance NIR and SWIR for each SPOT-5 HRV image acquisition date (Table 18).

Table 18: *Studied spectral indices derived from SPOT-5 sensor*

Indices	Equation	Properties	References
Normalised Difference Water Index ($NDWI_{Gao}$)	(Red – SWIR)/(Red + SWIR)	Vegetation water content Soil moisture content	Gao (1996); Hardisky et al. (1983)
Moisture Stress Index (MSI)	(SWIR/NIR)	Water content of leaves in vegetation water content	Hunt Jr and Rock (1989); Ceccato et al. (2001)

The next step consisted in generation of a mask of wheat sub-plots, using ENVI 5 software. The average values of the spectral indices (NDWIGao and MSI) were then computed for each corresponding sub-plot (7×7 pixels) where field measurements were conducted (Figure 28). In our case study, we took ½ ha (7×7 pixels) as a reference area, where irrigation applications are synchronous and homogeneous at this scale. Regression analysis was carried out between vegetation water content measurements, MSI and NDWIGao values. This permitted to establish the relationships

between the NDWIGao and MSI values derived from the SPOT-5 images dataset and the ground studied measurements.

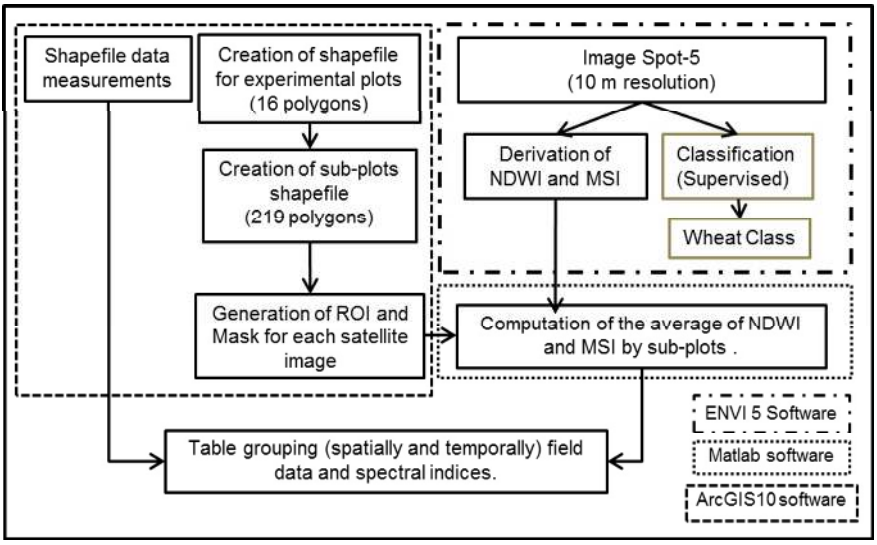

Figure 28: *Schematic diagram illustrating field data and Satellite images processing*

2.4 Supervised classification

In order to define the cereal area, which is our region of interest, we used a supervised classification method where 65 datasets have been taken for calibration and 112 sets for validation data. Separability analysis allow to determine how distinct, and thus separable, different surface types are from each other. Wheat, as a cereal, and other land occupations were categorized into two different classes to analyze their spectral separability. The Jeffries-Matusita (JM) distance was used to assess the potential of band pairs to discriminate between two different region classes. The values range between 0 and 2.

2.5 Model validation

Cross-validation is a technique to explore the reliability of a model to assess how the results of a statistical analysis will be applied to an independent data set (Kohavi, 1995). It is mainly used to estimate the accuracy of a predictive model. Several cross-validation techniques are used: "holdout method", "k-fold cross-validation" and "leave-one-out cross-validation" (LOOCV).

The k-fold cross validation (k-fold CV) approach was used to evaluate the accuracy of the obtained regression models between the two spectral indices and surface water content (Cassel, 2007). This approach uses k replicate samples of observation data, builds models with (k-1)/k of data and tests with the remaining 1/k. K-fold CV is an effective and widely used method. In our case, it involved 20% of the observations as the validation data, with the remaining 80% of the observations being the training data. We emphasize that the random k-fold CV takes k independent samples of size N*(k-1)/k (Cassel, 2007). We performed the cross-validation analysis using SAS 9.1 software.

2.6 Model evaluation

Different statistical indices were used to compare predicted and observed values. These indices were the coefficient of determination (R^2), the root mean square error (RMSE), the normalized RMSE (nRMSE) expressed as a percentage of the RMSE divided by the mean of observed values (Richter et al. 2012) and the mean absolute error (MAE):

$$RMSE = \left[\sum_{i=1}^{n} \frac{(Si-Oi)^2}{n}\right]^{0.5} \quad (1)$$

$$nRMSE = \left[\sum_{i=1}^{n} \frac{(Si-Oi)^2}{n}\right]^{0.5} \times \frac{100}{M} \quad (2)$$

Where Si and Oi refer to simulated and observed values of the studied variable, respectively; n is the number of observations; and M is the mean of the observed variable. The nRMSE indicates the accuracy of the model and the dispersion around the mean of the observed values.

2.7 Mapping of vegetation water content

To illustrate the practical use of this study, vegetation water content was mapped by using the validated linear regression model between vegetation water content and $NDWI_{Gao}$ index. Three maps were presented here for the east of Beni-Moussa irrigated area.

3. Results and discussions

3.1 Vegetation water content assessment at full vegetation cover

We compared the values of observed vegetation water content of 32 studied sub-plots and their spectral indices values derived from the three images acquired on 21 March 2013, 26 March 2013 and 11 April 2013. The results of this comparison were presented in figure 29.

The statistical indicators obtained from the previous comparison, presented in figure 29, showed that both spectral indices simulated well the vegetation water content. The values of statistical indicators R^2, RMSE, and nRMSE were 0.63, 3.19% and 4.24% for the $NDWI_{Gao}$ and 0.58, 3.22 and 4.27% for the MSI, respectively. Similar results were reported for the indices based on shortwave infrared band by Hunt Jr and Rock (1989) and QiuXiang et al. (2012) when simulating the vegetation water content.

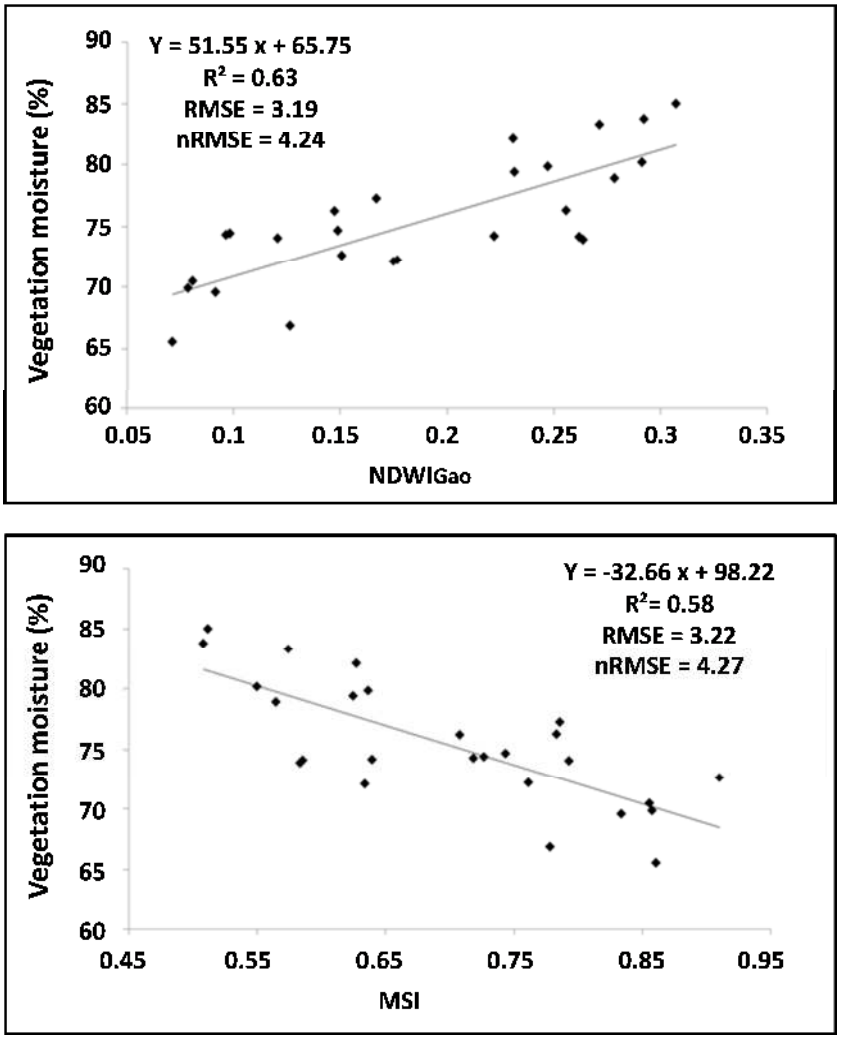

Figure 29: *Relationship between observed vegetation water content and derived spectral indices*

In order to validate these results, we compared observed vegetation water content values and those predicted using the k-fold CV method. As shown in figure 30, the errors were minimal for both the $NDWI_{Gao}$ and MSI. The evaluation model indicators obtained for predicted vegetation water content from the $NDWI_{Gao}$ were 3.39%, 4.52% and 0.52 for RMSE,

nRMSE and R^2, respectively. For the MSI, these values were 3.55%, 4.74% and 0.48 for RMSE, nRMSE and R^2, respectively (Figure 30). These results confirmed the ability of $NDWI_{Gao}$ to retrieve well the vegetation water content of wheat, while the values in MSI were comparatively less in agreement with the observed values.

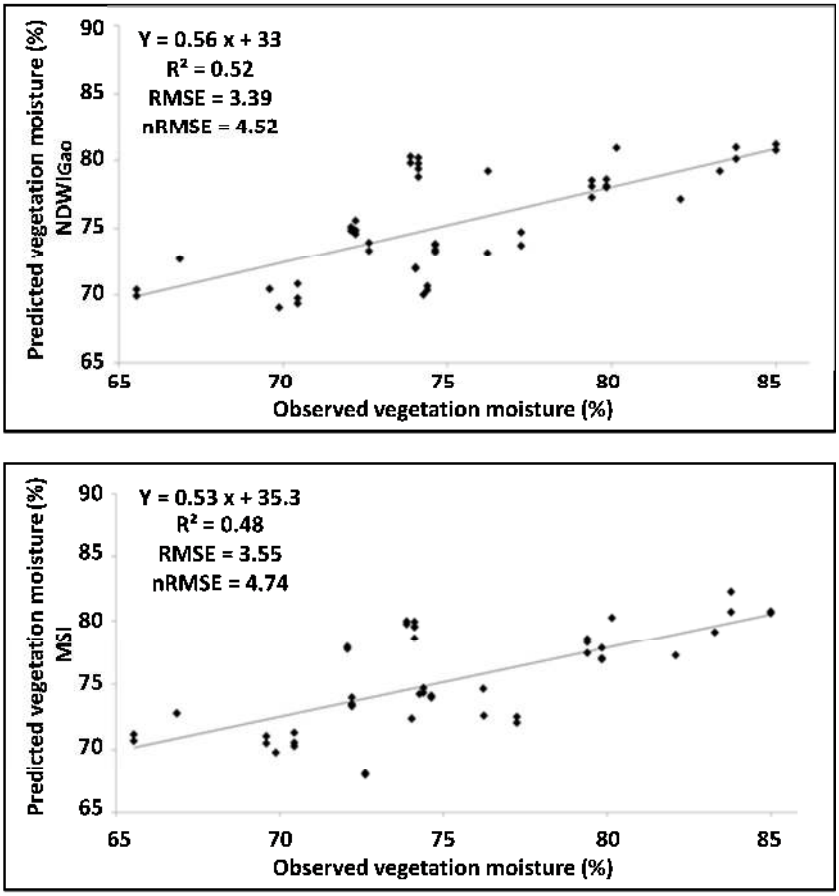

Figure 30: *Comparison between observed and predicted vegetation water content (%) using the k-fold CV of all acquired images*

3.2 Supervised classification

We performed a supervised classification to identify cereal area. The analysis of the numerical JM values allowed us to conclude that the separability results for training samples on final classification scheme are good. The estimated value of separability was 1.99.

The contingency matrix was used to evaluate the percentage of sampled pixels that were classified as expected. This classification was validated and the accuracy assessment and Kappa statistic indicated that it was a good classification. The overall accuracy is 0.95 while the overall Kappa is 96.7%.

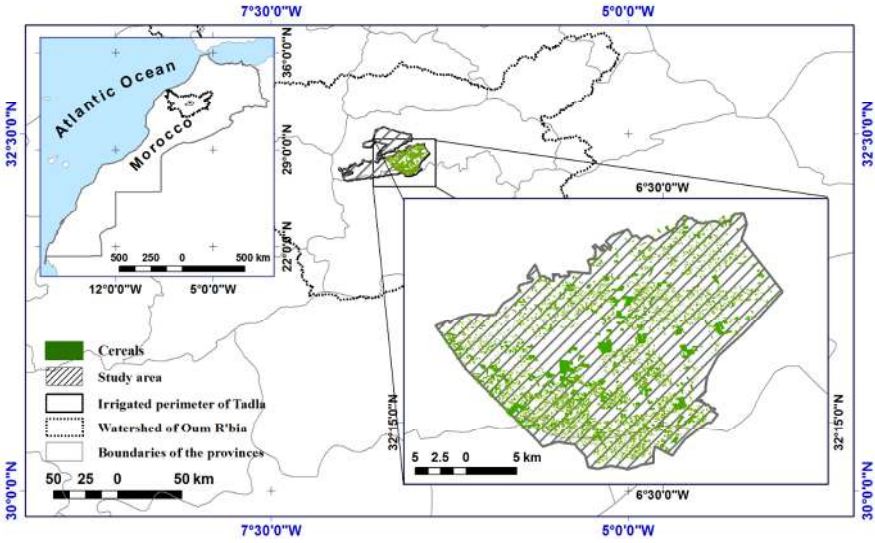

Figure 31: *Supervised classification map of wheat over the region of Beni-Moussa East (2012-2013)*

3.3 Mapping of vegetation water content

Figures (32, 33 and 34) show three maps of vegetation water content (VWC) of wheat class derived from the five SPOT-5 images. These maps were generated using the regression model (VWC = 51.55 * $NDWI_{Gao}$ + 65.75) obtained by comparing the three images on a pixel

basis and field measurements. The analysis of the three maps showed that vegetation water content ranged from 58% to 87% between the three considered dates. For these maps we had an RMSE of 3.19% and an nRMSE of 4.24%.

Figures (32 and 33) present a high homogeneity of vegetation water content (dominance of green color). Indeed, vegetation water content exceeded 70% for all plots. This is explained by important precipitation events that were recorded between 14 and 18 March 2013 (31.3 mm) and on 24 March 2013 (14 mm).

On the opposite, Figure 34 shows a strong heterogeneity in vegetation water content values after three weeks of precipitation and a homogeneous drying of several plots, with vegetation water content ranging from 58% to 76%.

Obtained maps allowed monitoring the variability of vegetation water content in wheat for each agricultural development center (ADC). Irrigation management is done independently at each development center. An overview of the maps allowed distinguishing between different levels of vegetation water content. Such information could be valuable for stakeholders and decision-makers in charge of irrigation areas and could help them to better manage irrigation at a large scale. It could also help judge the priority ADC to receive irrigation supplies according to the given state of vegetation water content.

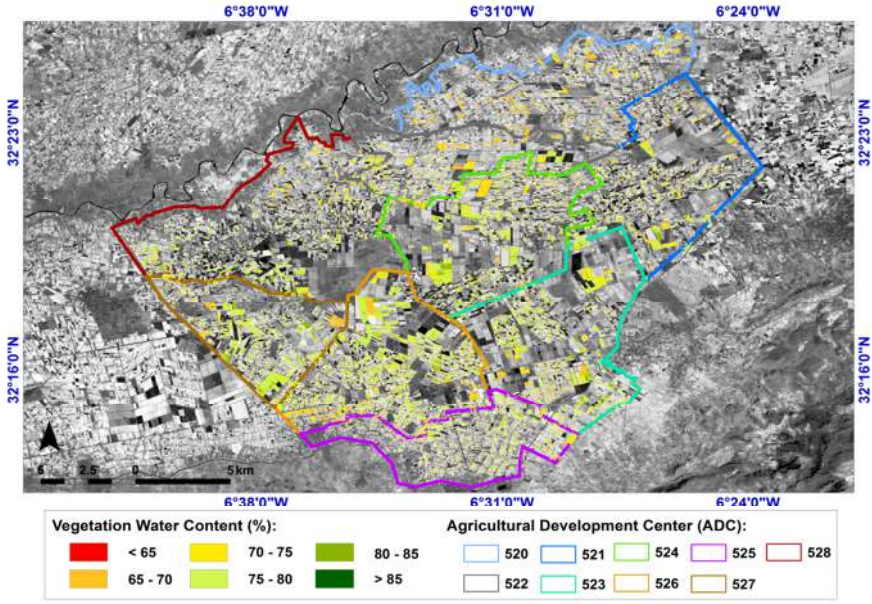

Figure 32: *Vegetation water content maps derived from* $NDWI_{Gao}$ *data (21/03/2013)*

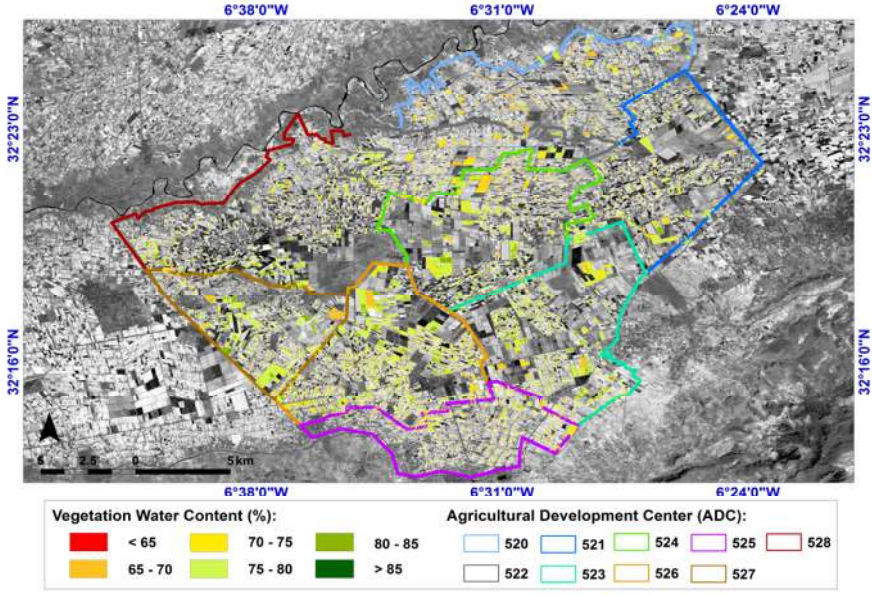

Figure 33: *Vegetation water content maps derived from* $NDWI_{Gao}$ *data (26/03/2013)*

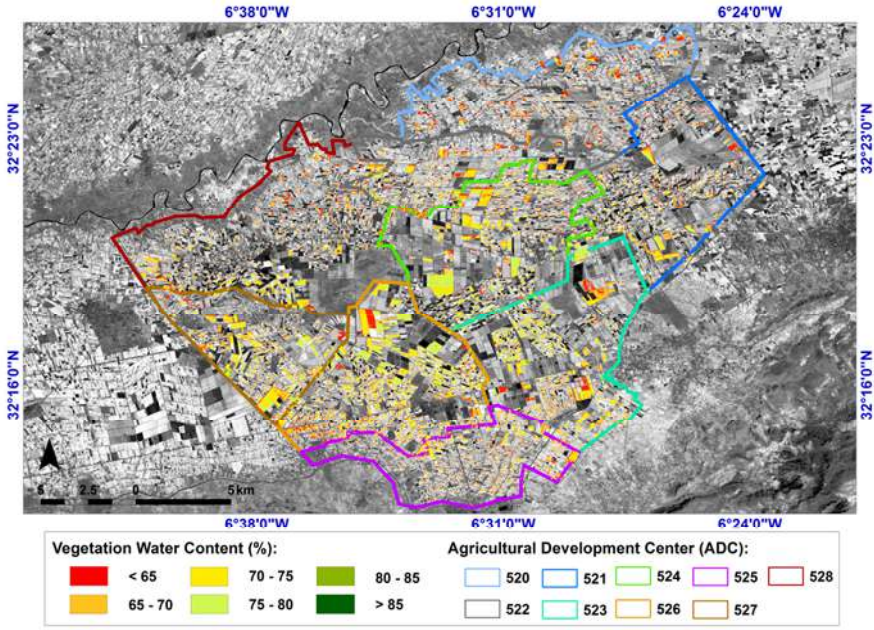

Figure 34: *Vegetation water content map derived from* $NDWI_{Gao}$ *data (11/04/2013)*

4. Conclusions

In this study, the ability of the two spectral indices ($NDWI_{Gao}$ and MSI) to monitor vegetation water content of wheat was assessed in a semi-arid irrigated area. These indices were calculated using the near and shortwave infrared band derived from SPOT-5 HRV satellite images.

The comparison between studied spectral indices values, based on SWIR and NIR, and vegetation water content measurements showed good correlations. This result demonstrated the potential of SWIR and NIR bands to improve irrigation and crop management based on vegetation water content changes per surface unit.

These indices ($NDWI_{Gao}$ and MSI) allowed vegetation water content to be assessed and quantified from anthesis to grain filling and showed their potential as an important tool for improving irrigation monitoring and water stress management at field and regional levels.

Appendix references

Cassel D.L. (2007) Re-sampling and simulation, the SAS way, in: Sas (Ed.), Proceedings of the SAS Global Forum 2007 Conference, SAS Institute Inc., Cary, NC.

Ceccato P., Flasse S., Grégoire J.M. (2002) Designing a spectral index to estimate vegetation water content from remote sensing data: Part 2. Validation and applications. Remote Sensing of Environment 82:198-207. DOI: http://dx.doi.org/10.1016/S0034-4257(02)00036-6.

Ceccato P., Flasse S., Tarantola S., Jacquemoud S., Grégoire J.M. (2001) Detecting vegetation leaf water content using reflectance in the optical domain. Remote Sensing of Environment 77:22-33. DOI: http://dx.doi.org/10.1016/S0034-4257(01)00191-2.

Cheng T., Riaño D., Koltunov A., Whiting M.L., Ustin S.L., Rodriguez J.C. (2013) Detection of diurnal variation in orchard canopy water content using MODIS/ASTER airborne simulator (MASTER) data. Remote Sensing of Environment 132:1-12. DOI: http://dx.doi.org/10.1016/j.rse.2012.12.024.

de San Celedonio R.P., Abeledo L.G., Miralles D.J. (2014) Identifying the critical period for waterlogging on yield and its components in wheat and barley. Plant and Soil 378:265-277. DOI: 10.1007/s11104-014-2028-6.

Duchemin B., Hadria R., Erraki S., Boulet G., Maisongrande P., Chehbouni A., Escadafal R., Ezzahar J., Hoedjes J.C.B., Kharrou M.H., Khabba S., Mougenot B., Olioso A., Rodriguez J.C., Simonneaux V. (2006) Monitoring wheat phenology and irrigation in Central Morocco: On the use of relationships between evapotranspiration, crops coefficients, leaf area index and remotely-sensed vegetation indices. Agricultural Water Management 79:1-27. DOI: 10.1016/j.agwat.2005.02.013.

Elvidge C.D., Lyon R.J.P. (1985) Influence of rock-soil spectral variation on the assessment of green biomass. Remote Sensing of Environment 17:265-279. DOI: http://dx.doi.org/10.1016/0034-4257(85)90099-9.

Feng H., Chen C., Dong H., Wang J., Meng Q. (2013) Modified Shortwave Infrared Perpendicular Water Stress Index: A

Farmland Water Stress Monitoring Method. Journal of Applied Meteorology and Climatology 52:2024-2032. DOI: 10.1175/jamc-d-12-0164.1.

Gao B.C. (1996) NDWI - A normalized difference water index for remote sensing of vegetation liquid water from space. Remote Sensing of Environment 58:257-266.

Geerts S., Raes D., Garcia M., Miranda R., Cusicanqui J.A., Taboada C., Mendoza J., Huanca R., Mamani A., Condori O., Mamani J., Morales B., Osco V., Steduto P. (2009) Simulating Yield Response of Quinoa to Water Availability with AquaCrop. Agron. J. 101:499-508. DOI: 10.2134/agronj2008.0137s.

Ghulam A., Qin Q., Teyip T., Li Z.L. (2007) Modified perpendicular drought index (MPDI): a real-time drought monitoring method. ISPRS Journal of Photogrammetry and Remote Sensing 62:150-164. DOI: http://dx.doi.org/10.1016/j.isprsjprs.2007.03.002.

Guo Y., Zeng F. (2012) Atmospheric correction comparison of SPOT-5 image based on model FLAASH and model QUAC. Int. Arch. Photogramm. Remote Sens. Spatial Inf. Sci. XXXIX-B7:7-11. DOI: 10.5194/isprsarchives-XXXIX-B7-7-2012.

Hadria R., Duchemin B., Jarlan L., Dedieu G., Baup F., Khabba S., Olioso A., Le Toan T. (2010) Potentiality of optical and radar satellite data at high spatio-temporal resolutions for the monitoring of irrigated wheat crops in Morocco. International Journal of Applied Earth Observation and Geoinformation 12, Supplement 1:S32-S37. DOI: 10.1016/j.jag.2009.09.003.

Hardisky M.A., Michael S.R., Klemas V. (1983) Growth response and spectral characteristics of a short Spartina alterniflora salt marsh irrigated with freshwater and sewage effluent. Remote Sensing of Environment 13:57-67. DOI: http://dx.doi.org/10.1016/0034-4257(83)90027-5.

Hunt Jr E.R., Li L., Yilmaz M.T., Jackson T.J. (2011) Comparison of vegetation water contents derived from shortwave-infrared and passive-microwave sensors over central Iowa. Remote Sensing of Environment 115:2376-2383. DOI: http://dx.doi.org/10.1016/j.rse.2011.04.037.

Hunt Jr E.R., Rock B.N. (1989) Detection of changes in leaf water content using Near- and Middle-Infrared reflectances. Remote Sensing of Environment 30:43-54.

Iqbal M.A., Bodner G., Heng L.K., Eitzinger J., Hassan A. (2010) Assessing yield optimization and water reduction potential for summer-sown and spring-sown maize in Pakistan. Agricultural Water Management 97:731-737. DOI: http://dx.doi.org/10.1016/j.agwat.2009.12.017.

Jacquemoud S., Baret F. (1990) PROSPECT: A model of leaf optical properties spectra. Remote Sensing of Environment 34:75-91. DOI: http://dx.doi.org/10.1016/0034-4257(90)90100-Z.

Jensen J.R. (2007) Remote Sensing of the Environment: An Earth Resource Perspective. 2nd ed. Prentice Hall.

Kohavi R. (1995) A study of cross-validation and bootstrap for accuracy estimation and model selection, Fourteenth International Joint Conference on Artificial Intelligence, San Mateo, CA: Morgan Kaufmann. pp. 1137–1143.

Liu S., Roberts D.A., Chadwick O.A., Still C.J. (2012) Spectral responses to plant available soil moisture in a Californian grassland. International Journal of Applied Earth Observation and Geoinformation 19:31-44. DOI: http://dx.doi.org/10.1016/j.jag.2012.04.008.

Ning Z., Yang H., Qiming Q., Lu L. (2013) VSDI: a visible and shortwave infrared drought index for monitoring soil and vegetation moisture based on optical remote sensing. International Journal of Remote Sensing 34:4585-4609. DOI: doi.org/10.1080/01431161.2013.779046.

ORMVAT. (2009) Rapport annuel de l'Office de la mise en valeur agricole de Tadla.

QiuXiang Y., AnMing B., Yi L., Jin Z. (2012) Measuring cotton water status using water-related vegetation indices at leaf and canopy levels. Journal of Arid Land 4(3):310−319. DOI: doi: 10.3724/SP.J.1227.2012.00310.

Seckler D., Barker R., Amarasinghe U. (1999) Water scarcity in the twenty-first century. Water Resources Development 15:29–42. DOI: 10.1080/07900629948916.

Trombetti M., Riaño D., Rubio M.A., Cheng Y.B., Ustin S.L. (2008) Multi-temporal vegetation canopy water content retrieval and interpretation using artificial neural networks for the continental USA. Remote Sensing of Environment 112:203-215. DOI: http://dx.doi.org/10.1016/j.rse.2007.04.013.

Yilmaz M.T., Hunt Jr E.R., Jackson T.J. (2008) Remote sensing of vegetation water content from equivalent water thickness

using satellite imagery. Remote Sensing of Environment 112:2514-2522. DOI: http://dx.doi.org/10.1016/j.rse.2007.11.014.